33. GEOCHEMISTRY OF IGNEOUS ROCKS RECOVERED FROM A TRANSECT ACROSS THE MARIANA TROUGH, ARC, FORE-ARC, AND TRENCH, SITES 453 THROUGH 461, DEEP SEA DRILLING PROJECT LEG 60[1]

D. A. Wood,[2] N. G. Marsh,[2] J. Tarney,[2] J.-L. Joron,[3] P. Fryer,[4] and M. Treuil[3]

ABSTRACT

Major and trace element analyses are presented for 110 samples from the DSDP Leg 60 basement cores drilled along a transect across the Mariana Trough, arc, fore-arc, and Trench at about 18°N. The igneous rocks forming breccias at Site 453 in the west Mariana Trough include plutonic cumulates and basalts with calc-alkaline affinities. Basalts recovered from Sites 454 and 456 in the Mariana Trough include types with compositions similar to normal MORB and types with calc-alkaline affinities within a single hole. At Site 454 the basalts show a complete compositional transition between normal MORB and calc-alkaline basalts. These basalts may be the result of mixing of the two magma types in small sub-crustal magma reservoirs or assimilation of calc-alkaline, arc-derived vitric tuffs by normal MORB magmas during eruption or intrusion.

A basaltic andesite clast in the breccia recovered from Site 457 on the active Mariana arc and samples dredged from a seamount in the Mariana arc are calc-alkaline and similar in composition to the basalts recovered from the Mariana Trough and West Mariana Ridge. Primitive island arc tholeiites were recovered from all four sites (Sites 458–461) drilled on the fore-arc and arc-side wall of the trench. These basalts form a coherent compositional group distinct from the Mariana arc, West Mariana arc, and Mariana Trough calc-alkaline lavas, indicating temporal (and perhaps spatial?) chemical variations in the arc magmas erupted along the transect.

Much of the 209 meters of basement cored at Site 458 consists of endiopside- and bronzite-bearing, Mg-rich andesites with compositions related to boninites. These andesites have the very low Ti, Zr, Ti/Zr, P, and rare-earth-element contents characteristic of boninites, although they are slightly light-rare-earth-depleted and have lower MgO, Cr, Ni, and higher CaO and Al_2O_3 contents than those reported for typical boninites. The large variations in chemistry observed in the lavas recovered from this transect suggest that diverse mantle source compositions and complex petrogenetic process are involved in forming crustal rocks at this intra-oceanic active plate margin.

INTRODUCTION

On DSDP Legs 59 and 60, 15 sites were drilled along an east–west transect at about 18°N from the West Philippine Basin to the Mariana Trench (Fig. 1) in order to study the nature of the back-arc and inter-arc basins, the remnant and active arcs, and the fore-arc of the region. One of the many aims of this drilling program was to elucidate the processes involved in crustal generation and the composition variation of active margin volcanics in an intra-oceanic environment, free of the complications associated with arc systems close to continental margins. On Leg 60, we recovered igneous rocks from the Mariana Trough, Sites 453, 454, and 456; the Mariana Ridge, Site 457; the Mariana fore-arc, Sites 458 and 459; and the arc-side wall of the Mariana Trench, Sites 460 and 461.

Detailed geophysical investigations and dredging operations have established that most back-arc or inter-arc basins are of extensional origin and are floored by basaltic crust, broadly comparable in structure and composition to those of the major ocean basins (Karig, 1971; Hart et al., 1972; Barker, 1972; Hawkins, 1974; Gill, 1976). Recent studies have shown that some of the basalts flooring back-arc basins are enriched in volatile and mobile elements (e.g., H_2O^+, K, Rb, Ba, Sr, U, and Cs) relative to normal mid-ocean ridge basalts (N-type MORB), and have some affinities with active margin magma types (Gill, 1976; Tarney et al., 1977; Hawkesworth et al., 1978; Saunders and Tarney, 1979; Weaver et al., 1979). In contrast, the basalts drilled in the Shikoku, West Philippine, and Parece Vela Basins on Legs 58 and 59 show no unequivocal chemical affinities with active margin magma types (Marsh et al., 1980, Mattey et al., 1980; Wood et al., 1980a, 1980b). The basalts recovered from the Mariana Trough provide us with an opportunity to compare the compositions of material from this relatively recently developed, narrow inter-arc basin with those of the broader, more mature back-arc basins of the West Pacific Ocean.

There is as yet no general consensus on the petrogenetic processes of active arc magma types. There are two main compositional end members of arc magmatism: a tholeiitic type showing iron enrichment trends and a calc-alkaline type showing enrichment in alkalis, corresponding broadly to Kuno's (1968) pigeonitic and hypersthenic series, respectively. In addition, there are very rare Mg-rich andesites or boninites, named after their type locality in the Bonin Islands (Kuroda and Shiraki, 1975) but also recently dredged from the Mariana Trench near the island of Guam (Dietrich et

[1] *Initial Reports of the Deep Sea Drilling Project*, Volume 60.

[2] Department of Geological Sciences, University of Birmingham, P.O. Box 363, Birmingham, B15 2TT, U.K. Dr. Wood's present address: Phillips Petroleum Co. Europe-Africa, Glen House, Stag Place, London SW1E 5DA, U.K. Dr. Marsh's present address: University of Leicester, Department of Geology, Leicester, LE1 7R4, U.K.

[3] Laboratorie de Géochimie Comparée et Systematique, UER des Sciences de la Terre et Institut de Physique du Globe, LA 196 CNRS, Université Pierre et Marie Curie, 4 Place Jussieu, 75230 Paris Cedex 05, France, and Laboratoire Pierre Sue CNRS, CEN Saclay, B. P. No. 2, 91190 Gif-sur-Yvette, France.

[4] Hawaii Institute of Geophysics, 2525 Collea Road, Honolulu, Hawaii 96822.

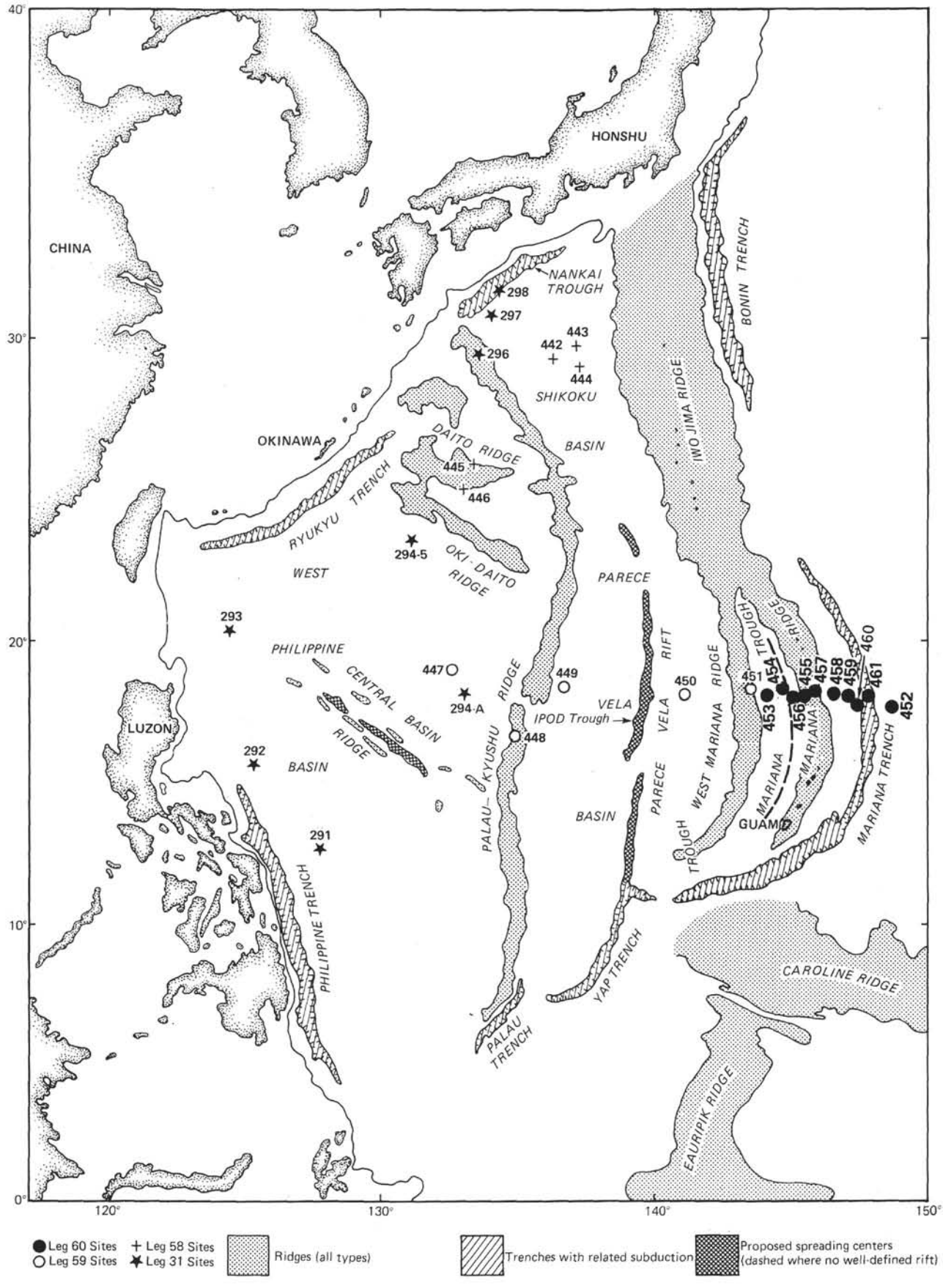

Figure 1. Location of drill sites from Legs 59 and 60.

al., 1978). These lavas are thought to be produced during the early stages of island arc development and are therefore important in understanding arc magmatism. Similar Mg-rich andesites were drilled at Site 458. These lavas, together with the primitive island arc tholeiites and calc-alkaline basalts recovered from the Kyushu-Palau, West Mariana, Mariana Ridges and the Mariana fore-arc and Trench during Legs 59 and 60, should help to constrain petrogenetic models for this tectonic environment.

REGIONAL AND TECTONIC SETTING

The southern Philippine Sea is divided into three major basins (Fig. 1) which are elongated in a north–south direction. From west to east the basins are: the West Philippine Basin, the Parece Vela Basin, and the Mariana Trough. The basins are separated by the Kyushu-Palau and West Mariana Ridges, respectively. The eastern boundary of the Southern Philippine Sea consists of the Mariana Arc and fore-arc, which overlie the Pacific plate presently being subducted at the Mariana Trench (Katsumata and Sykes, 1969).

The Mariana Trough is crescent-shaped, open at its southern end but closing at the junction between the Mariana and West Mariana Ridges in the north. The trough is approximately 1500 km long and 250 km across at its widest section. The Mariana Ridge is approximately 100 to 120 km across, and the fore-arc, or arc-trench gap, is approximately 150 to 180 km wide.

The crust flooring the Mariana Trough is characterized by rough topography (Hart et al., 1972) and high heat flow (Sclater et al., 1972). It is underlain by a mantle zone of high seismic wave attenuation (Barazangi et al., 1975). Poorly developed magnetic lineations have been reported for the Mariana Trough (Hussong, Uyeda, et al., 1978). The reasons for the poorly developed magnetic lineations are suspected to be the rough basement topography and low geomagnetic latitude of the region (Karig et al., 1978). On the basis of the sediment thickness, depth, the character of the acoustic basement, and the presence of a topographic axial high and mean heat flow, Karig (1971) suggested that the Mariana Trough is actively spreading, unlike the other basins of the Philippine Sea. Estimates for the spreading rate vary from slow, 1 cm yr^{-1} (Hart et al., 1972) and 2 cm yr^{-1} (Hussong et al., 1978), to fast, and 4 cm yr^{-1} (Karig et al., 1978). The uppermost crust in the axial region of the trough consists of basalts broadly similar to ocean floor tholeiites (Hart et al., 1972; Hawkins, 1977). The opening of the Mariana Trough appears to be a continuation of the processes involved with the opening of the Parece Vela and Shikoku Basins, to the west, during the middle to late Tertiary. However, the relationship of these eastern basins and ridges to the West Philippine Basin remains uncertain (Scott et al., 1980).

The Mariana arc can be divided into two sections: a northern section which is presently active and underlain by a steeply dipping Benioff zone, with seismic activity down to at least 600 km; and a southern section which is presently inactive and underlain by a poorly defined seismic zone less than 200 km deep (Katsumata and Sykes, 1969; Isacks and Barazangi, 1977). The two zones overlap between 16° and 17°30′N, the ridge of the southern section lying to the trench side. The northern ridge carries 10 subaerial volcanic islands and possibly several submarine volcanoes whose extrusive products are dominated by quartz-normative basalts and basaltic andesites. The lack of iron enrichment and high Ba and Sr contents in the basalts suggests that they have calc-alkalic affinities (Meijer, 1976; Dixon and Batiza, 1979). The volcanic islands of the southern ridge consist mainly of basalts and basaltic andesites interbedded with and overlain by, predominantly calcareous sediments (Stark, 1963), although more evolved igneous rocks occur, for example, dacite on Saipan (Cloud et al., 1956; Schmidt, 1957; Taylor et al., 1969). These lavas also lack a trend of strong iron enrichment and plot as a hypersthenic series on an AFM diagram (Stark, 1963). In contrast to the Mariana arc and trough, the fore-arc has not been studied in detail. It consists of crust which is seismically oceanic in character (Murauchi et al., 1968). Sedimentation on the fore-arc appears to be strongly controlled by tectonic activity, mainly block faulting in a tensional regime with subsidence since the early Tertiary. It is unlikely that slices of the main Pacific ocean floor have been imbricated into the fore-arc of the Mariana system (Hussong et al., 1978).

The Mariana Trench has been dredged previously during Cruise 17 of the RV *Dmitry Mendeleev* south of the Leg 60 transect, at approximately 12°N (Anonymous, 1977). The dredges recovered flysch-like sediments, gabbros, metagabbros, serpentinized and mylonitized periodotites, boninites, basalts, and metabasalts (Dietrich et al, 1978; Sharaskin et al., 1980). The boninites and flysch-like sediments suggest the presence of arc-derived material in the trench.

ANALYTICAL METHODS

We have analyzed 110 samples from the Leg 60 cores at Birmingham by X-ray fluorescence (XRF) for major and trace elements by the method given in Tarney et al. (1978). However, TiO_2, MgO, CaO, and Na_2O were analyzed using an Rh anode tube rather than a Cr anode tube. Instrumental conditions for major element analysis using an Rh anode X-ray tube are given by Marsh et al. (1980). We have also analyzed 63 samples from the Leg 60 sites at Saclay by instrumental neutron activation (INA) for additional trace elements by the method of Chayla et al. (1973).

RESULTS

The XRF data, together with CIPW norms and some trace element ratios, are given in Tables 1 through 6, 8, and 10. Some of the INA data have been presented by Bougault et al. (this volume), and only representative analyses of the main lithological units are given here (Table 11). The geochemical variations of the Leg 60 sites will be dealt with in two parts: first, the Mariana Trough and Ridge sites (Sites 453, 454, 456, and 457); and secondly, the Mariana fore-arc and Trench sites (Sites 458 through 461). This will be followed by a brief, essentially qualitative, discussion of the implications of the geochemical data for the processes involved in the

petrogenesis of this diverse suite of active plate margin volcanics.

The Mariana Trough and Ridge

Site 453
(17°54.42′N, 143°40.95′E)

This site was located 120 km west of the central graben of the Mariana Trough in a water depth of 4693 meters. The 150 meters of igneous and metamorphic polymict breccias recovered are more than 5.4 m.y. old and are predominantly gabbros with subordinate norites and metabasalts cemented by a calcite, clay and/or iron oxide matrix. The breccia sequence can be split into three units based on lithologic changes with depth in the hole. These are:

1) From 455.5 to 541 meters, sub-bottom depth (Cores 49 through 57), an igneous polymict breccia of large gabbroic clasts (>10 cm) with a few diabase and basalt clasts in a predominantly red-brown matrix. The core from Section 55-4 (Piece 4) through Section 57-2 (Piece 16), however, has a green matrix and the gabbros in it have been demagnetized as a result of hydrothermal alteration at elevated temperatures.

2) From 541 to 569.5 meters, sub-bottom depth (Cores 58 through 60), an igneous polymict breccia of predominantly metavolcanic clasts. Quartz veining is common, and pyrite is abundant in the matrix.

3) From 569.5 to 605 meters, sub-bottom depth (Cores 61 through 64), a breccia composed of sheared, mylonitized and serpentenized metagabbro clasts, with abundant pyrite set in a matrix of serpentine.

The analyzed samples cover virtually the full spectrum of gabbroic clasts recovered, which include gabbros, anorthositic gabbros, gabbro pegmatites, noritic gabbros, and hornblende gabbros. Hand-specimen descriptions of the analyzed clasts are given in the Appendix. Replacement of the original igneous mineral assemblage of plagioclase ± clinopyroxene ± orthopyroxene ± olivine ± brown hornblende ± accessory magnetite is common. Replacement minerals include green hornblende, chlorite, epidote, sericite, carbonates, clays, and alkali feldspars with accessory amounts of zeolites, prehnite, pumpellyite, and stilpnomelane. The volcanic clasts recovered are mainly doleritic in texture and aphyric to sparsely plagioclase phyric with rare small vesicles (<0.6 mm). Alteration is moderate to heavy with clinopyroxene being replaced by chlorite, stilpnomelane, and iron oxides, and plagioclase being replaced by sericite, albite, and clays.

The major and trace element chemistry of the plutonic rocks (Table 1) is consistent with many of them being cumulates (Figs. 2 and 3), which accounts for the very low abundances of several of the incompatible or hygromagmatophile (HYG) trace elements (e.g., Zr and Y) in some of the samples. The basaltic clasts vary from aphyric to sparsely plagioclase, and clinopyroxene phyric with rare pseudomorphs of olivine microphenocrysts. The compositions of these basaltic clasts are typical of arc magma types with high Sr and Ba but low Ta, Cr, and Ni contents. Of the two basalts analyzed by INA (Table 10), Sample 453-52-1, 30–36 cm has a more primitive arc tholeiite composition (lower Th and La and a depletion in the light rare earth elements (REE) relative to the heavy REE (i.e., chrondite-normalized La/Tb ratio less than 1).

The high Sr and Ba contents of the plutonic rocks from this site (Table 1) are consistent with an origin in the deep-seated portion of an island arc. Table 2 presents major and trace element analyses of plutonic rocks from the Masirah ophiolite, Indian Ocean crust (Abbotts, 1979) and calc-alkaline plutonic rocks from Chile (Marsh, 1977; Wells, 1978). Note the lower Sr and Ba of the plutonic rocks from oceanic crust relative to the rocks from Site 453. However, the very high Ba and K_2O contents of some Site 453 samples (e.g., Sample 453-52-4, 0–4 cm) are likely to be due to the presence of secondary potassium feldspar. The most plausible explanation for these breccias is a derivation from the West Mariana Ridge during the uplift resulting from the initial rifting of the Mariana Trough. We note that the basalt clasts in the breccia drilled on Site 451 (Leg 59) on the West Mariana Ridge also have calc-alkaline affinities (Mattey et al., 1980; Wood et al., 1980a). However, calc-alkaline magmas may have been erupted elsewhere in the Mariana Trough (see the following).

Site 454
(18°00.78′N, 144°31.92′E)

This site was located 28 km west of the central graben of the Mariana Trough in a water depth of 3819 meters. A basement section of 80 meters of basalts interbedded with sediments was recovered from Hole 454A. The oldest sediments are between 1.2 and 1.6 m.y. old. Five lithological units and three paleomagnetic units were distinguished by the shipboard party. The basalts are all considerably more vesicular than mid-ocean ridge basalts (MORB) erupted in similar water depths (e.g., Moore and Schilling, 1973).

The geochemical units correspond with the paleomagnetic units (Fig. 4). The basalts of Geochemical Unit 1 are olivine phyric (about 10% phenocrysts) with chrome spinel microphenocrysts and contain up to 14 weight percent MgO. The basalts in Geochemical Unit 2 are sparsely plagioclase, olivine, and clinopyroxene phyric, and those in Unit 3 are sparsely olivine phyric (up to 7% phenocrysts) with associated chrome spinel. The major element chemistry of the basalts (Table 3) is similar to normal or N-type MORB with high CaO (about 11 wt.%), but low K_2O and TiO_2 (about 1 wt.%). However, these basalts have higher Sr, Ba, Th, and light REE contents relative to Zr, Ti, Y, and the heavy REE than N-type MORB. In addition they also display a depletion of Ta relative to Th and La. These trace element characteristics are similar to those observed in island arc magmas. Their high vesicularity also indicates a volatile rich magma (Garcia et al., 1979).

Site 456
(17°54.7′N, 145°10.8′E)

This site was located 37 km east of the central graben of the Mariana Trough in a water depth of 3590 meters.

The sediment above the basement had an age of about 1.8 m.y. In two holes, short basement sections (Hole 456 about 35 meters; Hole 456A about 40 meters) of altered pillow basalt were recovered. The top of the basement sections in both holes has suffered intense hydrothermal alteration, under reducing conditions, with abundant pyrite mineralization and quartz veining. Toward the bottom of the basement sections in both holes, the basalts are only slightly to moderately altered, under oxidizing conditions, and contain fresh glass.

Two lithological units in Hole 456 and four lithological units in Hole 456A were distinguished by the shipboard party. Unit 1 of both holes includes intensely altered pillow basalts which are aphyric or sparsely plagioclase phyric (about 1 or 2% phenocrysts). Unit 456A-2[5] is a coarsely plagioclase phyric basalt (greater than 20% resorbed phenocrysts) with pseudomorphs of rare olivine phenocrysts. Unit 456A-3 is a highly vesicular (up to 30% vesicles of 0.2 to 2 mm diameter), aphyric basalt with up to 3 percent olivine microphenocrysts. Unit 456A-4 varies from aphyric to sparsely plagioclase phyric basalts with rare clinopyroxene phenocrysts. Unit 456-3 is also aphyric and similar to Units 456A-3 and 4. Units 456-3 and 456A-4 are vesicular but less so than Unit 456A-3. The shipboard party have grouped Units 456A-3 and 456-3 together, but from the geochemical data it is apparent that basalts corresponding to Units 456A-2 and 3 are not present in Hole 456 and that Unit 456-3 can probably be equated with Unit 456A-4 (see below and Fig. 5). Unit 456A-5 is petrographically similar to Unit 456A-3, although less vesicular, but chemically it is indistinguishable from Unit 456A-4.

Most of the basalts from both holes have major and trace element chemistry (Table 4) similar to N-type MORB, although with slightly higher Sr and Ba contents. However, the porphyritic Unit 456A-2 and the relatively Mg-poor Unit 456A-3 are significantly enriched in Th, Sr, Ba, K, and light REE relative to Zr, Ti, Y, and the heavy REE when compared to N-type MORB. They also show a depletion of Ta relative to Th and La (Table 11). The basalts from these units therefore have trace element characteristics that are quite similar to island arc tholeiites.

Site 457
(17°49.99′N, 145°49.02′E)

This site was located on the active Mariana arc in a water depth of 2630 meters. The hole penetrates only coarse sand and volcaniclastic breccias. We have analyzed one sample of a basaltic andesite clast from the breccia (Tables 5 and 11). There are no petrographic data available for the analyzed sample, but the crystal-vitric tuff clasts with which it is associated in the breccia included glass fragments with sparse euhedral plagioclase, clinopyroxene, and amphibole phenocrysts. The analysis indicates that the sample has calc-alkaline affinities with high Th, K, Ba, Sr, and light REE relative to Zr, Ti, Y, and heavy REE contents.

[5] Denotes lithologic unit, not to be confused with Core 456A-2.

Inter-Site Relationships of Basement Chemistry

The chemical data for the samples from Sites 454, 456, and 457 have been plotted on a series of major and trace element variation diagrams (Figs. 6 through 13). The main feature of the chemical variations in the basic lavas from these sites is the systematic gradation in chemistry from basalts similar to N-type MORB to basalts with calc-alkaline affinities. At Sites 454 and 456, which have penetrated inter-arc basin crust, both basalt types are found interlayered within a single hole. Geochemical Units 454A-1, 454A-2, 456A-2, 456A-3, and 457 have calc-alkaline affinities, whereas Geochemical Units 454A-3, 456-1 (and 456A-1?—extensive hydrothermal alteration), and 456A-4 have compositions quite similar to N-type MORB.

Figure 6 shows that for the same MgO contents the MORB-like lavas have higher Zr and Ti but lower Sr than the units with calc-alkaline affinities. Biaxial plots of HYG elements (Figs. 7 and 8) confirm that the different magma types cannot be related by simple crystal fractionation processes. On such diagrams, magmas related by crystal fractionation should conform to straight-line trends passing through the origin (Weaver et al., 1972; Treuil and Varet, 1973). On the contrary, the Mariana Trough basalts can be seen to follow several diverse trends.

The occurrence of lavas with MORB-like and arc-like characteristics interbedded in the crust of the Mariana Trough at two localities has important implications for the magmatic processes controlling the formation of this inter-arc basin. One possibility is that the two basalt types were co-magmatic. If so, such small scale lithostratigraphic variations indicate that eruptions are related to small, short-lived magma reservoirs. This has also been proposed for the slow-spreading Mid-Atlantic Ridge to explain similar interlayering of geochemically different basalt types which cannot be related by crystal fractionation processes (Wood et al., 1979a). Rocks previously dredged from the Mariana Trough also show a range of compositions (Hart et al., 1972), and, although some are similar to MORB, others have some geochemical affinities with arc magma types. Hart et al. (1972) distinguished those lavas from arc magmas on the basis of their low $^{87}Sr/^{86}Sr$ (less than 0.7030) and K/Ba (less than 85) ratios, despite them having Ba (25–50 ppm), K (2350–4200 ppm), and Sr (155–208) contents considerably higher than average MORB (Ba ~ 12 ppm, K ~ 1060 ppm, Sr ~ 124 ppm—Wood, 1979; Sun et al., 1979). Also, the dredged basalts studied by Hart et al. (1972) have flat or slightly light-REE-enriched, chondrite-normalized REE ratios.

Wood et al. (1980a) have recently noted that the abundance of Ba relative to K, Th, U, and Rb varies significantly in arc basalts from the West Pacific, with the Japanese arcs (Wood et al., 1980a) being most enriched in Ba. Hart et al. (1972) suggest that island arc tholeiites have K/Ba ratios invariably less than 30 to 40, based on the work of Philpotts et al. (1971) on Japanese

Table 1. Major and trace element analyses of igneous rocks from Hole 453.

Sample (interval (in cm)	42-1, 16-18	47-1, 99-101	49-1, 56-58	49-3, 52-54	50-2, 37-39	52-1, 96-98	52-2, 94-96	53-3, 0-2	54-1, 40-42	54-2, 84-86	54-3, 6	55-2, 14-16
SiO_2	56.0	50.2	46.2	55.9	45.1	51.0	46.0	45.3	46.6	52.4	51.4	45.9
TiO_2	0.82	0.94	0.07	0.74	0.21	1.00	0.18	0.17	0.21	0.81	1.00	1.08
Al_2O_3	13.4	11.1	23.8	17.1	14.0	15.7	19.3	19.1	21.3	16.1	15.1	14.7
tFe_2O_3	9.98	13.47	5.76	9.57	8.08	11.37	8.93	7.04	6.27	10.84	12.25	14.48
MnO	0.20	0.19	0.07	0.15	0.11	0.15	0.18	0.10	0.09	0.18	0.4	0.32
MgO	5.72	10.10	7.18	4.71	15.10	5.71	10.71	10.37	7.88	7.04	6.03	8.57
CaO	5.97	1.30	15.21	7.82	16.12	9.86	9.52	17.17	15.97	5.83	9.32	5.79
Na_2O	3.13	2.53	0.75	3.51	0.38	2.93	0.87	0.43	1.18	3.91	2.23	3.30
K_2O	0.71	3.69	0.54	0.82	0.18	0.56	2.43	0.36	0.59	1.66	1.18	0.58
P_2O_5	0.10	0.25	0.00	0.17	0.00	0.31	0.00	0.00	0.00	0.18	0.13	0.16
Total	95.99	93.75	99.60	100.55	99.28	98.67	98.09	100.08	100.10	98.99	98.87	94.84
Ni	9	15	24	4	58	11	36	39	20	5	6	3
Cr	36	27	25	8	304	16	146	122	123	13	21	13
Zn	83	86	8	43	21	34	58	20	27	48	75	92
Ga	20	18	15	20	11	17	11	12	14	17	18	20
Rb	8	35	5	8	<1	9	25	5	4	18	17	7
Sr	187	72	418	384	204	511	240	314	398	338	429	322
Y	29	46	3	25	3	25	<1	1	2	25	21	23
Zr	91	52	9	41	5	82	6	8	9	65	55	56
Nb	1	1	<1	<1	<1	<1	<1	<1	<1	<1	<1	<1
Ba	266	288	126	231	40	148	1018	72	297	429	326	144
La	8	15	3	9	9	20	7	2	2	9	12	11
Ce	15	21	1	11	4	27	3	5	<1	19	19	17
Nd	11	16	3	9	2	16	3	3	1	14	12	11
Pb	6	11	3	5	6	8	2	1	3	<1	7	1
Th	<1	<1	1	2	1	4	1	<1	2	3	5	2
Zr/Nb	91.0	52.0	>9.0	>41.0	>5.0	>82.0	>6.0	>8.0	>9.0	>65.0	>55.0	>56.0
Ti/Zr	54.0	108.0	45.0	108.0	253.0	73.0	176.0	131.0	143.0	74.0	109.0	116.0
Y/Zr	0.32	0.88	0.33	0.61	0.60	0.30	<0.17	0.13	0.22	0.38	0.38	0.41
Ce/Zr	0.16	0.40	0.11	0.27	0.80	0.33	0.50	0.63	<0.11	0.29	0.35	0.30
Ba/Zr	2.92	5.54	14.00	5.63	8.00	1.80	169.67	9.00	33.00	6.60	5.93	2.57
$(Ce/Y)_N$	1.27	1.12	0.82	1.08	3.27	2.65	—	12.28	—	1.87	2.22	1.82
Fe/Mg	2.02	1.55	0.93	2.36	0.62	2.31	0.97	0.79	0.92	1.79	2.36	1.96
K/Rb	740.0	875.0	903.0	852.0	>1461.0	513.0	807.0	603.0	1233.0	766.0	576.0	688.0
Ba/Sr	1.42	4.00	0.30	0.60	0.20	0.29	4.24	0.23	0.75	1.27	0.76	0.45
Q	10.5	0.0	0.0	5.5	0.0	0.7	0.0	0.0	0.0	0.0	2.1	0.0
Or	4.4	23.3	3.2	4.8	1.0	3.3	14.6	2.1	3.5	9.9	7.1	3.6
Ab	27.6	22.8	6.4	29.5	0.5	25.1	7.5	0.6	6.7	33.4	19.1	29.4
An	21.2	5.2	60.2	28.4	36.2	28.5	42.4	49.2	51.0	21.8	28.1	24.8
Ne	0.0	0.0	0.0	0.0	1.5	0.0	0.0	1.7	1.8	0.0	0.0	0.0
Di	7.5	0.0	12.6	7.7	35.5	15.9	4.9	28.9	22.8	5.3	15.0	3.7
Hy	24.2	31.1	6.0	19.8	0.0	20.8	3.8	0.0	0.0	13.6	23.3	9.2
Ol	0.0	10.2	9.9	0.0	22.8	0.0	24.2	15.4	12.2	11.2	0.0	22.7
Mt	1.8	2.5	1.0	1.7	1.4	2.0	1.6	1.2	1.1	1.9	2.2	2.7
Il	1.6	1.9	0.1	1.4	0.4	1.9	0.3	0.3	0.4	1.5	1.9	2.2
Ap	0.3	0.6	0.0	0.4	0.0	0.7	0.0	0.0	0.0	0.4	0.3	0.4

Note: All CIPW norms calculated assuming an Fe_2O_3/FeO ratio of 0.15.

lavas. However, island arc tholeiites recently recovered from DSDP Site 448 have K/Ba ratios greater than 90 (Mattey et al., 1980). We note also that the low-temperature sea-water alteration could significantly increase the K/Ba ratios of the lavas. Thus, the high K/Ba ratios of the dredged basalts do not necessarily distinguish them from arc magmas. The basalts recovered from the Leg 60 drill sites have suffered variable degrees of alteration, and consequently the K/Ba ratios vary considerably. Nevertheless, the K/Ba ratios of most samples from Units 457, 454A-1, and 454A-2 are less than 50, but in Unit 454A-3 K/Ba varies from 64 to 94. The calc-alkaline arc lavas drilled at Site 451 (Mattey et al., 1980) have K/Ba ratios less than 40.

In Figures 9 and 10, Ni versus Zr and Cr versus Zr, the units which have calc-alkaline affinities and those MORB-like units follow distinct trends. This is mainly due to the different Zr contents of the different magma types. The plot of Zr versus Ti (Fig. 11) shows that most of the lavas have Ti/Zr ratios between 75 and 100, whilst N-type MORB generally have Ti/Zr ratios in the range 90 to 120. Significantly, Units 456A-3 and 457 have Ti/Zr ratios less than 90. The main HYG element differences between the two magma types have been summarized in Figure 12. Here the HYG element abundances of three representative samples have been normalized to estimated primordial mantle abundances (Wood, 1979) and arranged in approximate order of in-

Table 1. (Continued).

55-3, 25-27	55-3, 90-92	55-4, 144-146	56-2, 33-35	56-2, 85-87	57-1, 30-32	57-3, 8-10	57-4, 36-38	57-4, 123-125	58-1, 6-8	59-1, 13-15	59-1, 47-49	63-1, 0-2
41.8	44.6	43.7	42.6	48.0	48.3	42.4	43.0	42.6	43.7	70.5	61.0	48.0
0.04	0.23	0.05	0.05	0.05	0.83	0.05	0.16	0.03	1.28	0.46	0.73	0.82
21.7	19.0	27.6	24.7	23.0	15.2	24.7	17.9	29.1	14.1	12.1	12.8	13.9
8.29	8.36	5.99	8.15	5.90	11.67	6.94	10.73	4.79	15.30	6.88	6.65	13.06
0.11	0.10	0.09	0.14	0.09	0.17	0.09	0.12	0.06	0.39	0.36	0.11	0.26
12.81	11.48	6.99	9.06	8.24	8.34	11.23	14.41	7.44	14.24	2.89	1.94	12.63
12.82	16.92	12.82	11.69	9.76	13.47	14.34	11.94	15.26	1.02	0.66	8.80	2.66
0.51	0.32	0.96	0.97	2.65	1.69	0.38	0.44	0.56	3.00	4.98	7.50	3.34
0.29	0.07	1.20	0.73	1.34	0.21	0.16	0.09	0.53	0.05	0.24	0.03	0.21
0.00	0.00	0.00	0.00	0.00	0.03	0.00	0.00	0.00	0.20	0.07	0.17	0.10
98.32	101.09	99.38	98.05	98.99	99.99	100.32	98.78	100.34	93.22	99.14	99.77	95.00
58	46	17	41	22	13	51	77	32	9	<1	7	10
8	234	2	<1	1	26	62	265	<1	40	<1	16	20
31	25	28	50	26	63	19	42	16	127	300	19	67
13	14	17	16	14	18	12	13	16	20	12	6	17
3	<1	11	7	14	2	1	1	4	<1	2	<1	3
413	311	456	418	354	387	427	364	523	222	108	124	275
<1	1	<1	<1	<1	12	<1	1	<1	32	30	13	16
7	10	7	7	10	21	6	10	10	77	84	44	45
<1	<1	<1	<1	<1	<1	<1	<1	<1	<1	<1	<1	<1
68	13	547	301	409	80	42	58	148	112	104	32	118
9	8	4	2	2	6	8	11	3	17	7	4	6
4	<1	4	6	<1	6	3	3	3	19	12	15	15
2	1	3	3	1	5	1	3	1	14	8	8	8
3	<1	2	1	3	5	2	5	2	6	4	4	3
2	<1	<1	<1	<1	<1	<1	<1	<1	<1	<1	2	5
>7.0	>10.0	>7.0	>7.0	>10.0	>21.0	>6.0	>10.0	>10.0	>77.0	>84.0	>44.0	>45.0
35.0	137.0	44.0	39.0	31.0	234.0	55.0	95.0	20.0	100.0	33.0	99.0	110.0
<0.14	0.10	<0.14	<0.14	<0.10	0.57	<0.17	0.10	<0.10	0.42	0.36	0.30	0.36
0.57	<0.10	0.57	0.86	<0.10	0.29	0.50	0.30	0.30	0.25	0.14	0.34	0.33
9.71	1.30	78.14	43.00	40.90	3.81	7.00	5.80	14.80	1.45	1.24	0.73	2.62
—	—	—	—	—	1.23	—	7.37	—	1.46	0.98	2.83	2.30
0.75	0.84	0.99	1.04	0.83	1.62	0.72	0.86	0.75	1.25	2.76	3.98	1.20
808.0	>623.0	906.0	869.0	795.0	884.0	1353.0	780.0	1100.0	>390.0	988.0	>282.0	592.0
0.16	0.04	1.20	0.72	1.16	0.21	0.10	0.16	0.28	0.50	0.96	0.26	0.43
0.0	0.0	0.0	0.0	0.0	0.0	0.0	0.0	0.0	0.0	31.2	1.3	0.0
1.8	0.3	7.1	4.4	8.0	1.3	1.0	0.6	2.1	0.3	1.4	0.2	1.3
1.8	0.0	5.6	7.7	19.7	14.3	0.9	3.8	0.0	27.2	42.5	63.6	29.7
56.9	49.6	64.2	59.3	47.4	33.4	64.9	47.1	75.0	4.1	2.9	1.2	13.3
1.4	1.5	1.4	0.4	1.6	0.0	1.2	0.0	2.5	0.0	0.0	0.0	0.0
6.3	27.0	0.0	0.0	1.4	27.4	4.9	10.4	0.5	0.0	0.0	25.6	0.0
0.0	0.0	0.0	0.0	0.0	10.6	0.0	6.4	0.0	36.6	16.6	0.0	34.6
29.5	19.0	18.6	25.0	20.3	8.4	25.1	28.5	17.8	16.1	0.0	0.0	11.7
1.5	1.4	1.0	1.4	1.0	2.0	1.2	1.9	0.8	2.9	1.2	1.2	2.4
0.1	0.4	0.1	0.1	0.1	1.6	0.1	0.3	0.1	2.6	0.9	1.4	1.6
0.0	0.0	0.0	0.0	0.0	0.1	0.0	0.0	0.0	0.5	0.2	0.4	0.3

compatibility with the major mantle mineral phases. The enrichment of Cs, Rb, Ra, Th, U, and K relative to Hf, Zr, Ti, Y, and the heavy REE and the marked depletion in Ta and Nb for the calc-alkaline magma types clearly distinguish them from MORB-like lavas.

In Figure 13 the lavas from Sites 454, 456, and 457 have been plotted in the Th–Hf/3–Ta discrimination diagram (Wood et al., 1979b; Wood, 1980) with the fields of N-type MORB (A), E-type MORB (B), within plate lava series (C), and active plate margin lava series (D) distinguished. The field of active margin lava series (D) has been enlarged relative to that originally proposed (Wood et al., 1979b, fig. 4) to include additional analyses of arc tholeiites from Japan and DSDP Site 448 as well as the fore-arc lavas from DSDP Sites 458 through 461 (described later). All the basalts from Site 456 except Unit 456A-3 plot within the field of N-type MORB, and Unit 454A-3 plots between fields *A* and *D* (Fig. 13). Units 456A-3, 454A-1, 454A-2, and 457 plot in field *D* as expected.

Interestingly, the Site 454 lavas plot along a trend in Figure 13 between N-type MORB and calc-alkaline magma types. We interpret this as a mixing line. There seem to be two possible explanations for this mixing relationship: (1) the two magma types were comagmatic in the crust of the Mariana Trough, being derived from small, short-lived magma chambers, in which mixing between the magma types could occur in some instances. Mixing due to episodic injection of magma into a small, sub-crustal reservoir is a common process at the

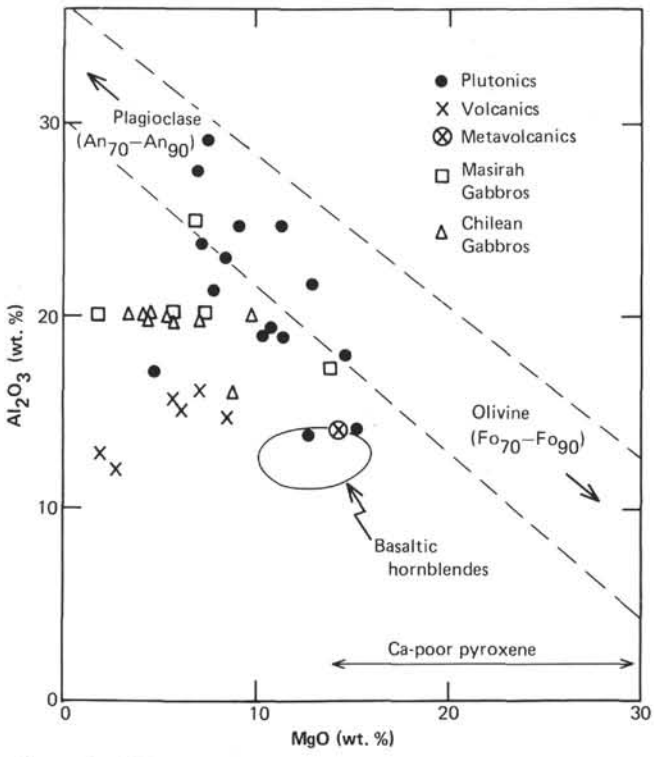

Figure 2. Al_2O_3 versus MgO for igneous rocks from Site 453, showing that most of the plutonic rocks contain cumulate plagioclase and a ferromagnesian mineral.

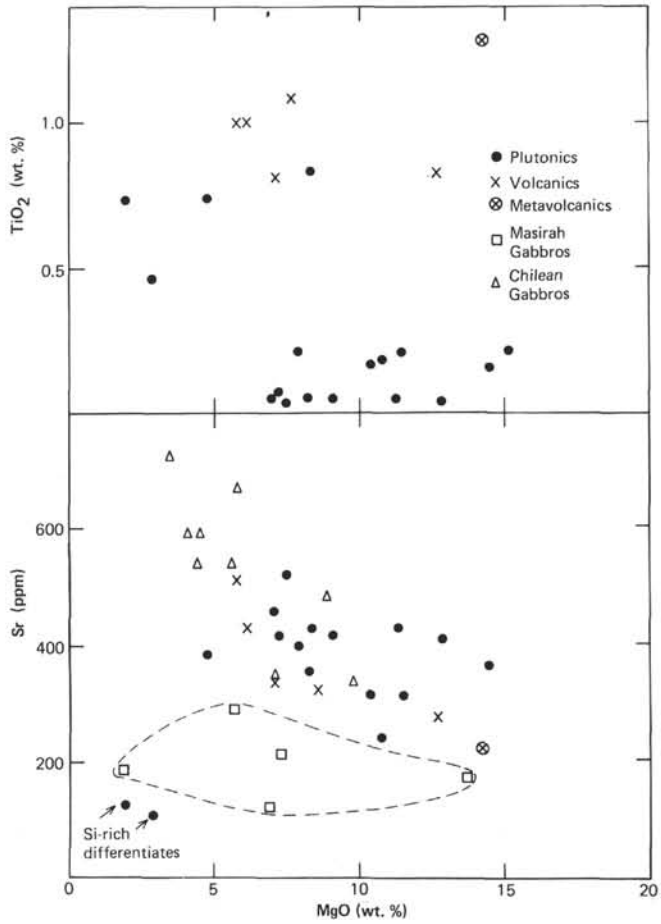

Figure 3. TiO_2 and Sr versus MgO for igneous rocks from Site 453. Gabbros from the Masirah Ophiolite, Oman (Abbotts, 1979), also plagioclase cumulates (cf. Table 2), considered to represent the cumulate layer of oceanic crust, have lower Sr than the Site 453 rocks.

Mid-Atlantic Ridge (Rhodes et al., 1979). Resorbed phenocrysts are present in the porphyritic Unit 456A-2 and could support a magma mixing hypothesis. The presently available data for petrography and mineralogy of the basalts from this site do not provide additional evidence of magma mixing (e.g., resorbed phenocrysts out of equilibrium with the bulk rock; differences in the composition of glass inclusions in the phenocrysts and bulk rock), but a more detailed study would clearly be worthwhile. (2) An N-type MORB magma type could have assimilated small but variable amounts of arc-derived sediments. Basalts from Sites 454 and 456 are associated with arc-derived vitric tuffs. One basalt at Site 456 actually contains a large recrystallized tuffaceous xenolith (see Site 456 summary, this volume). Low seismic velocities at Site 454 suggest that sediments may be interbedded with basalts for several hundred meters and some of the more massive basalts could be intrusive. This would provide a suitable environment for sediment assimilation. The fact that from the same cooling unit some samples have trace element characteristics of arc tholeiites, and other samples have trace element characteristics of N-type MORB, tends to support a heterogeneous assimilation process rather than a more homogeneous magma mixing process. Both processes could explain the lower $^{87}Sr/^{86}Sr$ and higher K/Ba ratios of these lavas (e.g., dredge samples of Hart et al., 1972) than most calc-alkaline basalts.

Magma mixing and/or sediment assimilation processes may be important in the initial stages of opening of an inter-arc basin and could explain the chemical variation in basalts dredged from several such basins, which seem to have compositions related to both N-type MORB and arc magma types, but cannot be classed as one or the other. For example, those from the Lau Basin (Gill, 1976, Hawkins, 1976), the East Scotia Sea (Saunders and Tarney, 1979; Hawkesworth et al., 1978), and the Mariana Trough (Hart et al., 1972; this study). Some basalts from those basins have affinities with arc magma types, sharing with them higher K, Rb, Ba, Th, Sr, and ^{87}Sr, and lower Ti, Zr, Hf, Ta, and Nb relative to N-type MORB. In contrast, basalts recovered from the broader, more developed marginal basins of the West Pacific—i.e., the Shikoku, West Philippine and Parece Vela Basins—show no clear chemical affinities with destructive margin magma types (Marsh et al., 1980; Mattey et al., 1980; Wood et al., 1980a, 1980b). Tarney et al. (1977) noted similar relationships in the marginal basins of the Scotia arc region. This may be due to the progressive decrease in arc magmatic activity or arc-derived volcaniclastic sediments in the basins as they become more developed. If so, it has important implications for the type of marginal basins sampled by ophiolites. For example, the Late Cretaceous Mediter-

Table 2. Major and trace element XRF analyses of basic plutonic rocks from different tectonic environments.

Sample	Gabbros from the Chilean Cordillera (Wells, 1978; Marsh, 1977)									Gabbros from the Masirah Ophiolite, Oman (Abbotts, 1979)				
Number	C378	C379	C387	C389	C397	C62	C184	C71	C117	X288	MA65	MA205	MA164	MA417
Major Element Oxides (wt.%)														
SiO_2	50.5	49.5	46.5	51.5	49.8	46.9	46.5	55.4	50.0	42.9	46.4	49.1	50.4	59.0
TiO_2	0.68	1.61	0.80	1.15	0.22	0.16	0.79	0.88	0.53	0.07	0.18	0.25	0.45	0.55
Al_2O_3	19.9	20.0	21.4	18.6	16.1	19.1	18.4	17.4	20.4	24.7	17.2	20.9	20.2	18.8
tFe_2O_3	9.01	9.57	8.89	9.82	8.10	6.44	10.2	7.52	3.30	1.08	4.87	4.29	4.05	2.87
MnO	0.14	0.18	0.11	0.14	0.13	0.13	0.17	0.13	0.11	0.02	n.d.	0.00	0.07	0.00
MgO	4.05	3.43	4.53	4.40	8.86	9.82	7.05	5.74	5.60	6.85	13.89	7.24	5.68	1.80
CaO	11.27	11.12	13.97	10.20	13.33	13.90	12.7	9.14	16.3	22.22	13.62	11.14	12.45	4.04
Na_2O	3.56	3.62	2.71	3.43	1.17	1.11	1.45	3.76	2.15	0.49	1.61	3.89	3.80	9.97
K_2O	0.50	0.23	0.09	0.41	0.12	0.09	0.45	0.15	0.08	0.03	0.09	0.28	0.08	0.05
P_2O_5	0.17	0.89	0.01	0.09	0.01	0.04	0.04	0.17	0.05	0.00	0.01	0.02	0.02	0.10
Total	99.77	100.13	98.99	99.79	97.83	97.70	97.84	100.29	98.50	98.27	97.48	96.77	97.20	97.18
Trace Elements (ppm)														
Ni	68	18	41	58	174	259	24	56	35	91	237	70	40	5
Cr	123	20	70	67	510	193	49	47	92	265	705	355	51	<1
Zn	60	108	59	65	63	56	55	22	23	15	24	9	20	4
Ga	22	25	20	21	17	15	21	23	21	8	14	15	20	24
Rb	1	<1	<1	5	<1	1	21	4	1	<1	<1	2	<1	<1
Sr	591	722	590	541	482	333	343	671	540	116	175	213	294	183
Y	11	21	<1	10	3	5	8	20	14	<1	3	3	4	57
Zr	76	77	35	80	30	34	37	190	54	8	8	19	28	711
Nb	<1	4	3	4	<1	2	4	6	1	<1	<1	4	5	52
Ba	179	152	59	141	33	43	59	175	53	7	16	41	33	87
La	10	19	3	7	7	3	5	12	3	2	<1	<1	2	44
Ce	<1	30	4	6	<1	11	11	26	14	3	<1	<1	4	88
Pb	8	6	<1	4	<1	12	6	<1	5	<1	<1	<1	<1	<1
Th	<1	3	<1	<1	<1	<1	<1	8	<1	n.d.	<1	<1	<1	17

Notes: C378, C379, C387, C397 = plagioclase-clinopyroxene leucogabbros from Puerto Aisen, Southern Chile. C389 = plagioclase-clinopyroxene leucogabbro with minor primary hornblende from Puerto Aisen. C62, C184, C71, C117 = plagioclase-clinopyroxene leucogabbros from Atacama Province, Northern Chile.
X288 = leuco-olivine gabbro (cumulus plagioclase ≫ olivine = diopside).
MA65 = clinopyroxene gabbro (plagioclase = diopside).
MA205 = clinopyroxene gabbro (screen to sheeted dykes).
MA164 = pegmatitic clinopyroxene gabbro.
MA417 = plagiogranite.

ranean ophiolites, which contain both MORB and arc-type lavas in their crustal sequences (Pearce, in press), may represent crust formed in narrow, poorly developed inter-arc basins, such as the Mariana Trough or Lau Basin, rather than broad, well-developed back-arc basins.

For comparison, Tables 6 and 7 present the major and trace element compositions of calc-alkaline basalts and andesites dredged by P. Fryer and D. Hussong from a seamount in the northern part of the active Mariana Arc (21°58′N, 143°28′E) following seismic activity suggesting a recent eruption in the area. These lavas are compositionally similar to the sub-aerially erupted lavas from the Mariana Islands (Dixon and Batiza, 1979; Stern, 1979; Chow et al., 1980) and the basalts from DSDP Sites 451, 453, and 457. They have been plotted in the Th–Hf/3–Ta discrimination diagram (Fig. 13) and plot close to the other calc-alkaline lavas. However, they are significantly more evolved (i.e., low MgO: 2 to 4 wt.%) than the drilled samples. This is consistent with the extensive near-surface crystal fractionation thought to prevail along the Mariana Arc (Stern, 1979).

Mariana Fore-arc and Trench

Site 458
(17°51.85′N, 146°56.06′E)

This site was located on the southeast flank of a 40 mgal. positive gravity anomaly, 120 km east of the active Mariana arc, on the fore-arc midway between the arc and the trench in a water depth of 3447 meters. The sediments overlying the basement were approximately 35 m.y. old. Hole 458 penetrated 209 meters of basement rocks including glassy pillow lavas and massive flows (Fig. 14). The shipboard party divided the basement section into five lithological units. Units 1, 2, and 3 are petrographically similar but distinguished by their form: massive, coarse-grained lavas of Unit 2 separate the vesicular, glassy, fine-grained pillows of Units 1 and 3. These three units make up 123.5 meters of the cored interval. They are petrographically unusual in having endiopside and bronzite phenocrysts (with no olivine), and significant quantities of plagioclase are only present in the more holocrystalline samples. The shipboard party noted that the two pyroxene, glassy samples with no plagioclase resembled the boninites or Mg-rich andesites previously reported from elsewhere on Western Pacific fore-arcs, for example, the Bonin Islands (Kuroda and Shiraki, 1975; Kuroda et al., 1978; Shiraki et al., 1979), the Mariana Trench (Dietrich et al., 1978; Cameron et al., 1979), and Cape Vogel in southeast Papua New Guinea (Dallwitz, et al., 1966; Dallwitz, 1968).

Unit 4 consists of about 75 meters of vesicular, glassy to fine-grained, sparsely plagioclase and augite phyric pillow and massive lavas, relatively rich in Fe–Ti oxides. The top 10 or so meters of this unit (Sections 41-1 and 41-2) are highly fractured and, although not distinguished petrographically, have a distinct chemistry from the rest of the unit (see below). We refer to this part as

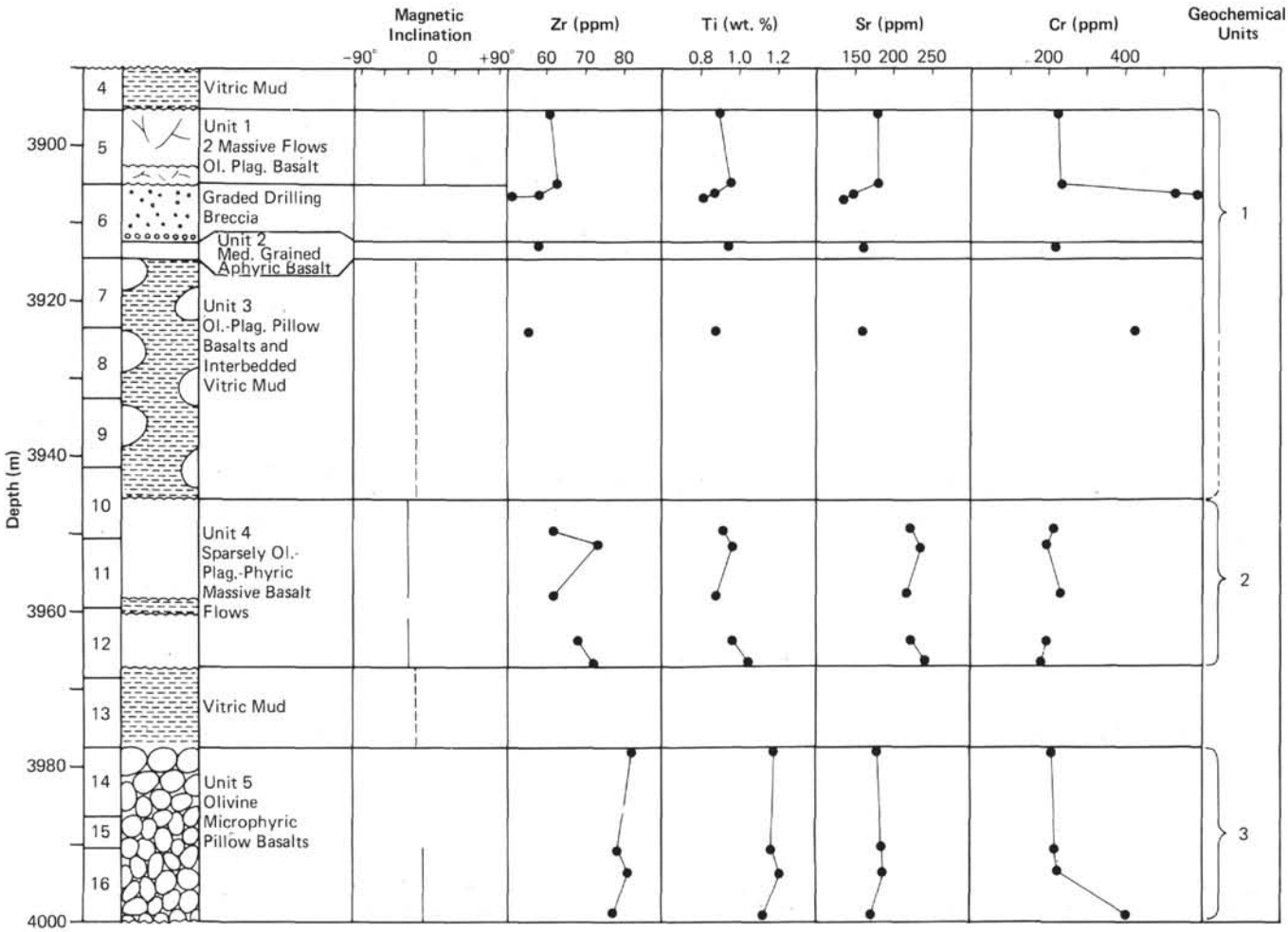

Figure 4. Geochemical and lithological stratigraphy of the basement sections of Hole 454A.

Unit 4a. Another highly fractured zone (~0.5 m) forms the lower part of Section 44-1 in Unit 4 and may be compositionally similar to Unit 4a but has not been sampled in this study. Unit 5 forms the lower 30 meters of the hole and consists of massive, fine-grained sparsely plagioclase and augite phyric lavas relatively rich in Fe-Ti oxides. All the units have suffered low-temperature (zeolite facies) alteration. Most of the glassy matrices are recrystallized to clays, although a few fresh glassy pillow rinds are preserved.

The lavas from Units 1, 2, and 3 show coherent chemical compositions (Table 8 and Fig. 14) with high SiO_2 (52 to 60 wt.%), moderate to high MgO (5 to 10 wt.%), high K_2O (0.5 to 1.5 wt.%), and very low TiO_2 (about 0.3 wt.%), P_2O_5 (about 0.03 wt.%), Zr, Hf, REE, and Y contents. Although they are chemically related to boninites, these Site 458 rocks are more evolved: previously described boninites (e.g., Table 9) generally have MgO contents >9 percent, Mg-numbers >0.7, Ca <8 percent, Al_2O_3 <14 percent, Ni >100 ppm, and Cr >600 ppm. Most of the Site 458 Units 1, 2, and 3 lavas have MgO <9 percent, Mg-numbers <0.7, CaO >8 percent, Al_2O_3 >14 percent, Ni <100 ppm, and Cr <300 ppm, and are probably best termed Mg-rich andesites. Unit 458-4 lavas are similar to those of the upper three units but with slightly higher abundances of Fe and the HYG elements and lower Mg-numbers and Cr and Ni contents. They are best termed andesites, but the relatively low abundances of the HYG elements in these lavas indicate that they are related to the Mg-rich andesites and boninites described earlier.

Units 458-4a and 458-5 are chemically different from the other Site 458 lavas and have the major element compositions of basaltic andesites. Both units have higher TiO_2 (about 1.1 wt.%) and HYG elements contents with low CaO (<7.5 wt.%) contents. Unit 458-4a has low MgO (<4 wt.%) and Unit 458-5 has very high Fe contents (ΣFe_2O_3 about 13.75 wt.%) and could be termed a ferrobasalt. Units 458-4a and 458-5 both have compositions similar to those of primitive island-arc tholeiites.

Site 459
(17°51.75′N, 147°18.09′E)

This site was located on the easternmost fore-arc basin, adjacent to the trench slope break in a water depth of 4120 meters. The basement was dated as prelate Eocene (74.5 m.y.) by the overlying sediments. Hole 459B penetrated 132.5 meters of basaltic basement divided into four lithologic units. The basalts are gener-

Table 3. Major and trace element analyses of igneous rocks from Hole 454A.

Sample (interval in cm)	5-1, 2-4	5-3, 106-108	5-4, 15-17	5-4, 16-18	6-2, 102-104	8-1, 2-4	10-1, 81-83	11-1, 40-42	11-4, 71-73	12-1, 100-102	12-2, 26-28	14-1, 2-4	15-1, 13-15	16-1, 32-35	16-1, 111-113
SiO_2	49.3	49.9	49.3	49.3	50.3	49.3	50.9	51.5	52.2	51.8	51.6	51.5	50.8	52.0	50.2
TiO_2	0.89	0.95	0.86	0.82	0.94	0.88	0.91	0.96	0.88	0.96	1.04	1.17	1.16	1.20	1.12
Al_2O_3	14.7	14.9	14.4	14.1	14.9	14.2	14.8	15.2	14.9	13.9	15.2	15.7	15.6	16.0	14.5
tFe_2O_3	8.50	8.58	9.42	9.37	8.99	9.41	8.34	8.52	8.69	8.83	9.08	9.44	9.45	9.23	9.92
MnO	0.17	0.10	0.12	0.12	0.11	0.14	0.12	0.12	0.12	0.11	0.13	0.14	0.14	0.14	0.16
MgO	8.85	10.54	13.30	14.17	10.87	10.17	9.96	8.90	12.20	9.89	8.53	6.55	7.49	6.64	8.73
CaO	14.22	11.97	10.97	11.05	11.74	11.80	11.37	11.41	10.70	11.24	11.53	10.75	11.04	11.08	10.42
Na_2O	2.73	3.13	2.36	2.30	2.93	2.66	3.21	3.36	2.52	2.78	3.32	2.68	2.69	2.89	2.64
K_2O	0.33	0.17	0.18	0.14	0.13	0.20	0.22	0.23	0.29	0.17	0.34	0.79	0.62	0.64	0.44
P_2O_5	0.11	0.10	0.09	0.08	0.10	0.07	0.09	0.11	0.11	0.10	0.13	0.10	0.09	0.11	0.09
Total	99.80	100.32	100.97	101.42	101.10	98.83	99.90	100.27	102.59	99.75	100.81	98.80	99.03	99.95	98.26
Ni	117	114	382	426	108	253	151	123	174	116	114	128	133	134	269
Cr	223	228	532	594	218	424	211	196	232	192	178	203	212	222	390
Zn	53	48	52	53	50	54	57	62	55	56	61	63	62	63	66
Ga	19	20	16	15	18	18	15	20	16	19	25	22	24	22	17
Rb	4	1	2	1	1	<1	<1	2	<1	<1	<1	8	5	3	3
Sr	176	178	143	137	161	160	221	234	214	221	239	179	183	185	170
Y	21	23	18	18	22	22	23	19	19	23	25	27	26	23	23
Zr	61	63	58	51	58	55	62	73	62	68	72	82	78	81	77
Nb	<1	1	<1	1	1	1	<1	<1	<1	<1	1	2	2	1	2
Ba	25	41	49	43	42	10	34	191	64	52	134	82	70	94	105
La	9	6	10	9	10	10	9	8	7	5	7	9	16	15	15
Ce	9	12	4	9	10	7	10	7	10	14	8	12	11	9	13
Nd	7	8	5	7	9	6	7	8	8	9	7	11	8	6	9
Pb	5	1	6	6	5	<1	7	9	<1	<1	4	<1	<1	—	—
Th	6	1	1	2	4	<1	<1	<1	<1	<1	<1	<1	<1	<1	2
Zr/Nb	>61.0	63.0	>58.0	51.0	58.0	55.0	>62.0	>73.0	>62.0	>68.0	72.0	41.0	39.0	81.0	39.0
Ti/Zr	87.0	90.0	89.0	97.0	97.0	96.0	88.0	79.0	85.0	85.0	87.0	86.0	89.0	89.0	87.0
Y/Zr	0.34	0.37	0.31	0.35	0.38	0.40	0.37	0.26	0.31	0.34	0.35	0.33	0.33	0.28	0.30
Ce/Zr	0.15	0.19	0.07	0.18	0.17	0.13	0.16	0.10	0.16	0.21	0.11	0.15	0.14	0.11	0.17
Ba/Zr	0.41	0.65	0.84	0.84	0.72	0.18	0.55	2.62	1.03	0.76	1.86	1.00	0.90	1.16	1.36
$(Ce/Y)_N$	1.05	1.28	0.55	1.23	1.12	0.78	1.07	0.90	1.29	1.50	0.79	1.09	1.04	0.96	1.39
Fe/Mg	1.11	0.94	0.82	0.77	0.96	1.07	0.97	1.11	0.83	1.04	1.23	1.67	1.46	1.61	1.32
K/Rb	689.0	1411.0	730.0	1179.0	1087.0	>1652.0	>1835.0	959.0	>2382.0	>1436.0	>2806.0	816.0	1026.0	1760.0	1229.0
Ba/Sr	0.14	0.23	0.34	0.31	0.26	0.06	0.15	0.82	0.30	0.24	0.56	0.46	0.38	0.51	0.62
Q	0.0	0.0	0.0	0.0	0.0	0.0	0.0	0.0	0.0	0.0	0.0	0.6	0.0	0.1	0.0
Or	2.0	1.0	1.0	0.8	0.8	1.2	1.3	1.4	1.7	1.0	2.0	4.7	3.7	3.8	2.7
Ab	17.9	24.3	19.8	19.2	24.5	22.8	27.2	28.4	20.8	23.6	27.9	23.0	23.0	24.5	22.7
An	27.0	25.9	27.8	27.3	26.9	26.6	25.2	25.6	27.8	25.0	25.2	28.8	28.8	28.8	26.9
Ne	2.8	1.1	0.0	0.0	0.0	0.0	0.0	0.0	0.0	0.0	0.0	0.0	0.0	0.0	0.0
Di	34.8	26.2	20.5	21.1	24.2	26.1	24.7	24.4	18.7	24.4	24.9	20.1	21.1	20.9	20.5
Hy	0.0	0.0	6.6	5.5	2.2	4.3	3.2	4.2	16.9	16.6	4.0	17.9	14.9	17.1	16.8
Ol	11.3	17.1	20.0	22.0	17.0	14.8	14.3	11.7	10.1	5.0	11.4	0.0	3.6	0.0	5.4
Mt	1.5	1.5	1.6	1.6	1.5	1.7	1.5	1.5	1.5	1.5	1.6	1.7	1.7	1.6	1.8
Il	1.7	1.8	1.6	1.5	1.8	1.7	1.7	1.8	1.6	1.8	2.0	2.2	2.2	2.3	2.2
Ap	0.3	0.2	0.2	0.2	0.2	0.2	0.2	0.3	0.2	0.2	0.3	0.2	0.2	0.3	0.2

ally sparsely clinopyroxene and plagioclase phyric with more than 10 percent vesicles (and in some cases more than 30%). The petrological and geochemical differences between the four units are subtle, and they have been distinguished by grain size, vesicularity, and magnetic intensity. The lavas contain up to about 3 percent Fe–Ti oxides and patches of quartz and alkali feldspar in the mesostasis. They are relatively rich in Fe with between 10 and 14 weight percent Fe_2O_3. Some of the fine-grained basalts contain spherulitic zones next to the vesicles with abundant needlelike opaque phases thought to be ilmenites.

The Site 459 basalts are quartz-normative and similar to primitive island arc tholeiites (Table 10 and Fig. 15) with low Ti and Zr, high K and a depletion of Ta relative to La and Th. The high vesicularity implies that the magmas from which the Site 459 basalts formed were rich in volatiles. Their low Sr (< 150 ppm) and Ba (generally < 50 ppm) contents and depletion of the light REE (chondrite-normalized La/Tb < 1) distinguish them from the calc-alkalic lavas from the Mariana Trough and Ridge.

Site 460
(17°40.14′N, 147°35.92′E)

This site is located 25 km from the center of the Mariana Trench in a sediment pond on the arc-side wall of the trench in a water depth of 6445 meters. Basement was not reached, but basaltic clasts were recovered from a conglomerate of early Miocene or late Oligocene age (25–27 m.y.). Three such basalt clasts have been studied. Samples 460-9,CC, 11–13 cm and 460-9,CC, 74–76 cm are sparsely plagioclase (about 2%), olivine (rare pseudomorphs), and clinopyroxene (trace) phyric basalts with abundant vesicles (about 20%). Sample 460A-11-1, 29–31 cm is an aphyric, coarse-grained basalt with abundant secondary amphibole replacing relict clinopyroxene. All three samples are primitive island arc tholeiites (Table 5) similar to those from Site 459 and Units 458-4a and 458-5 (Table 11).

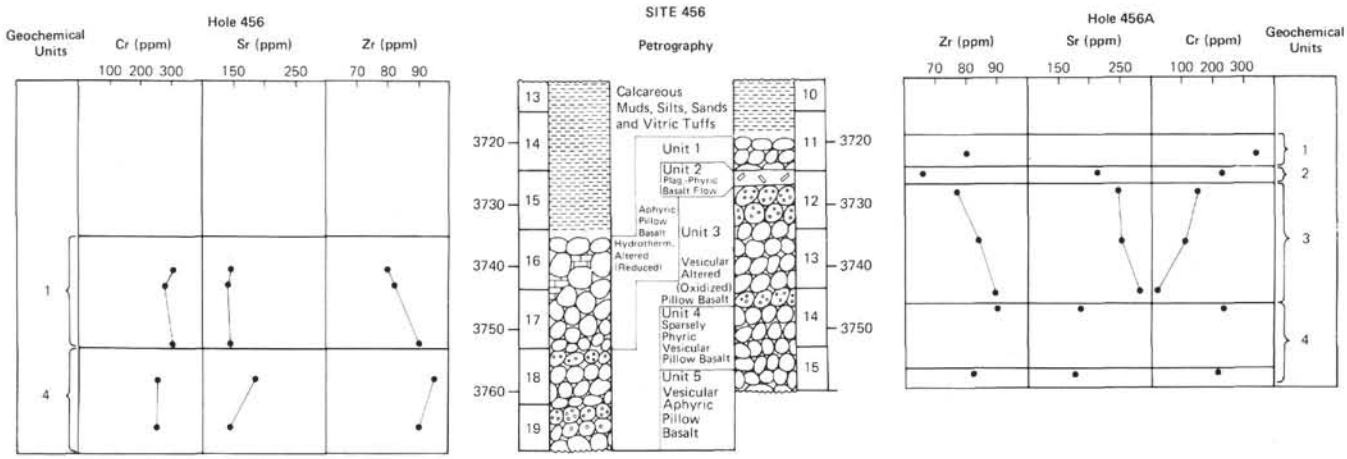

Figure 5. Geochemical and lithological stratigraphy of the basement sections of Holes 456 and 456A.

Site 461
(17°46.01′N, 147°41.26′E)

This site was located on a small patch of sediment on a local high in the arc-side wall of the Mariana Trench in a water depth of 7030 meters. Basement was not reached, but cobbles of igneous and metamorphic rocks were recovered in the few meters of sediment (about 20 m) of uncertain age. One metabasalt sample of unknown petrography has been sampled and has a composition (Table 5) similar to that of the primitive arc tholeiites of the other fore-arc and trench sites (Table 11).

DETAILED RELATIONSHIPS OF BASEMENT CHEMISTRY

The lavas from these Mariana fore-arc and Trench sites can be divided into two groups: (1) the Mg-rich andesites and andesites from Site 458 which are related to a boninite magma type. The Mg-rich andesites are probably derived from a boninite parental magma by crystal fractionation of the two pyroxene phases; (2) the primitive island arc tholeiites recovered from all four sites. Major and trace element variation diagrams for these rocks are presented in Figures 16 through 24. The Mg-rich andesites and andesites of Site 458 Units 1 through 3 follow a trend toward enrichment of Ca and Al with decreasing Mg (Fig. 15). This suggests that plagioclase has not fractionated from these magmas, at least from the more primitive ones. The Zr and Ti contents remain approximately constant with decreasing MgO in these units.

The andesites of Unit 458-4 have higher Fe, Ti and Zr, but lower Ca and Al contents than the andesites of Units 458-1 through 3 with similar MgO contents (Fig. 16). Most of the Unit 458-4 andesites also have lower K/Zr, Zr/Y, Sr/Zr ratios (Fig. 17) than the Units 458-1 through 3. These differences suggest that the Unit 458-4 andesites cannot be related to the Units 458-1 through 3 lavas by crystal fractionation processes. These HYG element ratios should remain approximately constant during crystal fractionation of two pyroxene assemblage. Units 458-1 through 4 have similar Ta/Tb, Th/Tb, and La/Tb ratios (Fig. 18) and have chondrite-normalized La/Tb and La/Eu ratios less than 1. Most of the previously described boninite-like lavas have been slightly enriched in the light REE relative to the heavy, REE—that is, chondrite-normalized La/Tb and La/Eu ratios greater than 1 (e.g., Sun and Nesbitt, 1978; Hickey and Frey, 1979). Also, Units 458-1 through 4 have low Ti/Zr (less than 75), Y/Ti, and Y/Zr (less than 0.35) ratios (Figs. 17 and 21). The low Ti/Zr ratios are characteristic of boninites from other localities (Sun and Nesbitt, 1978) and distinguish them from most other terrestrial magma types. Relative to estimated primordial mantle abundances for a chondritic earth model, Zr and Hf are enriched relative to Eu, Ti, Tb, and Y in these lavas (Fig. 23)—a point also noted by Bougault et al. (this volume). The significant fractionation of Ti, Zr, and Y relative to each other is difficult to achieve by mineral-melt processes unless garnet is involved (the heavy REE, Y, and Ti are partitional into garnet preferentially to Zr).

The primitive island arc tholeiite lavas from these sites have higher Fe, Ti, P, and HYG elements, but lower Ca and Al contents than the andesites of Site 458 with similar MgO contents (Fig. 16). Moreover, they have lower Sr/Zr, Zr/Y, Th/Tb, La/Eu, La/Tb, and Ta/Tb ratios (Figs. 17 and 18) and Ni and Cr abundances (Figs. 19 and 20). All these island arc tholeiites have Ti/Zr ratios close to 100 (Fig. 21)—except Unit 458-4a, which has low Mg and Fe and has probably resulted from crystal fractionation of an Fe-Ti oxide phase which would reduce the Ti/Zr ratios. Also they follow coherent trends on the trace element variation diagrams.

The lavas from the fore-arc and trench sites plot in a distinct and highly restricted field in the Th-Hf/3-Ta triangle (Fig. 22), close to the boundary between active margin and N-type MORB magma types. The andesites of Units 458-1 through 4 plot closer to the Th apex of the triangle than the arc tholeiites. All the lavas plot close to other primitive island arc tholeiites from the West Pacific active margins. However, these lavas are less depleted in Ta relative to the HYG elements than other active margin volcanics studied to date. This point

Table 4. Major and trace element analyses of igneous rocks from Site 456.

Sample (interval in cm)	Hole 456					Hole 456A							
	16-1, 145-147	16-2, 92-94	17-1, 95-97	18-1, 50-52	19-1, 18-20	10-1, 25-27	11-1, 76-78	12-1, 11-13	12-1, 41-43	13-1, 23-25	14-1, 12-14	14-1, 38-40	15-1, 27-29
SiO_2	49.3	46.2	49.3	50.2	48.2	45.7	48.2	48.0	49.7	50.7	52.5	48.4	49.5
TiO_2	1.25	1.26	1.33	1.20	1.14	0.62	1.38	0.77	1.15	1.18	1.30	1.18	1.12
Al_2O_3	14.5	12.3	13.3	14.5	15.5	8.1	14.0	18.6	15.5	16.6	16.2	15.0	15.5
tFe_2O_3	10.07	10.22	10.78	9.35	9.28	8.42	11.17	6.86	10.19	9.87	10.48	9.36	9.65
MnO	0.17	0.29	0.19	0.18	0.14	0.21	0.21	0.10	0.16	0.16	0.17	0.14	0.13
MgO	10.37	11.22	12.81	8.39	6.58	7.92	15.28	10.15	6.09	5.23	4.33	6.39	7.40
CaO	8.66	12.55	8.07	12.14	11.64	11.80	4.18	12.59	11.17	11.23	9.52	12.18	12.28
Na_2O	3.34	2.40	3.68	3.30	2.77	3.53	2.44	2.80	2.79	3.27	3.43	3.12	2.75
K_2O	0.09	0.06	0.10	0.31	0.54	0.75	0.06	0.13	0.58	0.62	0.98	0.47	0.40
P_2O_5	0.09	0.11	0.09	0.14	0.08	0.11	0.09	0.06	0.11	0.11	0.15	0.10	0.09
Total	97.92	96.56	99.66	99.63	95.94	87.21	96.99	100.09	97.46	98.92	99.10	96.38	98.84
Ni	90	74	90	99	85	26	85	109	68	51	23	71	88
Cr	305	276	297	254	253	14	338	226	152	106	18	234	214
Zn	118	93	86	64	61	80	198	34	68	77	79	63	68
Ga	21	18	18	22	19	15	15	20	24	16	22	14	14
Rb	<1	<1	<1	<1	1	11	<1	<1	4	8	12	6	4
Sr	146	141	146	184	176	138	100	212	246	251	280	185	173
Y	24	24	24	27	23	25	26	16	27	26	24	23	23
Zr	80	82	90	95	86	54	80	66	77	84	89	90	82
Nb	1	1	1	1	1	<1	<1	<1	1	2	2	1	1
Ba	109	67	87	22	21	136	54	117	75	81	87	43	43
La	6	7	6	8	7	7	17	11	11	10	12	15	13
Ce	11	12	9	7	9	10	5	7	14	17	21	12	8
Nd	10	9	8	6	8	8	7	6	11	12	14	9	7
Pb	—	—	—	<1	<1	7	5	<1	<1	3	<1	3	1
Th	—	—	—	<1	<1	<1	<1	<1	<1	<1	<1	<1	<1
Zr/Nb	80.0	82.0	90.0	95.0	86.0	>54.0	>80.0	>66.0	77.0	42.0	45.0	90.0	82.0
Ti/Zr	94.0	92.0	89.0	76.0	80.0	69.0	103.0	70.0	90.0	84.0	88.0	79.0	82.0
Y/Zr	0.30	0.29	0.27	0.28	0.27	0.46	0.33	0.24	0.35	0.31	0.27	0.26	0.28
Ce/Zr	0.14	0.15	0.10	0.07	0.10	0.19	0.06	0.11	0.18	0.20	0.24	0.13	0.10
Ba/Zr	1.36	0.82	0.97	0.23	0.23	2.52	0.68	1.77	0.97	0.96	0.98	0.48	0.52
$(Ce/Y)_N$	1.13	1.23	0.92	0.64	0.96	0.98	0.47	1.07	1.27	1.61	2.15	1.28	0.85
Fe/Mg	1.13	1.06	0.98	1.29	1.64	1.23	0.85	0.78	1.94	2.19	2.81	1.70	1.51
K/Rb	>747.0	>506.0	>789.0	>2532.0	>4474.0	563.0	>515.0	>1087.0	1195.0	647.0	681.0	647.0	836.0
Ba/Sr	0.75	0.48	0.60	0.12	0.12	0.99	0.54	0.55	0.30	0.32	0.31	0.23	0.25
Q	0.0	0.0	0.0	0.0	0.0	0.0	0.0	0.0	0.0	0.0	1.1	0.0	0.0
Or	0.5	0.4	0.6	1.8	3.3	5.1	0.4	0.8	3.5	3.7	5.9	2.9	2.4
Ab	28.9	17.5	31.2	26.3	24.4	21.2	21.3	18.5	24.2	28.0	29.3	25.3	23.5
An	24.9	23.3	19.5	23.9	29.6	4.7	20.8	37.8	28.9	29.0	26.2	26.6	29.2
Ne	0.0	1.9	0.0	0.9	0.0	7.1	0.0	2.8	0.0	0.0	0.0	1.1	0.0
Di	14.9	32.7	16.2	29.0	24.6	50.0	0.0	19.5	22.5	22.0	17.1	29.0	26.0
Hy	10.2	0.0	0.8	0.0	4.0	0.0	39.0	0.0	12.2	6.7	14.9	0.0	4.3
Ol	15.3	18.7	26.1	13.0	9.1	7.8	10.0	17.3	3.5	5.5	0.0	10.0	9.7
Mt	1.8	1.8	1.9	1.6	1.7	1.7	2.0	1.2	1.8	1.7	1.8	1.7	1.7
Il	2.4	2.5	2.5	2.3	2.3	1.3	2.7	1.5	2.2	2.3	2.5	2.3	2.2
Ap	0.2	0.3	0.2	0.3	0.2	0.3	0.2	0.2	0.3	0.3	0.3	0.2	0.2

is also apparent from Figure 20. Comparing this figure with Figure 10, it can be seen that the fore-arc tholeiites have a much smaller depletion in Ta relative to La and Ce, and the Mg-rich andesites from Unit 458-1 show no depletion in Ta relative to La. Figure 24 illustrates the large range of La/Ta ratios measured in the lavas recovered from the arcs and basins of the West Pacific Ocean; the Mariana fore-arc lavas and those from the Mariana Trough have La/Ta ratios less than 40 and, except for the Site 458 andesites, greater than 15; the lavas from Japan, the Mariana arc, the West Mariana Ridge and the Kyushu-Palau Ridge have La/Ta ratios greater than 40. These trace element variations suggest that several magma types, unrelated by crystal fractionation processes, have been erupted during the development of the island arcs and inter-arc basins of the west Pacific. The geochemical diversity of the lavas implies that the petrogenetic processes and mantle source compositions involved are complex.

DISCUSSION

The main aim of this chapter has been to provide a factual account of the geochemistry of Leg 60 igneous rocks. A detailed consideration of the petrogenetic implications of the data will be deferred to a subsequent paper. However, qualitative assessments can be made of some of the recently favored petrogenetic models for island arc and back-arc basin magmas, and constraints placed on them by the tectonic evolution of the Philippine Sea.

Most recent trace element and radiogenic isotope studies of continental margin, island arc, and marginal basin lavas have favored petrogenetic models invoking the involvement of fluids, probably of a supercritical

Table 5. Major and trace element analyses of igneous rocks from Holes 457, 460, and 461.

Sample (interval in cm)	Hole 457	Hole 460			Hole 461
	4,CC	9,CC, 74–76	9,CC, 11–13	11-1, 29–31	3-1, 60–62
SiO_2	53.4	52.5	53.6	55.5	58.7
TiO_2	0.89	0.87	1.34	0.61	1.01
Al_2O_3	15.6	15.2	16.6	13.3	13.2
tFe_2O_3	11.32	12.73	10.57	12.28	14.06
MnO	0.14	0.13	0.07	0.11	0.13
MgO	5.33	5.03	3.97	7.95	5.46
CaO	6.47	8.24	5.45	5.23	3.00
Na_2O	2.73	3.06	5.51	3.84	3.50
K_2O	1.13	0.91	1.68	0.57	0.22
P_2O_5	0.11	0.05	0.23	0.04	0.08
Total	97.09	98.75	99.00	99.40	99.43
Ni	17	22	2	16	27
Cr	29	51	5	10	15
Zn	80	98	91	59	60
Ga	16	18	25	16	17
Rb	18	8	22	4	4
Sr	305	122	154	104	113
Y	19	17	52	15	16
Zr	81	48	83	38	69
Nb	<1	<1	1	<1	<1
Ba	255	21	66	37	36
La	16	11	12	10	11
Ce	17	10	16	9	7
Nd	12	5	11	5	6
Pb	5	8	8	5	2
Th	<1	2	<1	1	4
Zr/Nb	>81.0	>48.0	83.0	>38.0	>69.0
Ti/Zr	66.0	108.0	96.0	97.0	88.0
Y/Zr	0.23	0.35	0.63	0.39	0.23
Ce/Zr	0.21	0.21	0.19	0.24	0.10
Ba/Zr	3.15	0.44	0.80	0.97	0.52
$(Ce/Y)_N$	2.20	1.44	0.76	1.47	1.07
Fe/Mg	2.46	2.93	3.09	1.79	2.99
K/Rb	521.0	940.0	634.0	1185.0	465.0
Ba/Sr	0.84	0.17	0.43	0.36	0.32
Q	6.4	2.3	0.0	2.6	15.2
Or	6.9	5.4	10.0	3.4	1.3
Ab	23.8	26.2	45.8	32.7	29.8
An	27.7	25.5	15.7	17.4	14.5
Ne	0.0	0.0	0.7	0.0	0.0
Di	4.0	13.1	8.5	6.9	0.0
Hy	26.3	22.4	0.0	32.5	31.4
Ol	0.0	0.0	13.4	0.0	0.0
Mt	2.0	2.2	1.9	2.1	2.5
Il	1.7	1.7	2.6	1.2	1.9
Ap	0.3	0.1	0.5	0.1	0.2

saline and siliceous nature, derived from the subducted oceanic lithosphere and infiltrating the mantle wedge above the Benioff zone from which the lavas are subsequently derived (Best, 1975; Hawkesworth et al., 1978; Saunders and Tarney, 1979; Saunders et al., 1980). This process would cause the mantle wedge above the subducted plate to become enriched in the mobile elements (Cs, K, Rb, Pb, Ba, Th, U, La, and Sr) which can be leached to varying degrees from altered oceanic crust after subduction. Because the altered oceanic crust is hydrated with sea water, hydrous fluids derived from it would be enriched in ^{87}Sr relative to radiogenic Nd (Nd content of sea water is very low). In addition, subducted sediments would also be expected to contribute certain mobile elements and radiogenic Pb to the fluids (Sun, 1980). Variations in the composition of the sediments and the proportions to which they contribute to fluids emanating from subducted oceanic crust might explain the geochemical diversity observed in arc magma types as a whole (e.g., the large range of HYG element ratios, such as Ba/La). However, we note that recent Pb, Sr, and Nd isotopic data for the Mariana arc (Meijer, 1976; DePaolo and Wasserburg, 1977; Dixon and Batiza, 1979; Stern, 1979) suggest that sediment contamination of the mantle source is minimal (<2%).

The introduction of a hydrous fluid into the mantle wedge would lower the solidus and induce partial melting under conditions of high P_{H_2O}. The HYG element variations measured in the active margin volcanics of the west Pacific are certainly consistent with this model. In order to be able to explain the extremely low Ta and Nb abundances in active margin volcanics in general (Wood et al., 1979b), it is necessary to invoke that these elements are held in a mineral phase in the mantle during the partial melting (Wood, 1979; Saunders et al., 1980). Ta and Nb are strongly partitioned into titanium mineral phases—for example, rutile and sphene. Recent experimental studies have shown that the stabilities of rutile and sphene are enhanced under hydrous conditions and may be refractory phases with even high degrees of melting of mafic material (Hellman and Green, 1979).

The major and trace element compositions of the Mg-rich andesites from Site 458 and boninite lavas can, in general terms, be reconciled with this model. Their major element compositions are similar to liquids produced experimentally by high degrees of partial melting of a hydrous peridotite at low pressures, ~10 kbars (Green, 1976). They have generally been interpreted as near-primary magmas derived by greater than 20 percent partial melting of a hydrous mantle source at depths less than 30 km (Sun and Nesbitt, 1978). The low absolute abundances of the immobile HYG elements in these lavas support a model invoking high degrees of partial melting. The absence of a negative Ta anomaly in the Site 458 andesites could reflect the total consumption of mantle titanium phases during high degrees of partial melting.

The Mg-rich andesites do show compositional relationships with other arc magma types for example, enrichment in volatile and mobile elements—yet there are some significant differences which suggest that they are not derived from the same mantle sources. For example, the high Zr/Ti and Ti/Y ratios of the Mg-rich andesites are similar to those observed in calc-alkaline magmas and probably indicate the involvement of garnet in their genesis; yet they are depleted in the light REE, whereas the calc-alkaline magmas are enriched. However, we note that previously described boninites are light-REE-enriched, and the Site 458 Mg-rich andesites are less depleted in the light REE than the island arc tholeiites with which they are associated. The Mg-rich andesites of Site 458 differ from primitive island arc tholeiites in being less depleted in the light REE and in having high Zr/Ti and Ti/Y ratios. Overall the Mg-rich andesites

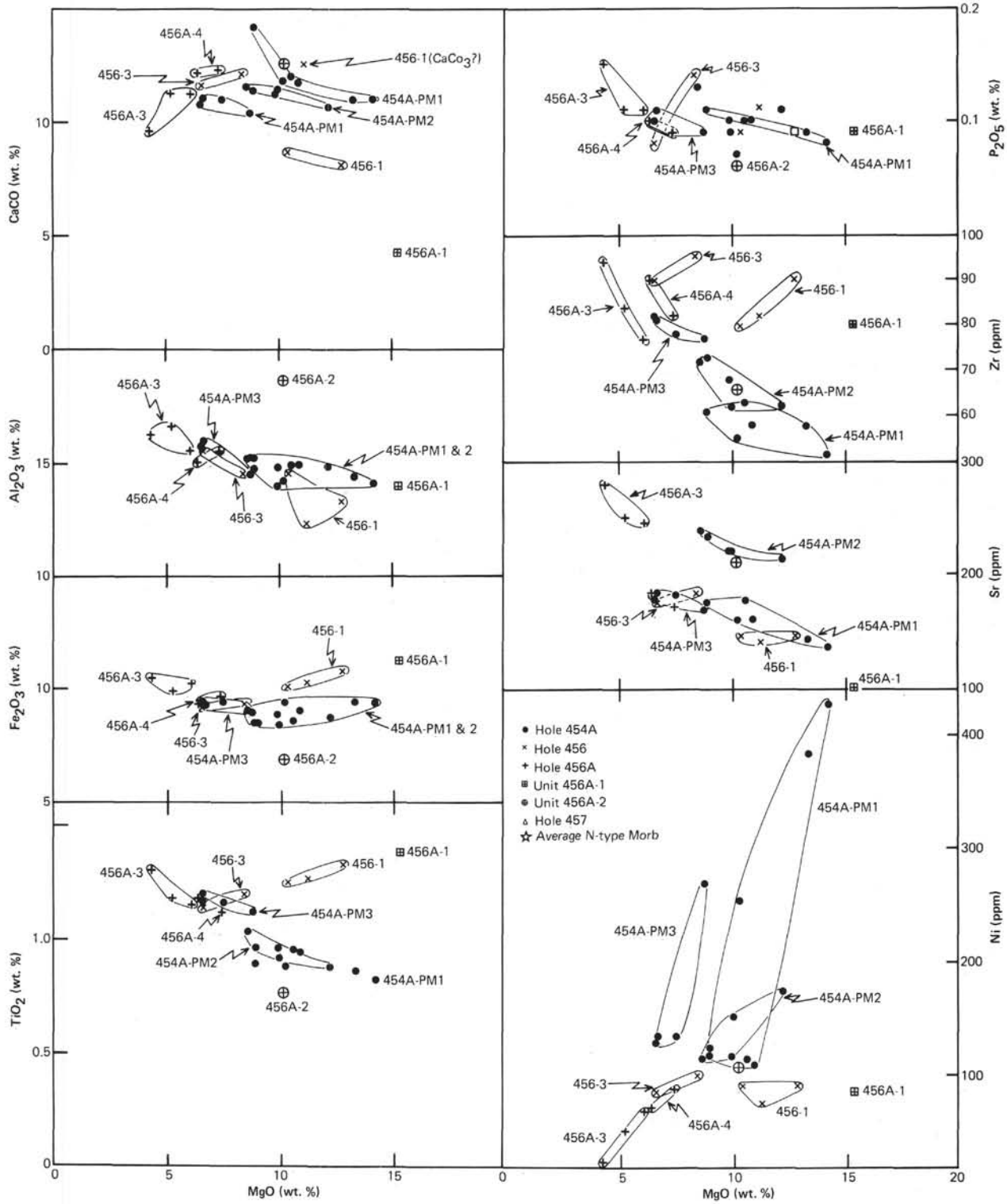

Figure 6. MgO variation diagram of selected major and trace elements for samples from Sites 454 and 456.

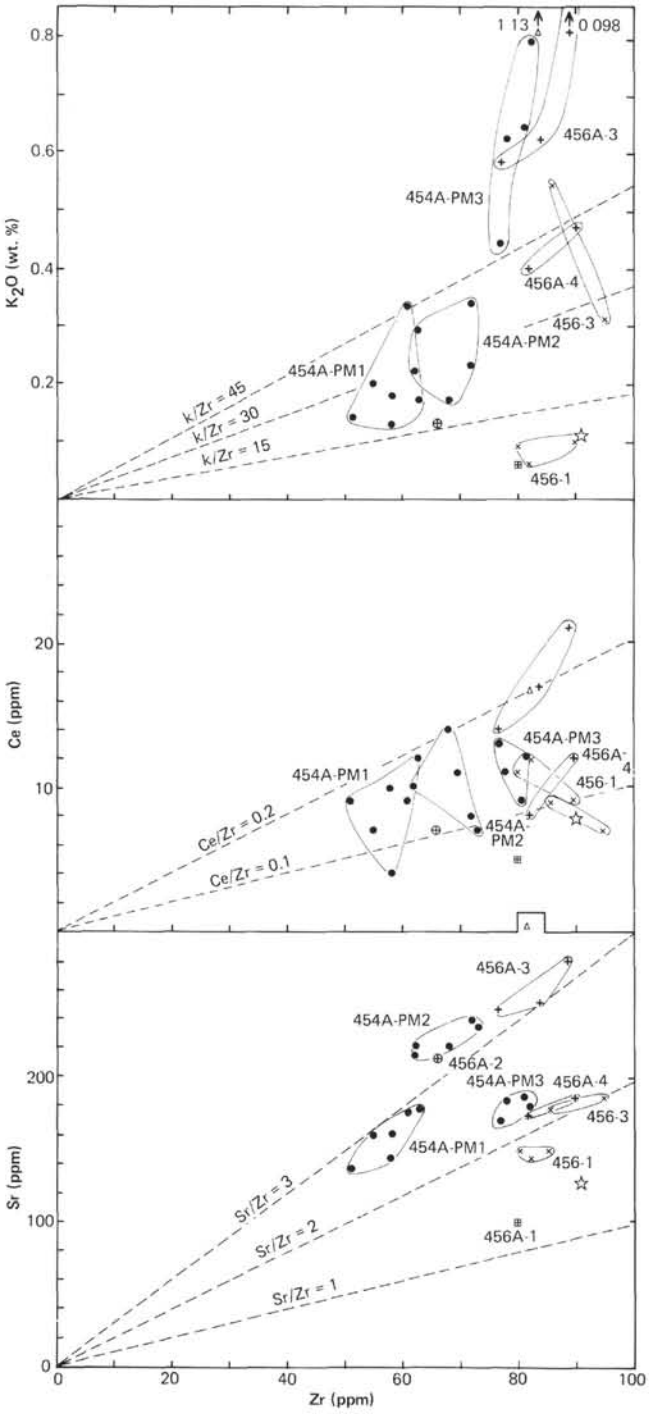

Figure 7. K_2O, Ce, and Sr versus Zr for samples from Sites 454, 456, and 457. Average N-type MORB from Wood (1979). (See Fig. 6 for legend.)

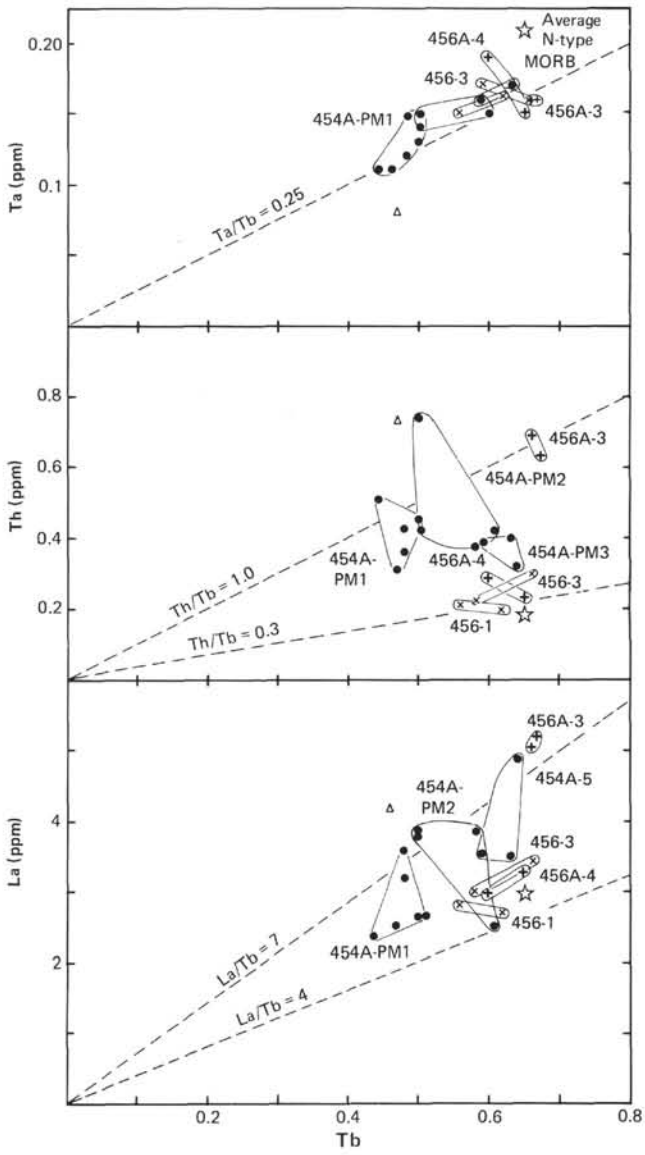

Figure 8. Ta, Th, and La versus Tb for samples from Sites 454, 456, and 457. (See Fig. 6 for legend.)

have more compositional similarities with calc-alkaline magma types than primitive island arc tholeiites. There are two important features of Mg-rich andesites and boninites which need to be considered when developing petrogenetic models for them: (1) They appear to be limited to the fore-arc of the West Pacific active margin and associated with the early development of an island arc system. (2) Their chemical compositions apparently result from high degrees of partial melting in the mantle source under hydrous conditions, which suggests certain thermal energy requirements.

The source of the Mg-rich andesites could be in the mantle wedge where the addition of excess slab-derived hydrous fluids temporarily suppresses its solidus below the geotherm and initiated extensive partial melting. As the descending slab tends to cool the mantle wedge as subduction continues, the solidus of the mantle wedge would cease to be significantly depressed below the geotherm. The Site 458 Mg-rich andesites overlie island-arc tholeiitic lavas which are more depleted in the light REE. The arc tholeiites could be generated during the initial stages of hydrous metasomatism of the previously depleted mantle wedge by small degrees of partial melting. More extensive metasomatism would enrich the source in a number of HYG elements as well as depressing its solidus and increasing the degree of partial melting so as to produce boninite-like magmas. As

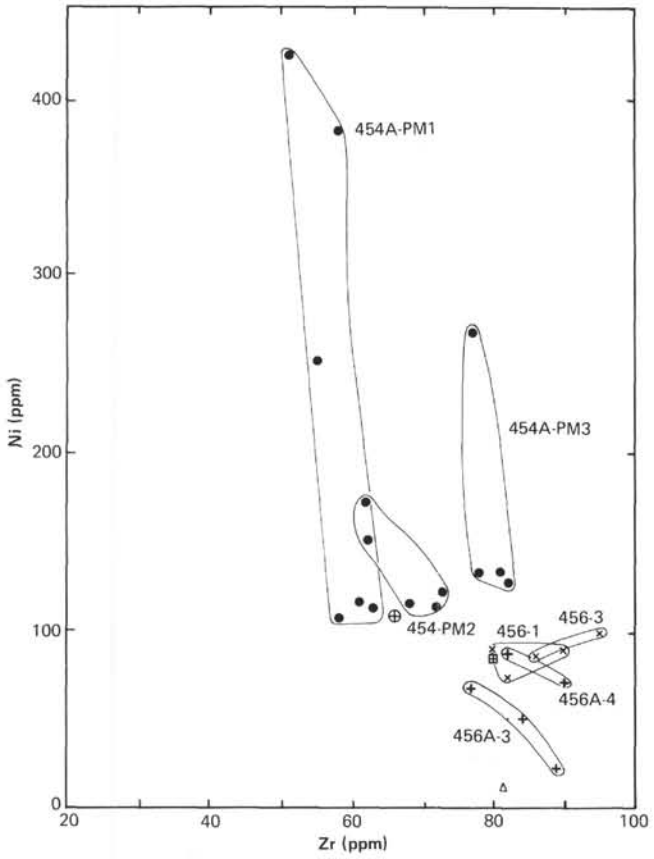

Figure 9. Ni versus Zr for samples from Sites 454, 456, and 457. (See Fig. 6 for legend.)

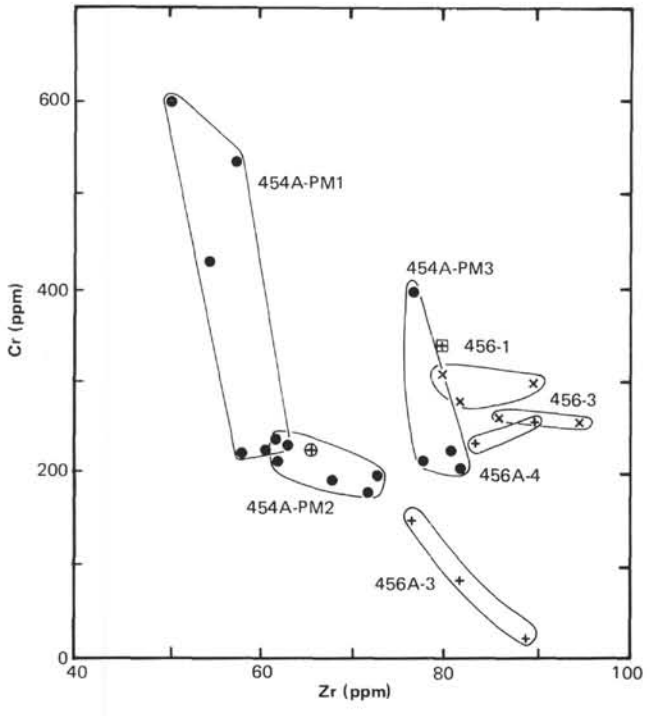

Figure 10. Cr versus Zr for samples from Sites 454, 456, and 457. (See Fig. 6 for legend.)

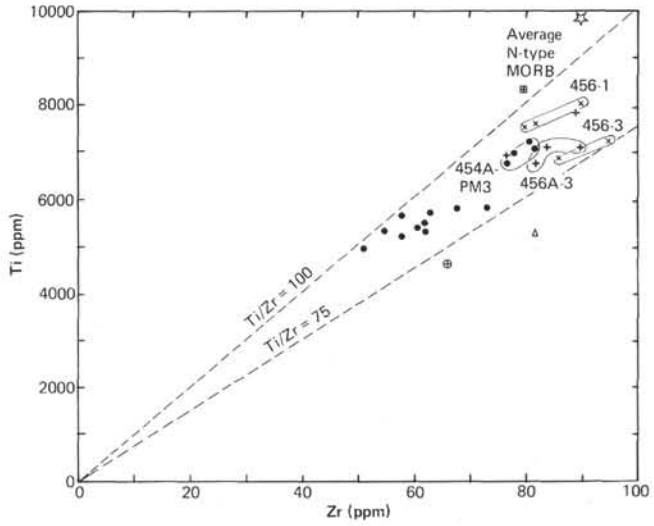

Figure 11. Ti versus Zr for samples from Sites 454, 456, and 457. (See Fig. 6 for legend.)

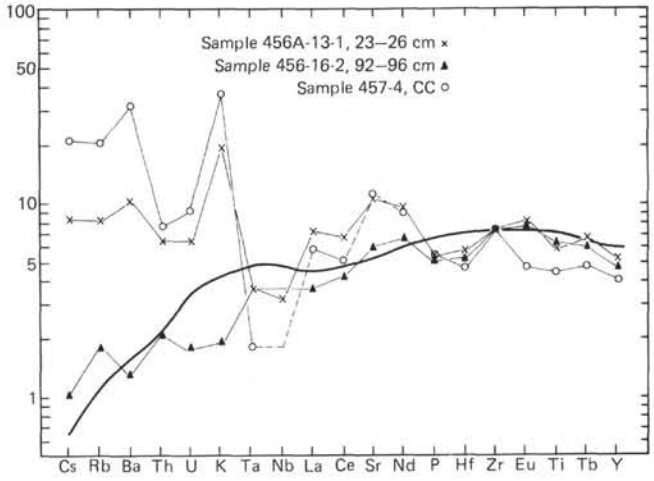

Figure 12. HYG element abundances of selected samples from Sites 456 and 457 normalized to estimated primordial mantle abundances (from Wood, 1979, except that a Ti value of 1500 ppm is used here). Continuous line is average N-type MORB.

metasomatism continued to cool and enrich the mantle wedge, the degree of partial melting would decrease and the magmas would develop a more calc-alkaline composition.

Alternatively, the difference between calc-alkaline and primitive island arc tholeiites could result from the mantle sources of the latter being metasomatized by hydrous fluids driven off the subducted slab at low pressures (perhaps during the prograde metamorphic reaction of greenschist to amphibolite), and the former from material infiltrated (veined) by hydrous melts (or fluids) derived from the slab at higher pressures (perhaps during the prograde metamorphic reaction amphibolite to eclogite). Ringwood (1974) proposed the involvement of a liquid component derived by partial

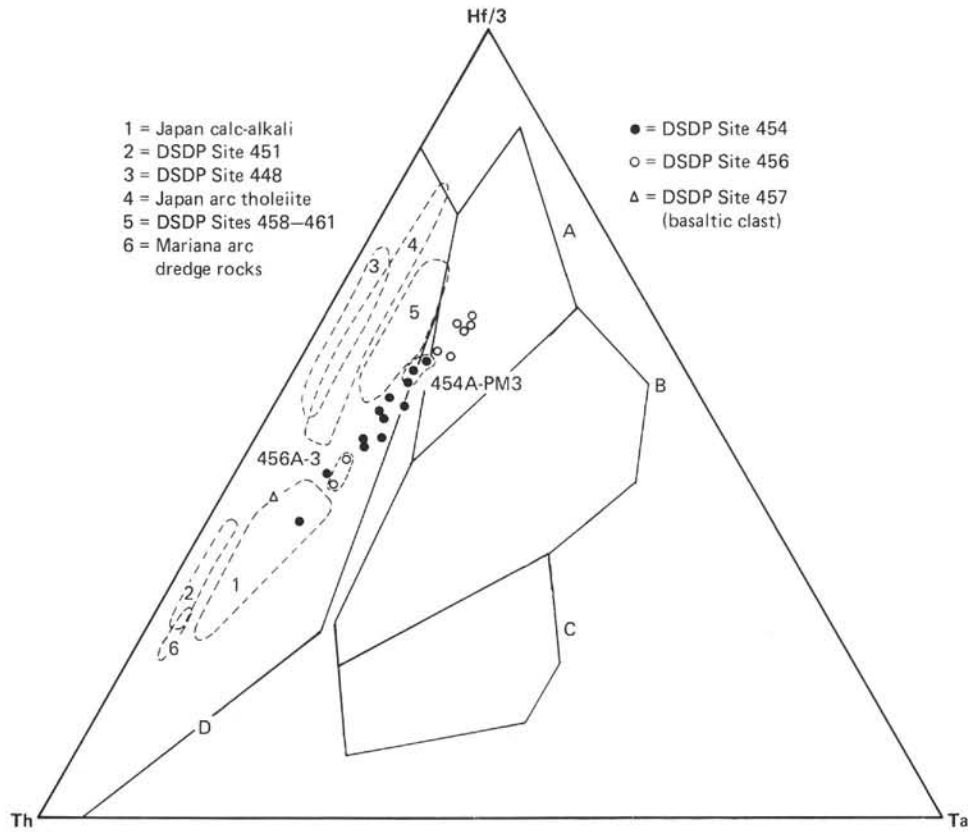

Figure 13. Th–Hf/3–Ta discrimination diagram (Wood et al., 1979b; Wood, 1980) for samples from Sites 454, 456, and 457. Areas: A = N-type MORB; B = E-type MORB; C = within plate lavas; D = active plate margin lavas. The fields of Japanese lava series and DSDP Leg 59 samples are from Wood et al., 1980a, 1980b.

melting of quartz eclogite in the genesis of calc-alkaline magmas. The partial dehydration of the slab at low pressures would leach much of the radiogenic Sr added to the ocean crust during alteration, so that the residue involved in the amphibolite to eclogite transformation could be isotopically similar to MORB. This might explain the low $^{87}Sr/^{86}Sr$ (~0.7032–0.7034) of the Mariana arc calc-alkaline lavas (Dixon and Batiza, 1979).

The most recent models for the tectonic evolution of the Mariana type plate boundary require that the position of the trench remains approximately fixed relative to the mantle. Poehls (1978) proposed that the Mariana Trough and other back-arc basins are caused by interaction between the subducted plate and the plate behind the trench in places where trenches are terminated or offset due to variations in subduction rates along the plate margin. He envisaged the slowing of the subduction rate where aseismic ridges (in this case the Caroline Ridge) collide with island arcs (Vogt et al., 1976). In this model the strike-slip motions occurring in the southern Marianas have induced the opening of the Mariana Trough, but the Mariana Trench has remained fixed. In their recent model, Uyeda and Kanamori (1979) propose that it is the westward motion of the Eurasian plate in the Philippine Sea area that has caused back arc extension in the area. In this model the downgoing slab is anchored to the mantle, and therefore the position of the trench remains fixed relative to the mantle.

Mattey et al. (1980) have pointed out that if the trench remains fixed relative to the mantle, the same mantle wedge would remain coupled to the Benioff zone and be repeatedly infiltrated with fluids or melts derived from the subducted plate. Moreover, these models imply that the Kyushu-Palau Ridge and West Mariana Ridge would have formed in the same position relative to the trench and Benioff zone as the active Mariana arc. The Parece Vela Basin (Fig. 1) was the first back-arc basin to open as a response to westerly movement of the West Philippine Basin or a strike-slip movement in the regions of the Palau and Yap Trenches. The arc magmatism became more calc-alkaline, forming the West Mariana Ridge followed by back-arc extension in the Mariana Trough.

Considered in these terms the observed temporal variations in the geochemistry of the lavas erupted in the Mariana system may be able to constrain some of the petrogenetic models: the lavas from the Mariana forearc and Kyushu-Palau Ridge are primitive arc tholeiites (although we note that there are some systematic differences in the trace element ratios of lavas from the two regions, e.g., La/Ta, Fig. 24); lavas from the younger West Mariana Ridge and active Mariana arc are calc-alkaline, as are some of the lavas in the Mariana Trough. Thus, there is a trend from early primitive island-arc tholeiites to subsequent calc-alkaline lavas erupted in the Mariana system. These variations suggest

Table 6. Major and trace element analyses of Recent basalts and andesites dredged from a seamount (latitude 21°57′N, longitude 143°27′E) in the northern Mariana arc.

	Andesites												
	MV 1801	MV 1802	MV 1803	MV 1804	MV 15101	MV 15117	MV 15146	MV 15188	MV 15197	MV 15220	MV 15214	MV 15268	MV 15295
SiO_2	53.1	51.5	52.8	54.2	55.3	60.6	56.7	52.7	56.9	55.3	55.5	53.0	55.4
TiO_2	0.82	0.74	0.80	0.82	1.13	1.11	1.28	0.79	1.13	1.14	0.92	0.88	0.88
Al_2O_3	19.1	18.3	18.6	19.7	15.0	14.0	13.8	18.7	15.1	14.8	16.6	18.6	16.9
tFe_2O_3	8.51	8.48	8.76	8.69	10.91	9.91	11.43	9.38	10.12	11.04	9.13	9.82	9.90
MnO	0.13	0.13	0.14	0.13	0.18	0.19	0.18	0.15	0.16	0.18	0.15	0.15	0.17
MgO	2.75	4.03	2.91	2.61	2.89	1.98	2.86	3.58	2.61	3.17	2.36	3.21	3.92
CaO	10.49	10.71	10.48	10.39	7.89	5.32	6.99	10.82	7.26	8.02	7.93	10.56	9.58
Na_2O	2.57	2.34	2.52	2.67	2.73	3.64	3.08	2.51	2.92	2.64	2.71	2.56	2.50
K_2O	0.92	1.20	0.58	1.13	1.21	1.47	1.29	0.89	1.41	1.20	1.22	1.02	1.01
P_2O_5	0.12	0.15	0.11	0.18	0.15	0.24	0.15	0.11	0.18	0.14	0.13	0.14	0.12
Total	98.51	97.49	97.66	100.51	97.39	98.47	97.81	99.61	97.73	97.56	96.73	99.99	100.37
Ni	4	36	4	6	1	<1	<1	9	<1	3	<1	4	13
Cr	13	104	13	10	11	<1	6	25	9	10	4	11	38
Zn	69	63	69	65	96	110	99	74	98	99	91	92	82
Ga	17	18	18	18	8	14	17	17	16	14	15	17	14
Rb	20	28	12	24	25	32	29	19	37	26	29	23	23
Sr	457	477	501	495	387	358	340	482	370	395	414	513	395
Y	17	19	19	20	28	40	33	19	31	29	27	20	24
Zr	62	76	57	68	82	105	98	59	105	82	87	65	66
Nb	<1	<1	<1	2	2	2	3	2	3	<1	<1	1	<1
Ba	331	283	307	337	481	633	536	327	555	476	509	340	388
La	10	13	11	11	15	19	17	11	17	17	15	13	11
Ce	25	30	26	28	38	44	32	25	43	37	34	32	27
Nd	13	18	14	16	20	25	20	13	22	20	19	16	16
Pb	4	6	8	10	12	7	10	7	8	9	10	9	5
Th	4	6	3	5	8	6	9	6	7	7	6	5	8
Zr/Nb	>62.0	>76.0	>57.0	34.0	41.0	52.0	33.0	29.0	35.0	>82.0	>87.0	65.0	>66.0
Ti/Zr	79.0	58.0	84.0	72.0	83.0	63.0	78.0	80.0	65.0	83.0	63.0	81.0	80.0
Y/Zr	0.27	0.25	0.33	0.29	0.34	0.38	0.34	0.32	0.30	0.35	0.31	0.31	0.36
Ce/Zr	0.40	0.39	0.46	0.41	0.46	0.42	0.33	0.42	0.41	0.45	0.39	0.49	0.41
Ba/Zr	5.34	3.72	5.39	4.96	5.87	6.03	5.47	5.54	5.29	5.80	5.85	5.23	5.88
$(Ce/Y)_N$	3.61	3.88	3.36	3.44	3.33	2.70	2.38	3.23	3.41	3.13	3.09	3.93	2.76
Fe/Mg	3.59	2.44	3.49	3.86	4.38	5.80	4.63	3.04	4.50	4.04	4.49	3.55	2.93
K/Rb	382.0	326.0	401.0	391.0	402.0	381.0	369.0	389.0	316.0	383.0	349.0	368.0	365.0
Ba/Sr	0.72	0.59	0.61	0.68	1.24	1.77	1.58	0.68	1.50	1.21	1.23	0.66	0.98
Q	6.6	3.9	7.5	6.3	11.0	16.5	12.0	4.5	12.6	10.9	12.1	4.9	8.5
Or	5.5	6.7	3.5	6.6	7.3	8.8	7.8	5.3	8.5	7.3	7.5	6.0	5.9
Ab	22.1	20.3	21.8	22.5	23.7	31.3	26.6	21.3	25.3	22.9	23.7	21.7	21.1
An	38.5	37.1	38.6	38.2	25.7	17.7	20.5	37.3	24.4	25.5	30.7	36.4	31.8
Ne	0.0	0.0	0.0	0.0	0.0	0.0	0.0	0.0	0.0	0.0	0.0	0.0	0.0
Di	11.6	13.8	11.9	10.2	11.6	6.6	12.0	13.4	9.7	12.2	7.9	12.9	12.5
Hy	11.7	14.2	12.5	12.0	15.1	13.8	15.2	14.0	14.2	15.7	13.6	13.6	15.7
Ol	0.0	0.0	0.0	0.0	0.0	0.0	0.0	0.0	0.0	0.0	0.0	0.0	0.0
Mt	1.5	1.5	1.6	1.5	1.9	1.8	2.0	1.6	1.8	2.0	1.6	1.7	1.7
Il	1.6	1.4	1.6	1.5	2.2	2.1	2.5	1.5	2.2	2.2	1.8	1.7	1.7
Ap	0.3	0.4	0.3	0.4	0.4	0.6	0.4	0.3	0.4	0.3	0.3	0.3	0.3

that the nature of the mantle wedge and/or the petrogenetic processes have changed with time. One possibility is that the mantle wedge has become more refractory (i.e., more Mg-rich) and depleted in the high-field-strength trace elements, despite being repeatedly replenished by a volatile (lithophile element-rich) fluid or melt phase. In this case, the primitive island-arc tholeiites could represent early melting of the mantle wedge, having essentially the composition of the N-type MORB mantle reservoir enriched in the volatile elements. Such mantle would melt to similar or slightly higher degrees than that feeding mid-ocean ridges. The calc-alkaline magmas would then represent partial melts derived from the re-enriched mantle residue of primitive arc-tholeiite magmatism. Such a refractory mantle is unlikely to melt to such high degrees, and the HYG element composition of the liquids produced would be much more influenced by the composition of the volatile phase producing the re-enrichment. In this model the proportion of the minor titanium phases (sphene or rutile) in the mantle wedge would increase with time; this, together, with a general decrease in the degree of partial melting could explain a general increase in the magnitude of the negative Ta anomaly with time: the tholeiites from the fore-arc are less depleted in Ta than the other arc lavas (Figs. 22 and 24). The mantle underlying the fore-arc at the present has been cooled sufficiently to preclude subsequent magmatism, and re-

Table 6. (Continued).

MV 15297	MV 15304	MV 15344	MV 1502	MV 1504	MV 1506	MV 1508	MV 1515	MV 1520	MV 1526	MV 1580	MV 17	MV 15132	MV 1517
58.0	54.9	55.1	54.4	52.3	59.6	57.3	54.8	52.0	55.4	59.7	54.0	60.5	52.5
0.95	0.89	1.00	0.71	0.80	0.98	1.14	1.26	0.71	0.88	1.10	0.98	1.11	0.93
15.4	16.7	17.0	20.5	19.2	14.9	13.7	14.8	19.3	18.6	13.4	15.4	13.9	15.7
9.62	9.87	9.83	8.00	8.75	9.72	10.53	9.79	8.14	7.99	9.85	10.88	9.82	10.51
0.18	0.16	0.15	0.12	0.13	0.18	0.17	0.14	0.12	0.11	0.19	0.18	0.19	0.17
2.52	3.82	2.81	3.17	2.87	2.63	2.90	3.54	3.58	3.44	2.00	3.28	1.90	2.85
7.08	9.40	8.92	11.13	10.27	6.38	6.81	8.72	10.88	9.67	5.14	8.37	5.21	8.70
3.21	2.47	2.70	2.66	2.39	3.27	2.85	2.17	2.37	3.50	3.49	2.56	3.67	2.66
1.20	1.04	1.03	0.69	1.30	1.33	1.31	1.49	1.18	1.17	1.48	1.32	1.48	1.26
0.18	0.13	0.12	0.16	0.17	0.17	0.14	0.17	0.16	0.22	0.22	0.16	0.23	0.15
98.40	99.31	98.70	101.53	98.22	99.20	96.86	96.85	98.48	100.97	96.58	97.18	98.02	95.42
2	13	4	<1	3	<1	3	12	28	3	<1	1	<1	2
10	34	11	7	8	3	6	37	65	11	<1	8	<1	5
90	95	85	58	70	98	92	82	66	48	121	97	112	104
13	16	16	17	20	15	14	16	19	19	16	17	15	18
26	26	23	35	35	27	31	36	33	18	32	32	31	33
364	392	374	509	568	355	324	359	512	467	350	432	350	430
30	22	24	17	22	35	31	31	19	20	39	23	38	24
82	70	77	55	90	91	92	107	77	71	103	83	104	81
<1	<1	<1	<1	<1	<1	<1	<1	<1	2	<1	2	<1	<1
500	395	414	215	339	562	574	612	265	326	644	394	644	398
15	14	12	9	18	16	16	21	12	12	21	17	20	16
37	29	33	24	40	39	38	46	31	29	41	38	45	34
20	16	16	12	21	22	21	23	18	15	24	19	25	18
9	8	<1	4	4	5	8	15	5	<1	6	14	7	6
7	8	2	5	7	4	6	9	3	7	10	8	6	6
>82.0	>70.0	>77.0	>55.0	>90.0	>91.0	>92.0	>107.0	>77.0	35.0	>103.0	41.0	>104.0	>81.0
69.0	76.0	78.0	77.0	53.0	65.0	74.0	71.0	55.0	74.0	64.0	71.0	64.0	69.0
0.37	0.31	0.31	0.31	0.24	0.38	0.34	0.29	0.25	0.28	0.38	0.28	0.37	0.30
0.45	0.41	0.43	0.44	0.44	0.43	0.41	0.43	0.40	0.41	0.40	0.46	0.43	0.42
6.10	5.64	5.38	3.91	3.77	6.18	6.24	5.72	3.44	4.59	6.25	4.75	6.19	4.91
3.03	3.24	3.38	3.47	4.47	2.74	3.01	3.64	4.01	3.56	2.58	4.06	2.91	3.48
4.43	3.00	4.06	2.93	3.54	4.29	4.21	3.21	2.64	2.69	5.71	3.85	5.99	4.28
383.0	332.0	372.0	164.0	308.0	409.0	351.0	344.0	297.0	540.0	384.0	342.0	396.0	317.0
1.37	1.01	1.11	0.42	0.60	1.58	1.77	1.70	0.52	0.70	1.84	0.91	1.84	0.93
13.2	8.6	9.8	6.2	5.3	14.8	14.4	11.5	4.1	4.1	17.1	8.7	16.7	7.3
7.2	6.2	6.2	4.0	7.8	7.9	8.0	9.1	7.1	6.8	9.1	8.0	8.9	7.8
27.6	21.0	23.1	22.2	20.6	27.9	24.9	19.0	20.4	29.3	30.6	22.3	31.7	23.6
24.6	31.5	31.6	41.3	38.6	22.3	21.4	27.1	39.1	31.2	17.2	27.5	17.3	28.5
0.0	0.0	0.0	0.0	0.0	0.0	0.0	0.0	0.0	0.0	0.0	0.0	0.0	0.0
8.6	12.4	10.6	10.2	10.4	7.3	10.7	13.9	12.3	12.5	6.8	12.1	6.6	13.5
14.0	15.7	13.8	12.4	13.0	14.9	15.2	14.0	13.2	11.7	14.0	16.2	13.5	14.3
0.0	0.0	0.0	0.0	0.0	0.0	0.0	0.0	0.0	0.0	0.0	0.0	0.0	0.0
1.7	1.7	1.7	1.4	1.5	1.7	1.9	1.8	1.4	1.4	1.8	1.9	1.7	1.9
1.8	1.7	1.9	1.3	1.5	1.9	2.2	2.5	1.4	1.7	2.2	1.9	2.2	1.9
0.4	0.3	0.3	0.4	0.4	0.4	0.3	0.4	0.4	0.5	0.5	0.4	0.6	0.4

Table 7. INA trace element analyses (ppm) of 15 andesites from the Mariana arc.

Sample Number	Sc	Cr	Co	Ni	Rb	Sr	Zr	Cs	Ba	La	Ce	Eu	Tb	Hf	Ta	Th	U	La/Ta	La/Th	La/Tb	Th/Hf	Ba/La	La/Ce
RD17	29.8	60	27.2	8	30.4	431	92	0.68	404	17.4	29.9	1.38	0.69	2.16	0.11	2.67	0.76	158	6.5	25.2	1.2	23.2	0.58
MV1502	23.8	47	19.5	6	29.6	502	66	1.73	2.19	9.4	16.2	1.14	0.44	1.27	0.06	1.23	0.39	157	7.6	21.4	1.0	23.3	0.58
MV1504	23.4	49	20.1	7	30.6	551	108	0.59	371	19.4	30.6	1.45	0.63	2.19	0.11	2.66	0.83	176	7.3	30.8	1.2	19.1	0.63
MV1508	27.2	53	20.6	8	25.6	307	88	0.82	557	16.6	27.9	1.34	0.78	2.68	0.14	2.71	0.78	119	6.1	21.3	1.0	33.6	0.60
MV1515	28.4	74	21.6	16	31.0	355	134	1.05	627	20.2	32.8	1.37	0.77	2.87	0.17	3.61	1.00	119	5.6	26.2	1.3	31.0	0.62
MV1520	23.6	99	23.2	36	30.4	508	106	0.47	298	15.7	27.7	1.45	0.58	2.15	0.11	2.00	0.64	143	7.9	27.1	0.9	19.0	0.57
MV1526	28.7	49	25.5	8	15.1	441	94	0.12	302	14.0	22.2	1.32	0.58	1.79	0.09	1.74	0.61	156	8.0	24.1	1.0	21.6	0.63
MV1580	24.4	47	16.4	0.5	30.8	343	136	0.89	626	20.5	33.6	1.69	0.99	3.02	0.15	3.08	0.86	137	6.7	20.7	1.0	30.5	0.61
MV15101	30.3	62	26.7	8	25.3	392	114	0.63	462	15.2	30.9	1.36	0.70	2.40	0.13	2.46	0.62	117	6.2	21.7	1.0	30.4	0.49
MV15117	24.8	48	16.4	0	29.3	349	126	0.86	613	19.5	33.2	1.72	0.96	3.03	0.15	3.03	0.87	130	6.4	20.3	1.0	31.4	0.59
MV15132	24.6	47	16.6	0.7	29.9	339	112	0.87	626	19.9	33.5	1.69	0.97	2.99	0.16	3.02	0.86	124	6.6	20.5	1.0	31.5	0.59
MV15146	32.2	66	27.7	9	27.0	340	89	0.78	527	16.4	27.7	1.49	0.83	2.69	0.13	2.65	0.67	126	6.2	19.8	1.0	32.1	0.59
MV15220	31.4	65	26.9	9	23.5	389	96	0.68	482	16.1	27.6	1.40	0.73	2.42	0.12	2.55	0.72	134	6.3	22.1	1.1	29.9	0.58
MV1801	24.5	53	22.3	10	18.4	468	70	0.48	322	11.5	18.6	1.14	0.49	1.76	0.09	1.75	0.49	128	6.6	23.5	1.0	28.0	0.62
MV1802	24.7	134	25.0	46	25.7	487	93	0.49	278	14.6	25.6	1.42	0.56	1.91	0.08	1.76	0.58	183	8.3	26.1	0.9	19.0	0.57

Note: Samples from P. Fryer; sample designations as in Table 6.

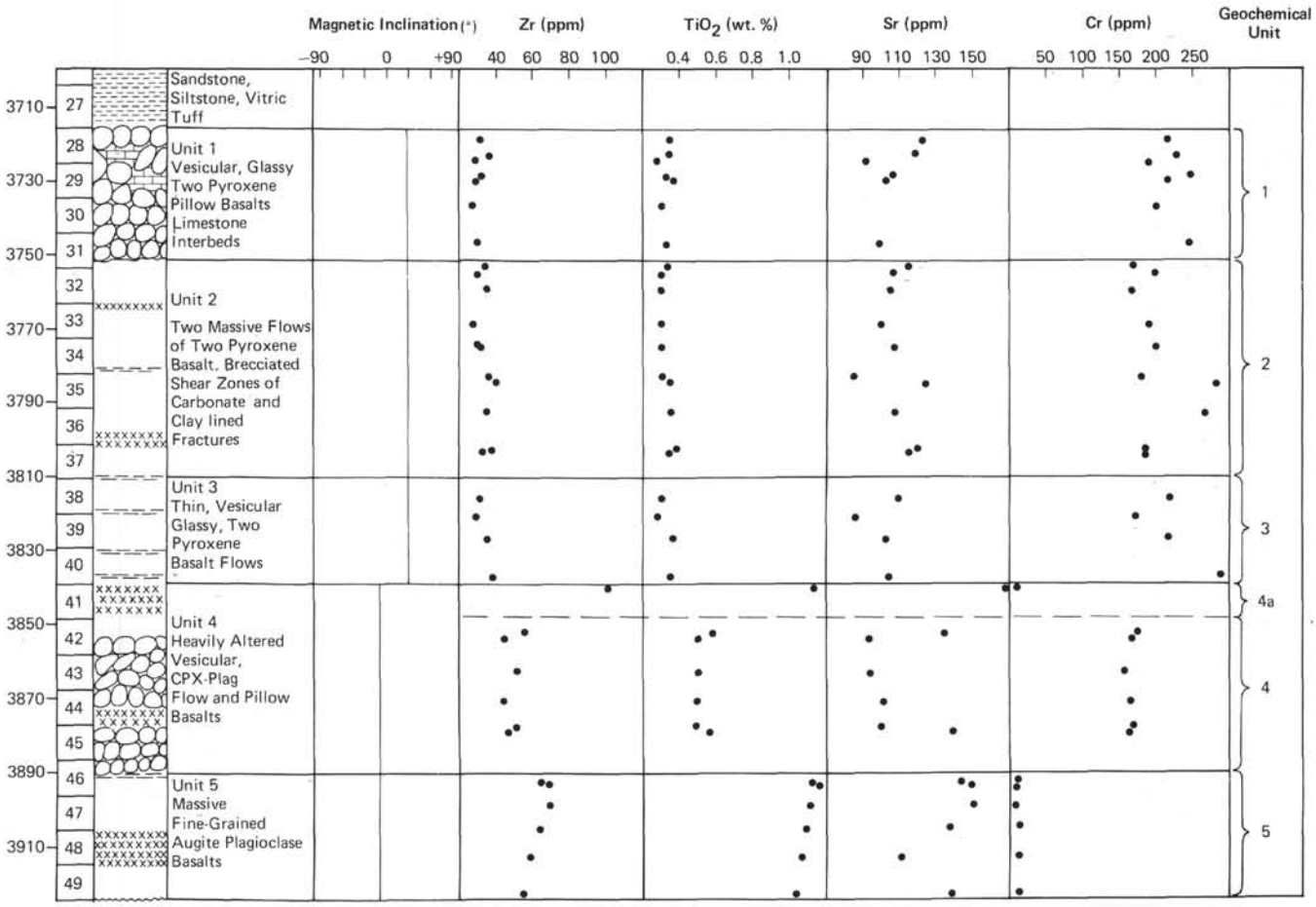

Figure 14. Geochemical and lithological stratigraphy of the basement sections of Hole 458.

cent arc magmatism has become restricted to a zone above the steeply dipping Benioff zone.

The possible coexistence of N-type MORB and calc-alkaline magmas in the initial period of inter-arc basin formation, as observed in the Mariana Trough (Sites 454 and 456), might be expected from this model. The general absence of basalts with calc-alkaline affinities in the Parece-Vela Basin and Shikoku Basin implies that the influence of the arc mantle sources disappears once the basins are well developed.

ACKNOWLEDGMENTS

The analytical work was carried out with financial support from the Natural Environment Research Council (NERC), U.K. and the Centre National de la Recherche Scientifique, France. DAW and NGM gratefully acknowledge NERC fellowships supporting work on samples recovered by DSDP. We thank Drs. J. H. Natland, J. A. Pearce, and A. D. Saunders for their reviews and comments on the manuscript.

REFERENCES

Abbotts, I. L., 1979. A field petrological and geochemical study of the Masirah Ophiolite, Oman [Ph.D. dissert.]. University of Birmingham, U.K.

Anonymous, 1977. Initial report of the geological study of oceanic crust of the Philippine Sea floor. *Ofioliti*, 2:137–168.

Barazangi, M., Pennington, W., and Isacks, B. L., 1975. Global study of seismic wave attenuation in the upper mantle behind island arcs using P waves. *J. Geophys. Res.*, 80:1078–1092.

Barker, P. F., 1972. A spreading centre in the East Scotia Sea. *Earth Planet. Sci. Lett.*, 15:123–321.

Best, M. G., 1975. Migration of hydrous fluids in the upper mantle and potassium variation in calc-alkalic rocks. *Geology*, 3: 429–432.

Cameron, W. E., Nisbet, E. G., and Dietrich, V. J., 1979. Boninites, komatiites and ophiolitic basalts. *Nature*, 280:550–553.

Chayla, B., Jaffrezic, H., and Joron, J.-L., 1973. Analyse par activation dans les mentions épithermiques. Application à la determination d'éléments en trace dans les roches. *Comptes Rendus Acad. Sci. Paris*, 277:273–275.

Chow, T. J., Stern, R. J., and Dixon, T. H., 1980. Absolute and relative abundances of K, Rb, Sr and Ba in circum-Pacific island-arc magmas, with special reference to the Marianas. *Chem. Geol.*, 28:111–121.

Cloud, P. E., Jr., Schmidt, R. G., and Burke, H. W., 1956. Geology of Saipan, Mariana Islands. *U.S. Geol. Surv. Prof. Paper*, 280A.

Dallwitz, W. B., 1968. Chemical composition and genesis of clinoenstatite-bearing volcanic rocks from Cape Vogel, Papua: a discussion. *Rept. 23rd Int. Geol. Congr.*, 2:229–242.

Dallwitz, W. B., Green, D. H., and Thompson, I. E., 1966. Clinoenstatite in a volcanic rock from Cape Vogel, Papua. *J. Petrol.*, 7: 375–403.

DePaolo, D. J., and Wasserburg, C. J., 1977. The sources of island arcs as indicated by Nd and Sr isotopic studies. *Geophys. Res. Lett.*, 4:465–468.

Dietrich, V., Emmermann, R., Oberhansli, R., et al., 1978. Geochemistry of basaltic and gabbroic rocks from the west Mariana basin and the Mariana Trench. *Earth Planet. Sci. Lett.*, 39:127–144.

Dixon, T. H., and Batiza, R., 1979. Petrology and chemistry of recent lavas in the Northern Marianas: Implications for the origin of island arc basalts. *Contrib. Mineral. Petrol.*, 70:167–181.

Garcia, M. O., Liu, N. W. K., and Muenow, D. W., 1979. Volatiles in submarine volcanic rocks from the Mariana Island arc and trough. *Geochim. Cosmochim. Acta*, 43:305–312.

Gill, J. B., 1976. Composition and age of Lau Basin and Ridge volcanic rocks: implications for evolution of an interarc basin and remnant arc. *Geol. Soc. Am. Bull.*, 87:1384–1395.

Green, D. H., 1976. Experimental testing of "equilibrium" partial melting of peridotite under water-saturated, high pressure conditions. *Can. Mineralogists*, 14:255–268.

Hart, S. R., Glassley, W. E., and Karig, D. E., 1972. Basalts and sea floor spreading behind the Mariana Island arc. *Earth Planet. Sci. Lett.*, 15:12–18.

Hawkesworth, C. J., O'Nions, R. K., Pankhurst, R. J., et al., 1978. A geochemical study of island arc and back-arc tholeiites from the Scotia Sea. *Earth Planet. Sci. Lett.*, 36:253–262.

Hawkins, J. W., 1974. Geology of the Lau Basin, a marginal basin behind the Tonga Arc. *In* Burke, C. A., and Drake, C. L. (Eds.), *The Geology of Continental Margins:* New York (Springer), pp. 505–520.

_____, 1976. Petrology and geochemistry of basaltic rocks of the Lau Basin. *Earth Planet. Sci. Lett.*, 28:283–297.

_____, 1977. Petrology and geochemical characteristics of marginal basin basalts. *In* Talwani, M., and Pitman III, W. C. (Eds.), *Island Arcs, Deep Sea Trenches and Back-Arc Basins: Maurice Ewing Series 1:* Washington (American Geophysical Union), 355–365.

Hellman, P. L., and Green, T. H., 1979. The role of sphene as an accessory phase in the high pressure partial melting of hydrous mafic compositions. *Earth Planet. Sci. Lett.*, 42:191–201.

Hickey, R., and Frey, F. A., 1979. Petrogenesis of high-Mg andesites: Geochemical evidence. *EOS*, 60:413.

Hussong, D. H., Uyeda, S., et al., 1978. Near the Philippines—Leg 60 ends in Guam. *Geotimes*, 23(10):19–22.

Isacks, B. L., and Barazangi, M., 1977. Geometry of Benioff zones: Lateral segmentation and downwards bending of the subducted lithosphere. *In* Talwani, M., and Pitman III, W. C. (Eds.), *Island Arcs, Deep Sea Trenches and Back-Arc Basins: Maurice Ewing Series 1:* Washington (American Geophysical Union).

Karig, D. E., 1971. Origin and development of marginal basins in the western Pacific. *J. Geophys. Res.*, 76:2542–2561.

Karig, D. E., Anderson, R. N., and Bibee, L. D., 1978. Characteristics of back arc spreading in the Mariana Trough. *J. Geophys. Res.*, 83:1213–1226.

Katsumata, M., and Sykes, L. R., 1969. Seismicity and tectonics of the western Pacific: Izu-Mariana-Caroline and Ryuku-Taiwan region. *J. Geophys. Res.*, 74:5923–5948.

Kuno, H., 1968. Differentiation of basalt magmas. *In* Hess, H. H., and Poldervaart, A. (Eds.), *Basalts* (Vol. 2): New York (Wiley), 623–688.

Kuroda, M., and Shiraki, K., 1975. Boninite and related rocks of Chichi-Jima, Bonin Islands. *Japan Rep. Fac. Sci. Shizuoka Univ.*, 10:145–155.

Kuroda, M., Shiraki, K., and Urano, H., 1978. Boninite as a possible calc-alkalic primary magma. *Proc. Tokyo Conf.*, pp. 280–281.

Marsh, N. G., 1977. The geochemistry of plutonic rocks from Atacama Province, North Chile [M.Sc. thesis]. University of Birmingham, U.K.

Marsh, N. G., Saunders, A. D., and Tarney, J., 1980. Geochemistry of basalts from the Shikoku and Daito Basins, DSDP Leg 58. *In* Klein, G. deV., Kobayashi, K., et al., *Init. Repts. DSDP*, 58: Washington (U.S. Govt. Printing Office), 805–842.

Mattey, D. P., Marsh, N. G., and Tarney, J., 1980. The geochemistry, mineralogy and petrology of igneous rocks from the West Philippine and Parece Vela Basins, and from the Kyushu-Palau and West Mariana Ridges, IPOD Leg 59. *In* Kroenke, L., Scott, R., et al., *Init. Repts. DSDP*, 59: Washington (U.S. Govt. Printing Office), 753–800.

Meijer, A., 1976. Pb and Sr isotopic data bearing on the origin of volcanic rocks from the Mariana island arc system. *Bull. Geol. Soc. Am.*, 87:1358–1369.

Moore, J., and Schilling, J-G., 1973. Vesicles, water and sulfur in Rejkjanes Ridge basalts. *Contrib. Mineral. Petrol.*, 41:105–118.

Murauchi, S., Den, N., Asaro, S., et al., 1968. Crustal structure of the Philippine Sea. *J. Geophys. Res.*, 73:3143–3171.

Pearce, J. A., in press. Geochemical evidence for the genesis and eruptive setting of lavas from Tethyan Ophiolites. *Proc. Symp. on Ophiolite Problems. Geol. Survey Cyprus.*

Philpotts, J. A., Martin, W., and Schnetzler, C. C., 1971. Geochemical aspects of some Japanese lavas. *Earth Planet. Sci. Lett.*, 12:89–95.

Poehls, K. A., 1978. Inter-arc basins: a kinematic model. *Geophys. Res. Lett.*, 5:325–328.

Rhodes, J. M., Dungan, M. A., Blanchard, D. P., et al., 1979. Magma mixing at mid-ocean ridges: evidence from basalts drilled near 22°N on the mid-Atlantic Ridge. *Tectonophysics*, 55:35–61.

Ringwood, A. E., 1974. The petrological evolution of island arc systems. *J. Geol. Soc. London*, 130:183–204.

Saunders, A. D., and Tarney, J., 1979. The geochemistry of basalts from a back-arc spreading centre in the East Scotia Sea. *Geochim. Cosmochim. Acta*, 43:555–572.

Saunders, A. D., Tarney, J., and Weaver, S. D., 1980. Transverse geochemical variations across the Antarctic Peninsula: Implications for the genesis of calc-alkalic magmas. *Earth Planet. Sci. Lett.*, 46:344–360.

Schmidt, R. G., 1957. Geology of Saipan, Mariana Islands, Chapter B. Petrology of the volcanic rocks. *U.S. Geol. Surv. Prof. Paper*, 280B:127–175.

Sclater, J. G., Hawkins, J. W., Mammerickx, J., et al., 1972. Crustal extension between the Tonga and Low Ridges: petrologic and geophysical evidence. *Bull. Geol. Soc. Am.*, 83:505–517.

Scott, R. B., Kroenke, L., et al., 1980. *Init. Repts. DSDP*, 59: Washington (U.S. Govt. Printing Office).

Sharaskin, A. Ya, Dobretsov, N. L., and Sobolev, N. V., in press. Marianites: the clinoenstatite bearing pillow lavas associated with ophiolite assemblage of the Mariana Trench. *Proc. Int. Ophiolite Symp. Cyprus.*

Shiraki, K., Kuroda, N., and Urano, H., 1979. Clinoenstative-bearing boninite of Muko-jima, Bonin Islands. *J. Geol. Soc. Japan*, 85:591–594.

Stark, J. T., 1963. Petrology of the volcanic rocks of Guam. *U.S. Geol. Surv. Prof. Paper*. 403C, 32.

Stern, R. J., 1979. On the origin of andesite in the northern Mariana Island Arc: Implications from Agrigan. *Contrib. Mineral. Petrol.*, 68:207–219.

Sun, S-S., 1980. Lead isotopic study of young volcanic rocks from mid-ocean ridges, ocean islands and island arcs. *Philos. Trans. Roy. Soc. Lond. Ser. A.*, 297:409–445.

Sun, S-S., and Nesbitt, R. W., 1978. Geochemical regularities and genetic significance of ophiolitic basalts. *Geology*, 6:689–693.

Sun, S-S., Nesbitt, R. W., and Sharaskin, A. Y., 1979. Chemical characteristics of mid-ocean ridge basalts. *Earth Planet. Sci. Lett.*, 44:119–138.

Tarney, J., Saunders, A. D., and Weaver, S. D., 1977. Geochemistry of volcanic rocks from the island arcs and marginal basins of Scotia Arc region. *In* Talwani, M., and Pitman III, W. C. (Eds.), *Island Arcs, Deep Sea Trenches and Back-Arc Basins: Maurice Ewing Series, 1:* Washington (American Geophysical Union), 367–377.

Tarney, J., Saunders, A. D., Weaver, S. D., Donnellan, N. C. B., and Hendry, G. L., 1978. Minor element chemistry of basalts from Leg 49, North Atlantic Ocean. *In* Luyendyk, B. P., Cann, J. R., et al., *Init. Repts. DSDP*, 49: Washington (U.S. Govt. Printing Office), 567–691.

Tarney, J. Wood, D. A., Saunders, A. D., et al., 1980. Nature of mantle heterogeneity in the North Atlantic: evidence from deep sea drilling. *Philos. Trans. Roy. Soc. Lond. Ser. A.*, 297:179–202.

Taylor, S. R., Capp, A. C., Graham, A. L., et al., 1969. Trace element abundances in andesite 11. Saipan, Bougainville and Fiji. *Contr. Mineral. Petrol.*, 23:1–26.

Treuil, M., and Varet, J., 1973. Critères volcanologiques, pétrologiques et géochimiques de la genèse et de la différentiation des magmas basaltiques: exemple de l'Afar. *Bull. Soc. Geol. France*, 15:506–540.

Uyeda, S., and Kanamori, H., 1979. Back-arc opening and the mode of subduction. *J. Geophys. Res.*, 84:1049–1061.

Vogt, P. R., Lowrie, A., Bracey, D. R., et al., 1976. Subduction of aseismic ocean ridges: Effects on shape, seismicity, and other characteristics of consuming plate boundaries. *Geol. Soc. Am. Special Paper 172.*

Weaver, S. D., Saunders, A. D., Pankhurst, R. J., et al., 1979. A geochemical study of magmatism associated with the initial stages of back-arc spreading: the Quaternary volcanics of Bransfield Strait, South Shetland Islands. *Contr. Mineral. Petrol.*, 68:151–169.

Weaver, S. D., Sceal, J. S. C., and Gibson, I. L., 1972. Trace element data relevant to the origin of trachytic and pantelleritic lavas in the East African Rift System. *Contrib. Mineral. Petrology*, 36:181–190.

Wells, P. 1978. The geochemistry of the Patagonia batholith between 45°S and 46°S latitude [M.Sc. thesis]. University of Birmingham, U.K. (unpublished).

Wood, D. A., 1979. A variably veined sub-oceanic upper mantle: genetic significance for mid-ocean ridge basalts from geochemical evidence. *Geology*, 7:499–503.

_____, 1980. The application of a Th-Hf-Ta diagram to problems of tectonomagmatic classification and to establishing the nature of crustal contamination of basaltic lavas of the British Tertiary Volcanic Province. *Earth Planet. Sci. Lett.*, 50:11–30.

Wood, D. A., Joron, J. L., Marsh, N. G., et al., 1980a. Major and trace element variations in basalts from the North Philippine Sea drilled during DSDP Leg 58: A comparative study of back-arc basin basalt with lava series from Japan and mid-ocean ridges. *In* Klein, G. deV., Kobayashi, K., et al., *Init. Repts. DSDP*, 58: Washington (U.S. Govt. Printing Office), 873–894.

Wood, D. A., Joron, J. L., and Treuil, M., 1979b. A re-appraisal of the use of trace elements to classify and discriminate between magma series in different tectonic settings. *Earth Planet. Sci. Lett.*, 45:326–336.

Wood, D. A., Mattey, D. P., Joron, J. L., et al., 1980a. A geochemical study of 17 selected samples from the basement cores recovered at Sites 447, 448, 449, 450, and 451 DSDP Leg 59. *In* Kroenke, L., Scott, R., et al., *Init. Repts. DSDP*, 59: Washington (U.S. Govt. Printing Office), 743–752.

Wood, D. A., Tarney, J., Varet, J., et al., 1979a. Geochemistry of basalts drilled in the North Atlantic by IPOD Leg 49: implications for mantle heterogeneity. *Earth Planet. Sci. Lett.*, 42:77–97.

Table 8. Major and trace element analyses of igneous rocks from Hole 458.

Sample (interval in cm)	27-1, 130–132	28-1, 58–60	28-1, 125–127	28-1, 140–142	29-1, 54–60	29-2, 37–39	30-1, 56–58	31-1, 39–41	31-1, 131–133	32-1, 116–118	32-3, 34–36	33-2, 19–21	34-1, 34–41	35-1, 42–44	35-2, 69–71	36-1, 27–29	37-1, 52–54
SiO_2	54.6	52.5	52.8	56.1	53.1	52.0	51.5	53.2	57.1	58.8	59.0	56.9	59.8	53.3	52.4	52.4	
TiO_2	0.15	0.34	0.34	0.28	0.33	0.36	0.30	0.33	0.33	0.30	0.30	0.30	0.30	0.30	0.35	0.35	0.37
Al_2O_3	7.9	18.0	18.3	13.7	15.4	14.4	17.8	16.1	15.2	14.2	13.9	13.2	14.7	13.8	16.5	15.1	15.1
tFe_2O_3	11.92	9.31	8.55	9.32	9.16	10.23	9.36	9.24	9.38	9.32	9.34	8.98	8.95	8.75	9.20	10.13	9.36
MnO	0.42	0.11	0.11	0.14	0.10	0.12	0.17	0.10	0.11	0.10	0.11	0.12	0.12	0.11	0.12	0.14	0.10
MgO	16.35	5.09	5.35	6.11	8.97	9.71	6.32	7.47	5.19	5.02	4.62	8.13	5.53	5.23	7.12	8.73	7.63
CaO	1.83	11.17	11.32	9.59	9.26	8.70	7.99	9.49	10.45	9.60	9.24	8.93	10.76	9.74	9.76	7.90	10.13
Na_2O	2.67	2.77	2.67	1.97	2.60	2.63	3.13	2.65	2.81	2.36	2.50	2.24	2.61	2.33	2.81	3.04	2.87
K_2O	1.64	0.63	0.96	0.44	1.23	0.88	1.53	1.12	0.85	1.20	1.16	0.61	1.12	0.83	0.79	1.05	1.38
P_2O_5	0.00	0.03	0.02	0.02	0.01	0.01	0.01	0.01	0.05	0.04	0.04	0.03	0.04	0.04	0.01	0.01	0.05
Total	97.45	99.97	100.41	97.70	100.13	99.01	98.17	99.73	101.48	100.94	100.24	101.73	101.02	100.97	99.93	98.88	99.40
Ni	315	80	79	74	91	76	81	73	56	59	59	67	65	60	101	97	62
Cr	1303	214	229	189	244	216	201	245	168	199	168	191	200	181	282	267	184
Zn	57	71	64	54	74	76	55	65	48	50	48	52	52	55	76	73	57
Ga	5	14	15	14	17	15	9	11	14	16	14	15	15	14	17	13	16
Rb	21	7	7	8	13	5	11	9	46	61	113	13	24	13	8	5	33
Sr	55	122	119	92	106	103	69	99	116	106	105	100	107	85	124	107	119
Y	<1	8	6	7	3	2	5	2	8	6	8	6	9	12	3	5	12
Zr	24	31	36	28	31	30	27	30	33	30	35	28	30	36	39	34	36
Nb	2	<1	<1	2	<1	<1	<1	<1	<1	<1	<1	<1	<1	<1	<1	<1	<1
Ba	59	41	22	33	13	15	54	6	35	49	29	51	47	19	46	30	54
La	11	6	7	6	7	7	7	6	6	6	6	6	6	7	7	8	5
Ce	<1	6	<1	7	5	2	5	6	<1	2	<1	4	4	<1	2	5	2
Nd	<1	3	2	3	3	2	2	4	2	1	<1	3	3	1	2	3	3
Pb	3	6	3	3	2	4	<1	<1	2	1	2	5	4	<1	<1	2	2
Th	<1	2	<1	<1	<1	<1	7	9	2	<1	<1	2	<1	<1	<1	<1	<1
Zr/Nb	12.0	>31.0	>36.0	14.0	>31.0	>30.0	>27.0	>30.0	>33.0	>30.0	>35.0	>28.0	>30.0	>36.0	>39.0	>34.0	>36.0
Ti/Zr	37.0	66.0	57.0	59.0	65.0	71.0	66.0	67.0	59.0	60.0	52.0	64.0	60.0	50.0	54.0	62.0	61.0
Y/Zr	<0.04	0.26	0.17	0.25	0.10	0.07	0.19	0.07	0.24	0.20	0.23	0.21	0.30	0.33	0.08	0.15	0.33
Ce/Zr	<0.04	0.19	<0.02	0.25	0.16	0.07	0.19	0.20	<0.03	0.07	<0.03	0.14	0.13	<0.03	0.05	0.15	0.06
Ba/Zr	2.46	1.32	0.61	1.18	0.42	0.50	2.00	0.20	1.06	1.63	0.83	1.82	1.57	0.53	1.18	0.88	1.50
$(Ce/Y)_N$	2.46	1.84	—	2.46	4.09	2.46	2.46	7.37	—	0.82	—	1.64	1.09	—	1.64	—	0.41
Fe/Mg	0.85	2.12	1.85	1.77	1.18	1.22	1.72	1.43	2.10	2.15	2.34	1.28	1.88	1.94	1.50	1.35	1.42
K/Rb	648.0	747.0	1141.0	452.0	785.0	1453.0	1155.0	1033.0	154.0	163.0	85.0	391.0	387.0	531.0	817.0	1743.0	347.0
Ba/Sr	1.07	0.34	0.18	0.36	0.12	0.15	0.78	0.06	0.30	0.46	0.28	0.51	0.44	0.22	0.37	0.28	0.45
Q	0.0	1.3	0.8	12.3	0.0	0.0	0.0	0.5	7.3	11.8	12.6	11.3	6.9	14.2	0.9	0.0	0.0
Or	9.9	3.7	5.7	2.6	7.3	5.2	9.2	6.6	5.0	7.0	6.9	3.6	6.6	4.9	4.7	6.3	8.2
Ab	23.2	23.4	22.5	17.1	22.0	22.5	27.0	22.5	23.4	19.8	21.1	18.6	21.9	19.5	23.8	26.0	24.4
An	4.8	34.9	35.0	28.0	26.6	25.2	30.6	28.7	25.9	24.3	23.3	23.8	24.8	24.5	30.1	24.8	24.4
Ne	0.0	0.0	0.0	0.0	0.0	0.0	0.0	0.0	0.0	0.0	0.0	0.0	0.0	0.0	0.0	0.0	0.0
Di	3.6	16.8	17.2	16.9	15.6	14.9	8.0	15.0	20.6	18.7	18.4	15.9	22.9	19.1	15.0	12.1	21.1
Hy	49.3	16.6	16.0	20.0	22.2	23.5	14.7	23.5	14.7	15.3	14.6	23.8	14.0	14.9	22.5	21.7	11.7
Ol	5.6	0.0	0.0	0.0	3.3	5.3	7.4	0.0	0.0	0.0	0.0	0.0	0.0	0.0	0.0	5.8	6.9
Mt	2.1	1.6	1.5	1.7	1.6	1.8	1.7	1.6	1.6	1.6	1.6	1.5	1.5	1.5	1.6	1.8	1.6
Il	0.3	0.6	0.6	0.5	0.6	0.7	0.6	0.6	0.6	0.6	0.6	0.6	0.6	0.6	0.7	0.7	0.7
Ap	0.0	0.1	0.1	0.0	0.0	0.0	0.0	0.0	0.1	0.1	0.1	0.1	0.1	0.1	0.0	0.0	0.1

Table 8. (Continued).

37-2, 62-64	38-1, 51-53	39-1, 37-39	39-2, 94-96	40-2, 90-92	41-1, 22-24	42-1, 61-63	42-1, 86-88	43-1, 118-120	44-1, 53-55	45-1, 8-10	45-1, 24-26	46-1, 75-77	46-1, 83-85	47-1, 67-69	47-2, 90-92	48-1, 79-81	49-1, 136-138
54.2	54.9	54.8	52.5	52.8	53.2	52.7	54.8	54.5	54.7	54.1	52.8	52.8	52.6	52.0	51.8	52.2	50.6
0.34	0.30	0.28	0.36	0.35	1.13	0.58	0.49	0.51	0.49	0.49	0.56	1.13	1.16	1.11	1.09	1.07	1.04
15.0	14.7	14.4	15.7	14.9	15.5	15.5	13.6	14.2	14.3	12.9	15.3	13.6	14.0	14.3	14.2	13.8	13.9
9.02	8.92	9.34	9.43	10.24	9.66	11.11	10.37	10.61	10.19	10.29	10.69	13.82	13.74	13.05	13.53	13.88	13.73
0.10	0.12	0.15	0.15	0.09	0.06	0.08	0.16	0.16	0.15	0.15	0.08	0.10	0.09	0.10	0.10	0.16	0.09
7.34	6.36	6.42	9.16	8.97	3.73	6.76	6.12	6.25	5.78	5.64	6.71	6.17	6.33	6.85	7.32	5.51	7.96
9.89	10.68	9.40	8.39	7.98	6.12	8.51	8.35	7.88	7.97	8.20	9.09	5.88	6.06	7.42	6.78	6.65	6.51
2.79	2.66	2.14	2.63	2.47	5.70	2.94	2.54	2.48	2.45	2.54	2.95	3.41	3.46	3.55	3.20	2.59	3.63
1.27	1.14	0.54	0.86	1.03	1.52	0.83	0.57	0.57	0.53	0.51	0.97	0.75	0.69	0.48	0.49	0.72	1.36
0.05	0.04	0.01	0.01	0.01	0.20	0.05	0.02	0.02	0.02	0.02	0.07	0.06	0.09	0.14	0.10	0.02	0.11
100.02	99.81	97.49	99.20	98.86	96.83	99.03	96.98	97.22	96.66	94.81	99.16	97.74	98.26	98.99	98.66	96.58	98.95
65	75	71	99	97	11	65	75	82	76	77	71	23	28	21	35	24	19
185	219	172	217	290	11	176	170	157	164	167	165	11	10	10	16	14	13
53	53	60	51	83	88	82	59	65	60	60	68	109	111	92	102	92	69
18	16	12	14	16	25	18	13	12	13	14	17	18	20	26	24	15	21
34	19	7	3	12	25	15	6	7	8	8	19	13	12	8	7	9	20
115	109	86	102	104	169	134	94	94	101	100	139	144	149	151	138	111	138
9	8	6	<1	2	31	20	11	10	11	11	25	20	26	25	34	17	19
32	31	29	35	38	101	58	44	51	44	51	47	65	68	69	64	59	47
<1	<1	<1	<1	<1	1	<1	<1	<1	<1	<1	<1	<1	<1	<1	<1	<1	<1
44	39	25	20	18	79	19	42	49	29	41	80	63	43	44	37	77	83
6	6	6	4	7	9	7	5	6	6	5	9	10	9	8	11	7	8
2	4	<1	<1	5	15	9	3	3	8	<1	9	10	12	7	7	5	8
3	4	<1	<1	2	11	6	2	4	4	.2	6	7	8	5	6	3	7
1	2	3	11	<1	6	3	6	1	4	4	<1	1	<1	4	3	2	3
<1	<1	<1	<1	<1	<1	<1	<1	1	<1	2	<1	2	2	6	<1	<1	<1
>32.0	>31.0	>29.0	>35.0	>38.0	101.0	>58.0	>44.0	>51.0	>44.0	>51.0	>47.0	>65.0	>68.0	>69.0	>64.0	>59.0	>47.0
64.0	58.0	59.0	61.0	55.0	67.0	60.0	67.0	61.0	66.0	57.0	72.0	104.0	102.0	96.0	102.0	109.0	133.0
0.28	0.26	0.21	<0.03	0.05	0.31	0.34	0.25	0.20	0.25	0.22	0.53	0.31	0.38	0.36	0.53	0.29	0.40
0.06	0.13	<0.03	<0.03	0.13	0.15	0.16	0.07	0.06	0.18	<0.02	0.19	0.15	0.18	0.10	0.11	0.08	0.17
1.37	1.26	0.86	0.57	0.47	0.78	0.33	0.95	0.96	0.66	0.80	1.70	0.97	0.63	0.64	0.58	1.31	1.77
0.55	1.23	—	2.46	6.14	1.19	1.11	0.67	0.74	1.79	—	0.88	1.23	1.13	0.69	0.51	0.72	1.03
1.43	1.63	1.69	1.19	1.32	3.00	1.91	1.97	1.97	2.04	2.12	1.85	2.60	2.52	2.21	2.14	2.92	2.00
310.0	498.0	644.0	2382.0	713.0	505.0	462.0	784.0	681.0	550.0	533.0	425.0	479.0	479.0	501.0	575.0	665.0	564.0
0.38	0.36	0.29	0.20	0.17	0.47	0.14	0.45	0.52	0.29	0.41	0.58	0.44	0.29	0.29	0.27	0.69	0.60
1.0	3.4	9.2	0.0	0.7	0.0	1.0	8.7	8.5	9.9	9.7	0.5	2.7	1.9	0.0	0.7	6.2	0.0
7.5	6.7	3.3	5.1	6.2	9.3	5.0	3.5	3.5	3.2	3.2	5.8	4.5	4.2	2.9	2.9	4.4	8.1
23.6	22.5	18.6	22.4	21.1	45.7	25.1	22.2	21.6	21.4	22.7	25.2	29.5	29.8	30.3	27.4	22.7	31.0
24.6	24.9	28.7	28.9	26.9	12.5	26.9	24.7	26.7	27.5	23.5	25.8	20.1	21.0	21.9	23.3	24.7	17.9
0.0	0.0	0.0	0.0	0.0	2.2	0.0	0.0	0.0	0.0	0.0	0.0	0.0	0.0	0.0	0.0	0.0	0.0
19.7	22.9	15.6	10.6	10.7	14.6	12.7	14.7	11.1	11.0	15.9	15.8	7.8	7.5	11.9	8.4	7.8	11.5
20.5	16.5	21.5	28.1	31.0	0.0	25.1	22.4	24.8	23.2	21.1	22.9	29.3	29.5	25.7	31.3	28.3	8.6
0.0	0.0	0.0	1.6	0.0	10.4	0.0	0.0	0.0	0.0	0.0	0.0	0.0	0.0	1.4	0.0	0.0	16.8
1.6	1.6	1.7	1.7	1.8	1.7	2.0	1.9	1.9	1.8	1.9	1.9	2.5	2.4	2.3	2.4	2.5	2.4
0.6	0.6	0.6	0.7	0.7	2.2	1.1	1.0	1.0	1.0	1.0	1.1	2.2	2.2	2.2	2.1	2.1	2.0
0.1	0.1	0.0	0.0	0.0	0.5	0.1	0.1	0.0	0.1	0.1	0.2	0.1	0.2	0.3	0.2	0.1	0.3

Table 9. Representative major element analyses of boninites selected from the literature.

	1	2	3	4	5
SiO_2	53.76	56.88	56.46	55.56	54.09
TiO_2	0.24	0.28	0.29	0.21	0.30
Al_2O_3	12.53	13.76	14.65	10.25	8.39
Fe_2O_3	0.63	1.59	5.07	2.85	3.65
FeO	6.48	6.41	3.06	5.86	6.54
MnO	0.16	0.22	0.13	0.18	0.15
MgO	11.93	5.44	6.92	13.57	13.03
CaO	6.44	7.99	8.19	5.91	5.46
Na_2O	1.90	2.17	2.69	1.51	0.75
K_2O	0.68	0.49	1.28	0.69	0.41
P_2O_5	0.06	0.07	0.05	0.03	0.07
H_2O^+	5.13	4.40	2.42	3.65	7.4
Total	99.94	99.70	101.21	100.29	100.20

Notes:
1 = boninite, Bonin Islands, Kuroda et al. (1978).
2 = bronzite andesite, Bonin Islands, Kuroda et al. (1978).
3 = 1403-24 contact rock, Mariana Trench, Dietrich et al. (1978).
4 = 1403-34 enstalite porphyritic boninite, Mariana Trench, Dietrich et al. (1978).
5 = LB105 clinoenstatite-bearing, high-Mg andesite, Dabi Volcanics, Cape Vogel, Papua, Dallwitz et al. (1966).

Table 10. Major and trace element analyses of igneous rocks from Hole 459B.

Sample (interval in cm)	60-2, 80-82	61-1, 115-117	61-2, 47-49	63-1, 53-55	64-1, 41-43	65-1, 59-61	66-1, 73-75	66-2, 147-149	67-1, 118-120	68-1, 51-53	69-1, 144-146	69-3, 83-85	70-1, 49-51	71-2, 38-40	71-2, 105-107	73-1, 38-40	73-3, 118-120
SiO_2	54.6	53.8	54.4	51.1	51.3	52.6	56.2	56.5	57.4	58.6	56.8	56.0	55.4	57.2	57.2	53.1	52.9
TiO_2	0.74	0.66	0.67	0.83	0.82	1.21	0.99	0.98	0.93	0.72	0.76	0.94	0.88	1.14	1.12	1.14	1.11
Al_2O_3	14.7	14.9	14.2	14.8	13.8	13.9	13.4	13.2	12.8	12.2	14.4	14.3	14.2	12.8	13.4	14.0	15.3
tFe_2O_3	10.13	9.90	9.83	10.02	11.31	13.63	11.85	11.98	11.84	11.41	10.23	11.18	10.86	12.29	11.93	12.03	11.38
MnO	0.14	0.14	0.14	0.14	0.14	0.16	0.15	0.15	0.14	0.12	0.11	0.11	0.11	0.11	0.11	0.13	0.10
MgO	5.55	6.40	5.40	9.37	9.90	6.07	5.53	4.80	4.95	5.17	5.87	5.17	5.62	5.07	5.37	5.77	4.54
CaO	10.27	10.65	11.53	8.77	8.17	6.06	7.35	7.38	7.02	6.82	8.43	7.93	8.57	6.71	7.02	8.17	7.67
Na_2O	2.98	2.96	2.67	3.30	3.32	3.73	3.27	3.12	3.14	2.89	3.40	3.83	3.58	3.64	3.86	4.02	4.57
K_2O	0.47	0.44	0.54	0.68	0.57	0.89	0.63	0.86	1.45	1.89	0.69	1.00	0.82	1.03	0.84	0.98	1.22
P_2O_5	0.07	0.07	0.07	0.08	0.09	0.06	0.08	0.08	0.08	0.07	0.08	0.10	0.09	0.10	0.11	0.11	0.14
Total	99.69	99.97	99.48	99.12	99.38	98.35	99.41	99.03	99.70	99.90	100.81	100.59	100.13	100.07	100.89	99.44	98.88
Ni	43	57	54	68	52	24	24	21	24	30	28	22	30	11	14	20	11
Cr	131	159	141	67	56	13	17	13	16	22	23	20	55	14	13	22	14
Zn	60	65	60	90	87	115	72	70	107	85	66	74	65	82	89	83	80
Ga	16	17	16	18	22	25	22	19	18	17	20	21	21	21	22	22	23
Rb	27	24	15	6	5	13	28	46	22	26	12	28	11	16	11	13	19
Sr	121	120	116	127	123	125	109	107	109	115	144	131	139	121	123	134	159
Y	15	15	15	20	37	27	24	22	22	19	19	24	27	34	30	27	38
Zr	38	38	36	53	52	68	56	54	50	46	51	61	57	63	73	66	75
Nb	<1	<1	<1	<1	<1	<1	<1	1	<1	<1	<1	<1	1	<1	1	<1	<1
Ba	38	24	20	19	86	77	33	31	37	38	28	40	75	48	51	46	37
La	7	7	8	5	5	6	6	7	12	10	9	10	9	11	8	9	11
Ce	<1	3	3	5	8	11	4	9	4	5	7	5	9	10	7	9	17
Nd	2	2	3	4	7	10	4	6	5	5	6	5	5	7	8	8	11
Pb	<1	1	2	4	2	2	3	<1	2	5	4	2	5	2	4	4	2
Th	<1	<1	1	<1	<1	3	<1	2	2	1	1	1	4	<1	2	1	3
Zr/Nb	>38.0	>38.0	>36.0	>53.0	>52.0	>68.0	>56.0	54.0	>50.0	>46.0	>51.0	>61.0	57.0	>63.0	73.0	>66.0	>75.0
Ti/Zr	117.0	104.0	111.0	94.0	95.0	107.0	106.0	109.0	112.00	94.0	89.0	93.0	92.0	108.0	92.0	104.0	89.0
Y/Zr	0.39	0.39	0.42	0.38	0.71	0.40	0.43	0.41	0.44	0.41	0.37	0.39	0.47	0.54	0.41	0.41	0.51
Ce/Zr	<0.03	0.08	0.08	0.09	0.15	0.16	0.07	0.17	0.08	0.11	0.14	0.08	0.16	0.16	0.10	0.14	0.23
Ba/Zr	1.00	0.63	0.56	0.36	1.65	1.13	0.59	0.57	0.74	0.83	0.55	0.66	1.32	0.76	0.70	0.70	0.49
$(Ce/Y)_N$	—	0.49	0.49	0.61	0.53	1.00	0.41	1.00	0.45	0.65	0.90	0.51	0.82	0.72	0.57	0.82	1.10
Fe/Mg	2.12	1.79	2.11	1.24	1.32	2.60	2.49	2.89	2.77	2.56	2.02	2.51	2.24	2.81	2.58	2.42	2.91
K/Rb	144.0	153.0	301.0	938.0	955.0	566.0	186.0	156.0	547.0	603.0	477.0	295.0	619.0	534.0	633.0	623.0	533.0
Ba/Sr	0.31	0.20	0.17	0.15	0.70	0.62	0.30	0.29	0.34	0.33	0.19	0.31	0.54	0.40	0.41	0.34	0.23
Q	5.0	2.7	5.4	0.0	0.0	0.5	7.8	9.3	8.5	9.9	6.1	3.4	3.4	7.2	5.9	0.0	0.0
Or	2.8	2.6	3.2	4.0	3.4	5.3	3.7	5.1	8.6	11.2	4.0	5.9	4.8	6.1	4.9	5.8	7.3
Ab	25.3	25.1	22.7	28.2	28.3	32.1	27.8	26.7	26.6	24.5	28.5	32.2	30.3	30.8	32.4	34.2	39.1
An	25.5	26.1	25.3	23.8	21.2	18.9	20.1	19.5	16.6	14.7	21.9	18.9	20.3	15.6	16.5	17.3	17.7
Ne	0.0	0.0	0.0	0.0	0.0	0.0	0.0	0.0	0.0	0.0	0.0	0.0	0.0	0.0	0.0	0.0	0.0
Di	20.8	21.6	26.2	15.9	15.5	9.4	13.4	14.1	14.9	15.5	15.7	16.3	17.9	14.2	14.4	18.9	16.5
Hy	16.4	17.9	13.1	11.2	14.4	27.7	22.0	20.1	19.8	19.7	19.5	18.4	18.6	20.5	20.5	13.9	4.5
Ol	0.0	0.0	0.0	12.5	12.5	0.0	0.0	0.0	0.0	0.0	0.0	0.0	0.0	0.0	0.0	4.4	9.3
Mt	1.8	1.7	1.7	1.8	2.0	2.4	2.1	2.1	2.1	2.0	1.8	1.9	1.9	2.1	2.1	2.1	2.0
Il	1.4	1.3	1.3	1.6	1.6	2.3	1.9	1.9	1.8	1.4	1.4	1.8	1.7	2.2	2.1	2.2	2.1
Ap	0.2	0.2	0.2	0.2	0.2	0.2	0.2	0.2	0.2	0.2	0.2	0.2	0.2	0.2	0.2	0.3	0.3

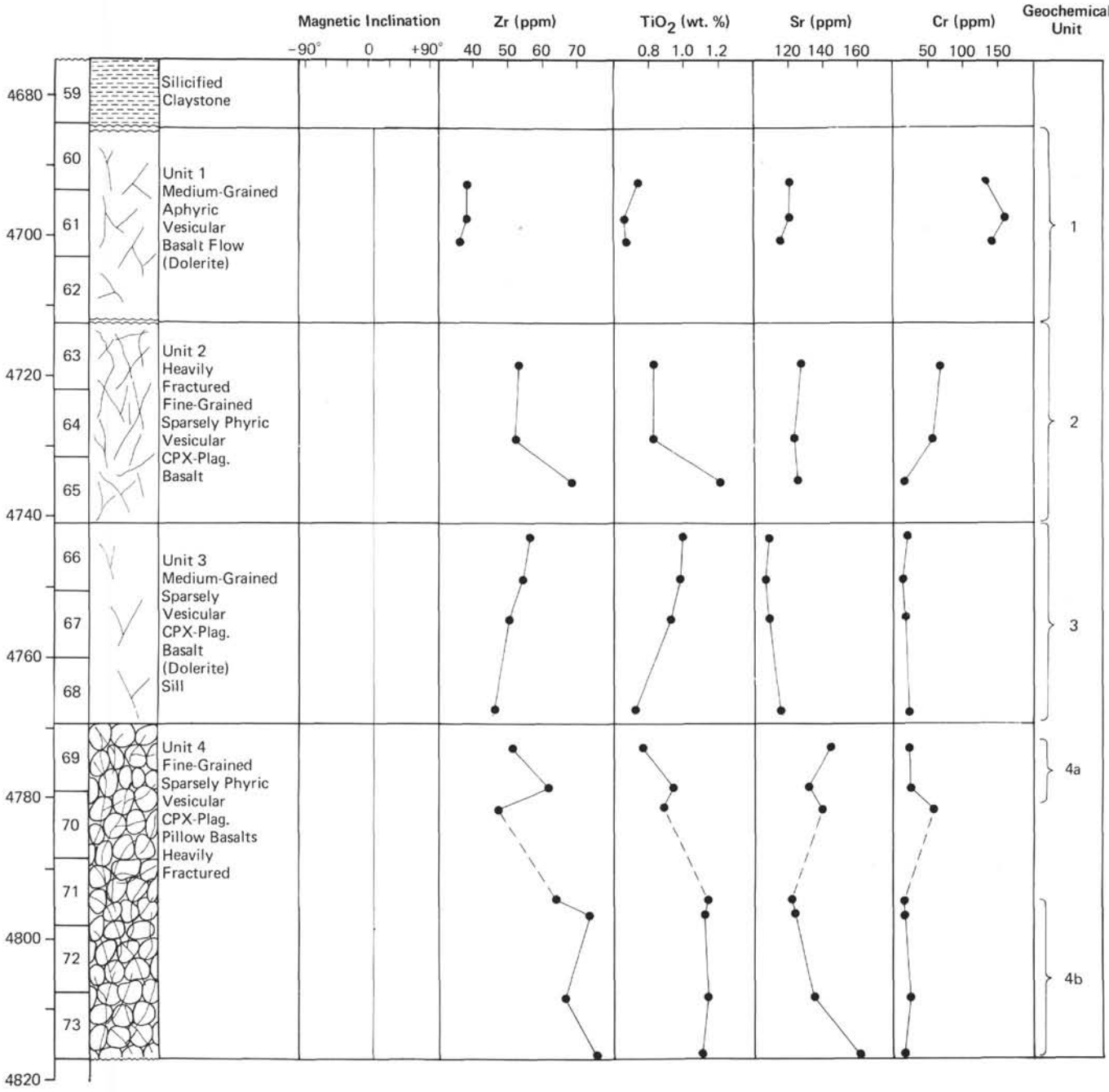

Figure 15. Geochemical and lithological stratigraphy of the basement sections of Hole 459B.

Table 11. Representative major and trace element analyses of basement rocks recovered on DSDP Leg 60. Major element oxides in weight percent, trace elements in parts per million.

Location	Mariana Trough				Mariana Ridge			Mariana Fore-Arc					Mariana Trench			
Lithological Unit	453-1	453-2	454A-pm1	454A-pm3	456-1	456A-3	457	458-1	458-4a	458-5	459B-1	459B-4a	460-1	460-2	461A	
SiO_2	51.0	48.3	49.3	50.2	46.2	50.7	53.4	52.5	53.2	52.8	53.8	57.2	53.6	52.5	58.7	SiO_2
TiO_2	1.00	0.83	0.86	1.12	1.26	1.18	0.89	0.34	1.13	1.13	0.66	1.14	1.34	0.87	1.01	TiO_2
Al_2O_3	15.7	15.2	14.4	14.5	12.3	16.6	15.6	18.0	15.5	13.6	14.9	12.8	16.6	15.2	13.2	Al_2O_3
Fe_2O_3	1.35	1.39	1.12	1.18	1.22	1.17	1.35	1.11	1.15	1.64	1.18	1.46	1.26	1.51	1.67	Fe_2O_3
FeO[a]	9.01	9.25	7.47	7.86	8.10	7.82	8.97	7.38	7.66	10.96	7.85	9.74	8.38	10.09	11.15	FeO[a]
MnO	0.15	0.17	0.12	0.16	0.29	0.16	0.14	0.11	0.06	0.10	0.14	0.11	0.07	0.13	0.13	MnO
MgO	5.71	8.34	13.30	8.73	11.22	5.23	5.33	5.09	3.73	6.17	6.40	5.07	3.97	5.03	5.46	MgO
CaO	9.86	13.47	10.97	10.42	12.55	11.23	6.47	11.17	61.2	5.88	10.65	6.71	5.45	8.24	3.00	CaO
Na_2O	2.93	1.69	2.36	2.64	2.40	3.27	2.73	2.77	5.70	3.41	2.96	3.64	5.51	3.06	3.50	Na_2O
K_2O	0.56	0.21	0.18	0.44	0.06	0.62	1.13	0.63	1.52	0.75	0.44	1.03	1.68	0.91	0.22	K_2O
P_2O_5	0.31	0.03	0.09	0.09	0.11	0.11	0.11	0.03	0.20	0.06	0.07	0.10	0.23	0.05	0.08	P_2O_5
H_2O^-	n.d.	n.d.	n.d.	n.d.	n.d.	n.d.	n.d.	n.d.	n.d.	n.d.	n.d.	n.d.	n.d.	n.d.	n.d.	H_2O^+
Total	97.66	98.96	100.14	97.38	95.66	98.05	96.02	99.15	95.98	96.52	99.10	98.99	98.07	97.62	98.19	Total
$Mg/(Mg + Fe^{2+})$	0.530	0.616	0.760	0.664	0.711	0.543	0.513	0.551	0.464	0.500	0.592	0.480	0.457	0.470	0.465	$Mg/(Mg + Fe^{2+})$
Total Fe as FeO	10.23	10.50	8.48	8.93	9.20	8.88	10.19	8.38	8.69	12.43	8.91	11.06	9.51	11.45	12.65	Total Fe as FeO
Sc	30.5	49.7	27.1	28.7	31.1	32.8	24.1	36.9	21.4	27.7	35.2	27.2	23.8	31.9	23.9	Sc (INA)
Cr	16	21	532	390	276	106	29	214	11	11	159	14	5	51	15	Cr (XRF)
Co	33.1	45.6	49.9	42.4	35.4	32.3	27.3	28.1	14.2	33.7	39.6	32.9	20.6	26.8	29.2	Co (INA)
Ni	11	6	382	269	74	51	17	80	11	23	57	11	2	22	27	Ni (XRF)
Zn	34	75	52	66	93	77	80	71	88	109	65	82	91	98	60	Zn (XRF)
Ga	17	18	16	17	18	16	16	14	25	18	17	21	25	18	17	Ga (XRF)
Rb	9	17	2	3	<1	8	18	7	25	13	24	16	22	8	4	Rb (XRF)
Sr	511	429	143	170	141	251	305	122	169	144	120	121	154	122	113	Sr (XRF)
Y	25	21	18	23	24	26	19	8	31	20	15	34	52	17	16	Y (XRF)
Zr	82	55	58	77	82	84	81	31	101	65	38	63	83	48	69	Zr (XRF)
Cs	0.08	0.03	0.01	0.02	0.02	0.16	0.41	0.09	0.44	0.18	1.14	0.25	0.38	0.06	0.25	Ca (INA)
Ba	148	326	49	105	67	81	255	41	79	63	24	48	66	21	36	Ba (XRF)
La	12.50	1.32	1.98	4.90	2.67	5.15	4.20	1.18	3.03	2.80	1.13	1.93	3.99	2.02	1.81	La (INA)
Ce	24.3	—	6.6	9.2	8.1	13.1	9.7	2.3	7.5	6.1	2.9	6.0	8.4	1.3	4.0	Ce (INA)
Eu	1.12	0.56	0.86	1.01	1.18	1.25	0.71	0.28	1.03	0.88	0.52	0.91	1.34	0.70	0.30	Eu (INA)
Tb	0.62	0.34	0.48	0.64	0.62	0.67	0.47	0.20	0.57	0.50	0.34	0.55	0.84	0.38	0.32	Tb (INA)
Hf	2.26	0.63	1.35	2.01	1.91	2.02	1.66	0.82	2.23	1.70	1.01	1.82	2.85	1.39	1.90	Hf (INA)
Ta	0.11	0.02	0.11	0.16	0.16	0.16	0.08	0.06	0.12	0.09	0.05	0.07	0.13	0.09	0.08	Ta (INA)
Th	2.38	0.14	0.24	0.32	0.20	0.63	0.73	0.15	0.23	0.16	0.10	0.18	0.32	0.21	0.25	Th (INA)
U	0.63	—	0.12	—	0.05	0.18	0.25	—	0.13	0.10	0.03	0.17	0.13	0.26	0.15	U (INA)

Notes:

[a] Fe calculated as $Fe_2O_3/FeO = 0.15$.

453-1 = Sample 453-52-1, 96–102 cm; 453-2 = Sample 453-57-1, 30–36 cm; 454A-pm1 = Sample 454A-5-4, 15–18 cm; 454A-pm3 = Sample 454A-16-1, 111–114 cm.
456-1 Sample 456-16-2, 92–96 cm; 456A-3 = Sample 456A-13-1, 23–26 cm; 457 = Sample 457-4,CC; 458-1 = Sample 458-28-1, 58–64 cm.
458-4a = Sample 458-41-1, 22–26 cm; 458-5 = Sample 458-46-1, 75–81 cm; 459B-1 = Sample 459B-61-1, 115–118 cm; 459B-4a = Sample 459B-71-2, 38–40 cm.
460-1 = Sample 460-9,CC, 11–13 cm; 460-2 = Sample 460-9,CC, 74–76 cm; 461A-3-1, 60–62 cm.

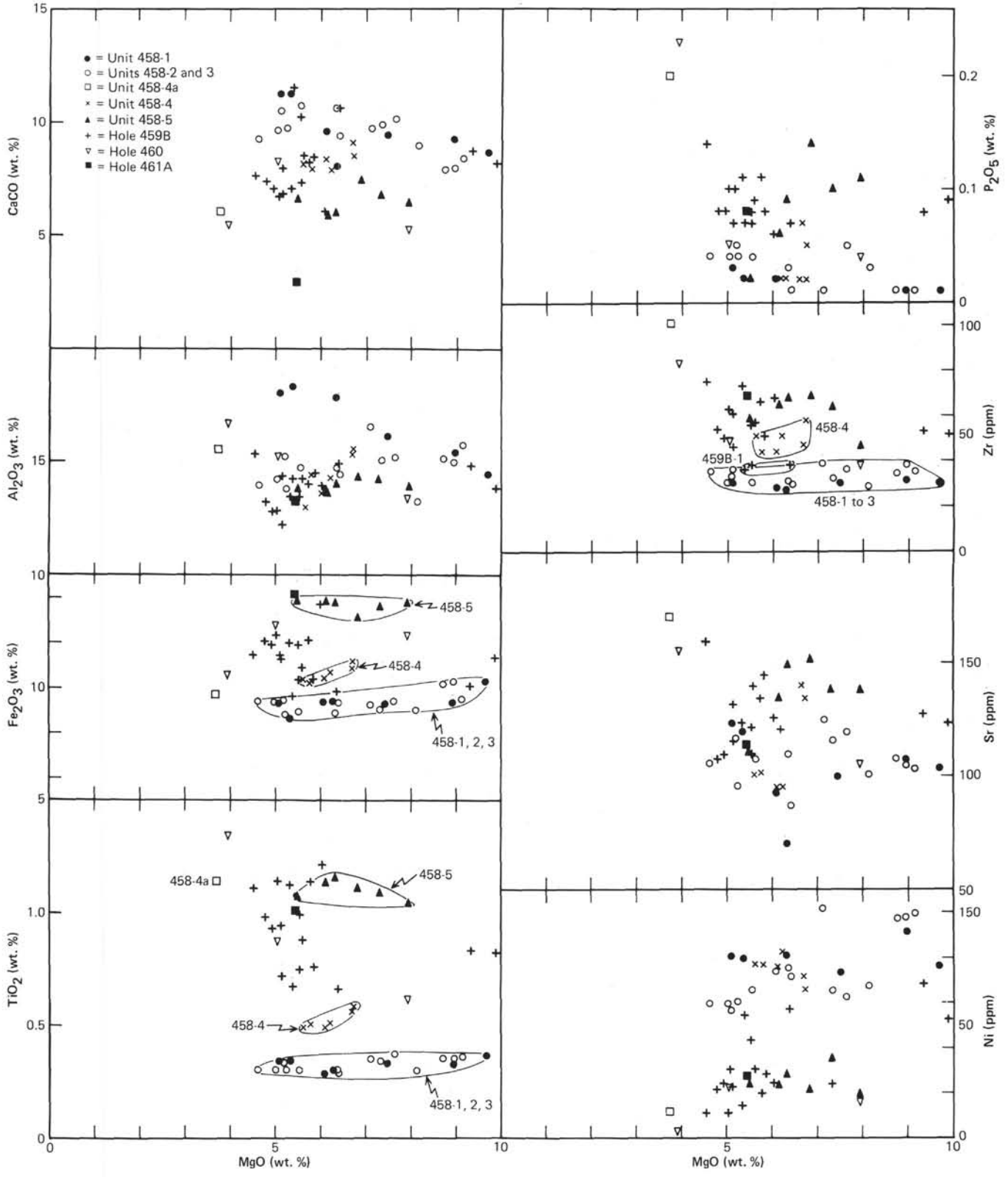

Figure 16. MgO variation diagram of selected major and trace elements for samples from Sites 458 through 461.

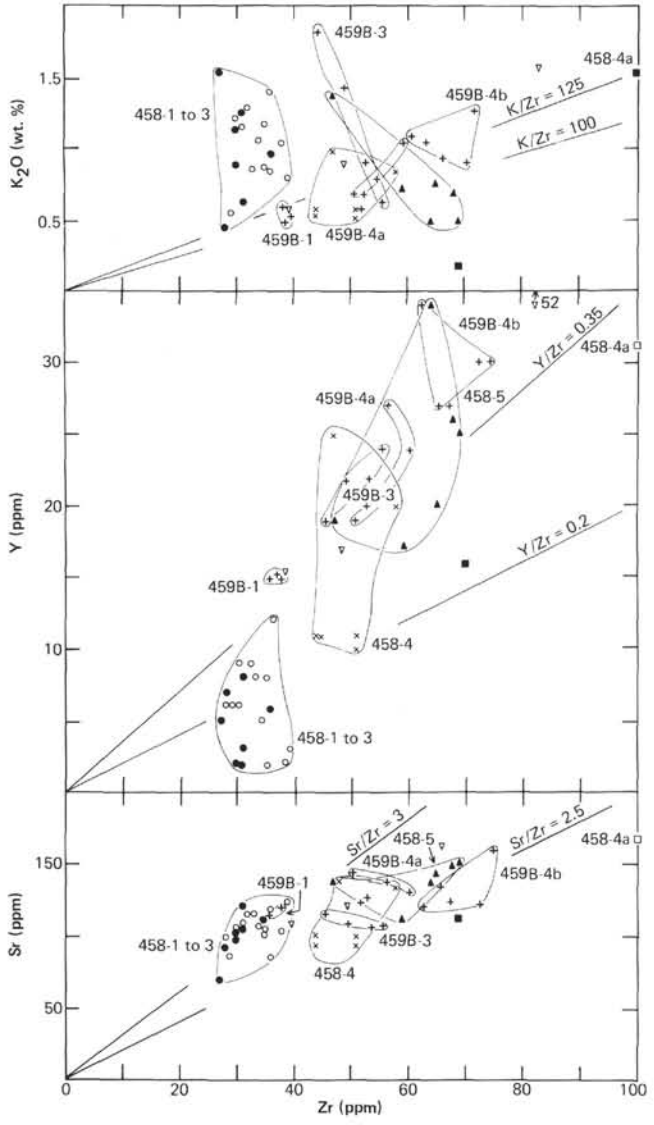

Figure 17. K_2O, Y, and Sr versus Zr for samples from Sites 458 through 461. (See Fig. 16 for symbols.)

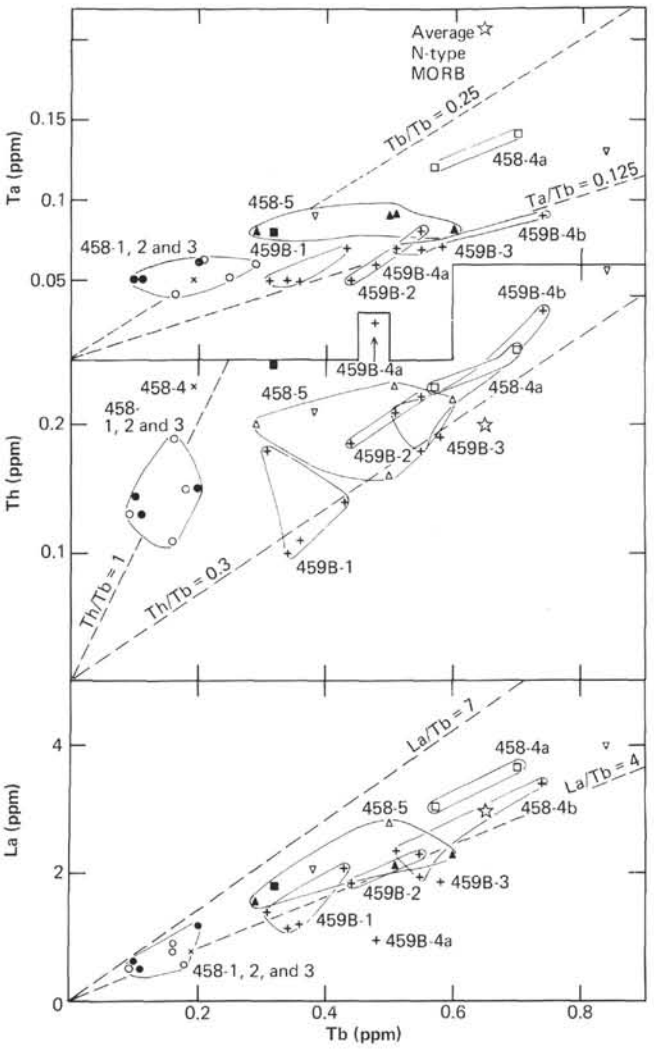

Figure 18. Ta, Th, and La versus Tb for samples from Sites 458 through 461. (See Fig. 16 for symbols.)

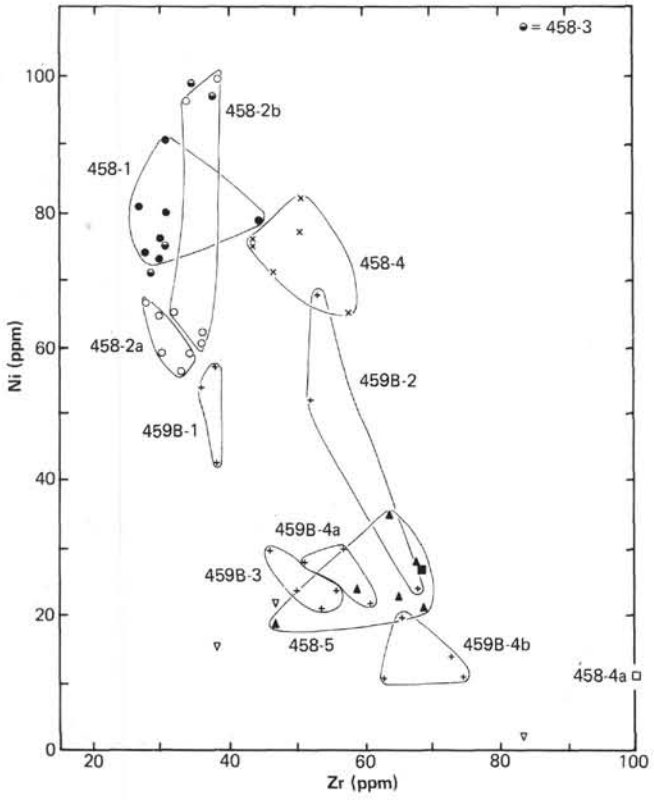

Figure 19. Ni versus Zr for samples from Sites 458 through 461. (See Fig. 16 for symbols.)

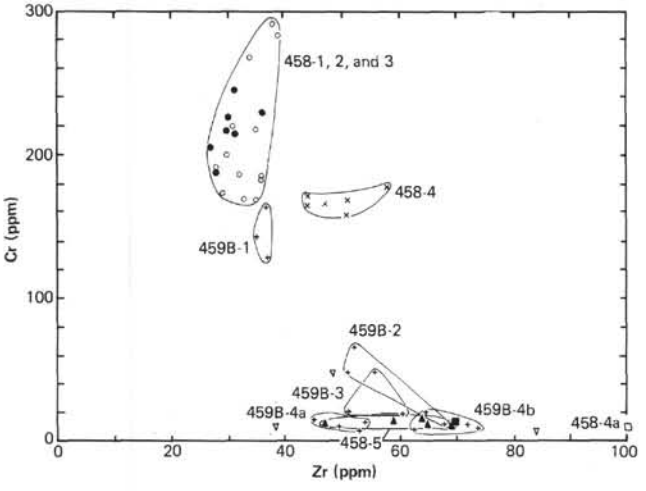

Figure 20. Cr versus Zr for samples from Sites 458 through 461. (See Fig. 16 for symbols.)

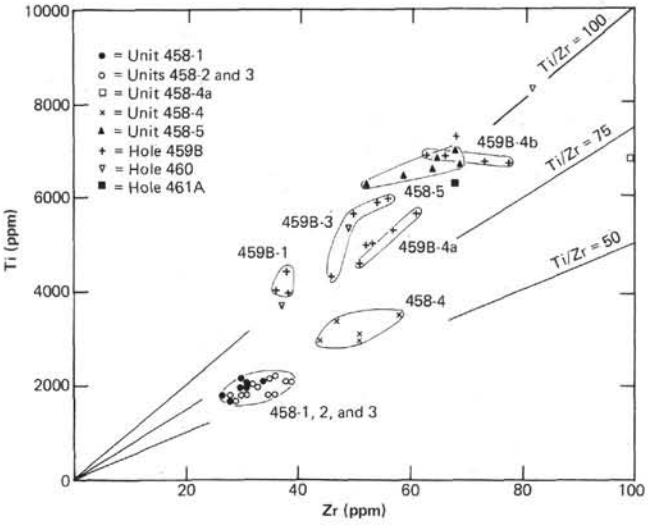

Figure 21. Ti versus Zr for samples from Sites 458 through 461. (See Fig. 16 for symbols.)

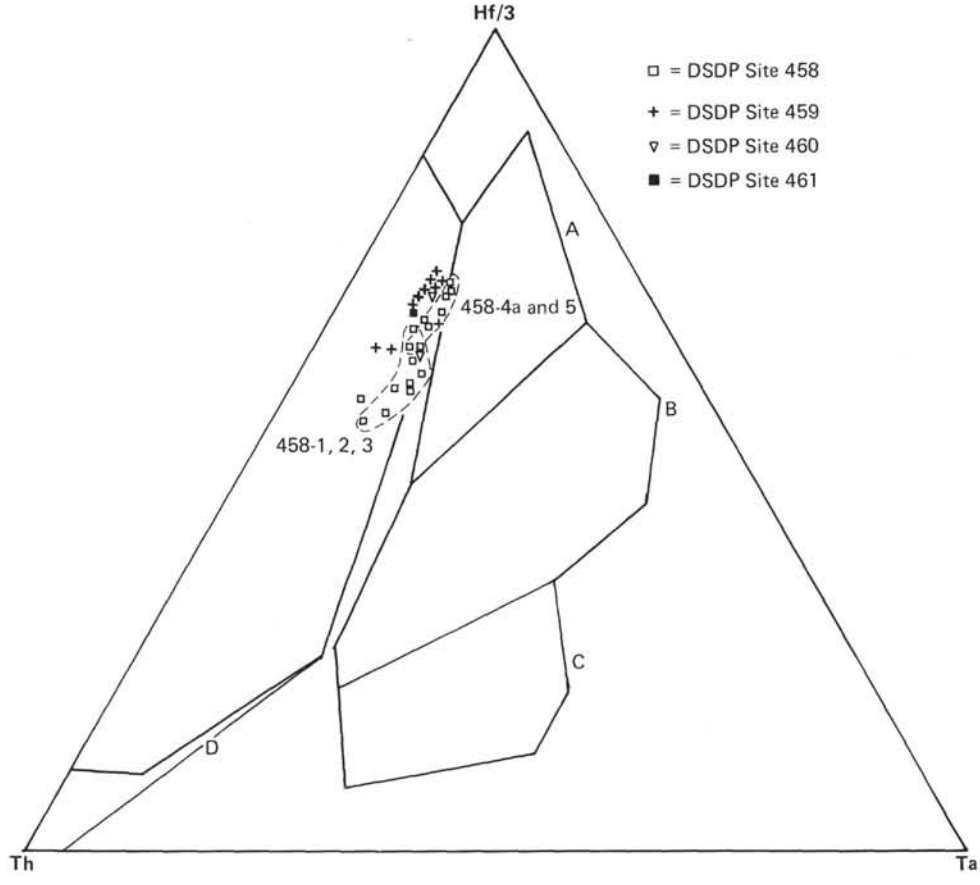

Figure 22. Th–Hf/3–Ta discrimination diagram for samples from Sites 458 through 461. See Figure 11 for description of the marked areas.

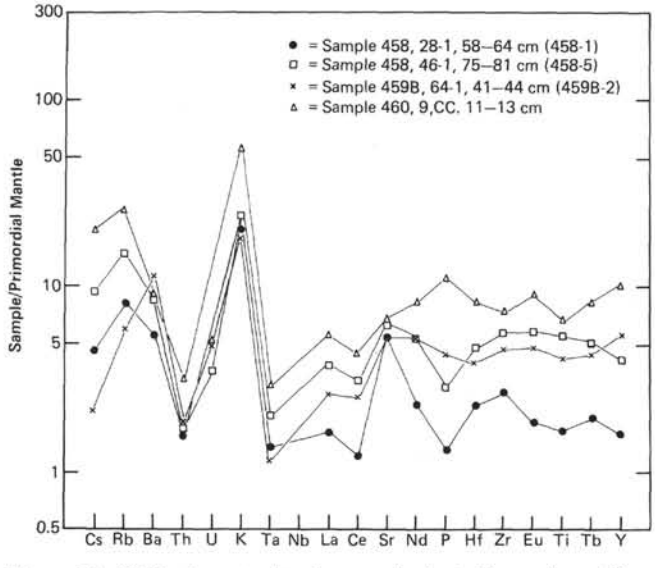

Figure 23. HYG element abundances of selected lavas from Sites 458, 459, and 460 normalized to estimated primordial mantle abundances (from Wood, 1979, except that a Ti value of 1500 ppm is used here).

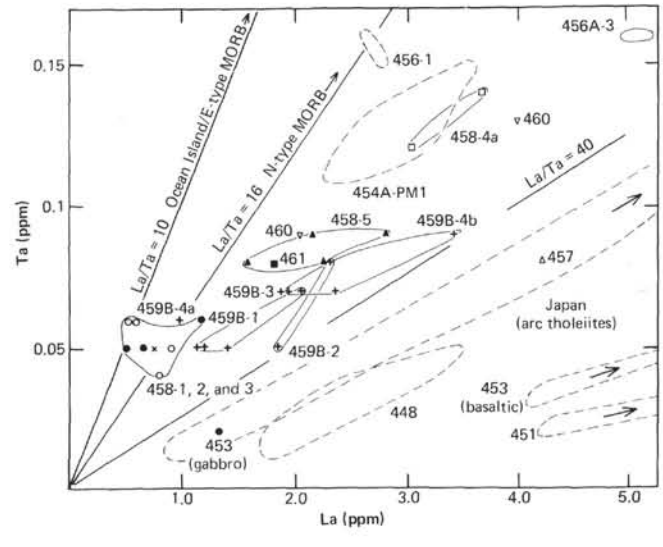

Figure 24. La versus Ta for Leg 60 samples. The fields of Japanese lava series and DSDP Leg 59 samples are from Wood et al., in press a and b. La/Ta ratios for E-type and N-type MORB are from Wood et al. 1979a.

APPENDIX

Table 1. XRF sample descriptions (hand-specimen), Leg 60.

Sample (interval in cm)	
Hole 453	
42-1, 16–18	Mudstone–siltstone, dark greenish gray.
47-1, 99–101	Bioturbated mudstone, brownish green.
49-1, 56–61	Coarse-grained leuco gabbro, 70 percent feldspar, ferromagnesian minerals replaced by clays/chlorite/serpentine ± amphibole(?).
49-3, 52–58	Fine- to medium-grained, leucocratic gabbro(?), pink coloration around feldspars, 60 percent felsic, altered ferromagnesian minerals [clay/chlorite(?)].
50-2, 37–42	Coarse-grained leucocratic gabbro, 70 percent feldspar, altered ferromagnesian minerals [clays/chlorite/serpentine(?)].
52-1, 96–102	Sparsely plagioclase-phyric basalt.
52-2, 94–97	Heavily altered, leucocractic gabbro, 60 percent feldspar, altered ferromagnesian minerals [clays/chlorite/serpentine(?)].
53-3, 0–5	Gabbro, 50 percent feldspar, 50 percent altered ferromagnesian minerals [clays/chlorite/serpentine(?)].
54-1, 40–47	Badly altered, leucocratic(?) gabbro.
54-2, 84–91	Arkose, various lithic fragments, one half of sample dark gray, possibly plagioclase-phyric basalt; the other half, brownish gray matrix with felsic grains.
54-3, 6–10	Basalt (dolerite) plagioclase and possibly olivine or clinopyroxene-phyric.
55-2, 14–18	Aphyric basalt clast, dark gray clay alteration products, fracture lined by red-brown clays.
55-3, 25–29	Leuco-gabbro, 60 percent feldspar, 40 percent altered ferromagnesian minerals.
55-3, 90–94	Leuco-gabbro, 65 percent feldspar, 40 percent altered ferromagnesian minerals.
55-4, 144–148	Leuco-gabbro, 70 percent feldspar, 30 percent chloritic alteration products.
56-2, 33–35	Leuco-gabbro, 70 percent feldspar, 30 percent chloritic alteration products, similar to previous sample.
56-2, 85–90	Anorthosite, interstitial chlorite/clay.
57-1, 30–35	Gabbro, dark-gray feldspar, red-brown alteration products after ferromagnesian minerals.
57-3, 8–12	Leuco-gabbro, 70 percent feldspar, 30 percent dark-brown and red-brown alteration products after ferromagnesian minerals.
57-4, 123–130	Coarse-grained leuco-gabbro, 70 percent feldspar, 30 percent interstitial altered ferromagnesian minerals.
57-4, 36–81	Equigranular gabbro, 50 percent altered ferromagnesian minerals, 50 percent feldspar.
58-1, 6–10	Greenish gray, plagioclase-phyric metabasalt (15% phenocrysts), occasional vesicles, some containing pyrite.
59-1, 13–15	Sparsely feldspar-phyric (1–2%), metavolcanic rock, aphanitic, Prussian gray groundmass, a few vesicles; quartz and carbonate vein cuts sample; quartz coating on one side of sample.
59-1, 47–52	Gray-purple metavolcanic rock, carrying pyrite.
63-1, 0–5	Prussian gray, plagioclase-phyric metabasalt(?), a few vesicles, some of which are carbonate-lined.

Table 1. (Continued).

Sample (interval in cm)	
Site 454	
454A-5-1, 2–8	Medium-grained aphyric, altered greenish gray basalt, 2 percent vesicles.
454A-5-3, 106–110	Medium-grained, altered, gray-green basalt, 10 percent vesicles.
454A-5-4, 15–18	Medium-grained, altered, aphyric, gray-green basalt, 5 percent vesicles.
454-6-2, 102–106	Medium- to coarse-grained basalt (dolerite), 2 percent vesicles; outer surface of sample covered by light-green clays.
454A-8-1, 2–7	Gray, aphyric, aphanitic basalt, 2 percent vesicles lined by dark gray-brown clay.
454A-10-1, 81–84	Gray, medium-grained, altered basalt, 10 percent vesicles, 2 percent large vesicles (1–2 mm across), often lined by light-green clay, other vesicles <0.5 mm.
454A-11-1, 40–44	Gray, medium-grained, altered basalt, 10 percent vesicles, 2 percent (1–2 mm) lined by light-green clay, other vesicles <0.5 mm, similar to previous sample.
454A-11-4, 71–75	Gray, medium-grained, altered basalt, 5 percent vesicles (<0.5 mm).
454-12-1, 100–104	Gray, medium-grained, altered basalt, 5 percent vesicles (<0.5 mm) similar to previous sample.
454A-12-2, 26–29	Gray, fine-grained, aphyric basalt, 10 percent vesicles (<2 mm), larger vesicles lined by blue-gray clay.
454A-14-1, 2–4	Gray, fine-grained, aphyric basalt, 10 percent vesicles (<2 mm).
454-15-1, 13–16	Gray, fine-grained, aphyric basalt, 10 percent vesicles, slightly altered.
454A-16-1, 33–36	Olive-green-gray, fine-grained, aphyric basalt, 5 percent vesicles, slightly altered.
454A-16-1, 111–114	Olive-green-gray to gray, aphanitic, aphyric basalt, 2 percent vesicles.
Site 456	
456-16-1, 145–148	Olive-green-brown, aphanitic, aphyric basalt, 3 percent large vesicles (1–2 mm), some with calcite and/or pyrite lining.
456-16-2, 92–96	Fine-grained, blue-gray, plagioclase-phyric basalt. (5% phenocrysts, 0.5–2 mm across), 1 percent vesicles.
456-17-1, 95–99	Fine-grained, blue-gray, plagioclase-phyric (5% phenocrysts, 0.5–2 mm across) basalt, 1 percent vesicles, some containing calcite crystals.
456-18-1, 50–53	Medium-grained, olive-gray basalt, 3 percent vesicles, some lined by calcite and green clay.
456-19-1, 18–21	Sparsely plagioclase-phyric, dark gray, medium-grained basalts, 5 percent vesicles, sample cut by fracture lined by Fe oxides/hydroxides.
456A-10-1, 25–27	Purple-gray mudstone.
456A-11-1, 76–79	Green-gray, aphyric, aphanitic metavolcanic rock, 10 percent vesicles (<2 mm), some contain pyrite.
456A-12-1, 11–15	Green-gray, fine-grained basalt, 2 percent vesicles, patches of dark-gray clay alteration products.
456A-13-1, 23–26	Dark-gray, aphyric, aphanitic basalt, 5 percent vesicles (<2 mm), 5 percent vesicles (2–10 mm) lined by or filled by light-brown clays.

Table 1. (Continued).

Sample (interval in cm)	
456A-14-1, 12–16	Dark-gray, aphyric, aphanitic basalt, 5 percent vesicles (< 2 mm), 5 percent vesicles (2–10 mm), lined by yellow, red-brown and purple alteration products.
456A-14-1, 38–42	Olive-gray, aphyric, aphanitic basalt, 2 percent vesicles (< 0.5 mm), concentric zoning of alteration colors through sample suggests part of pillow interior.
456A-15-1, 27–31	Gray, aphyric, fine-grained basalt, 4 percent vesicles concentrated in "pipes," vesicles often lined by gray or light-brown clays.
Hole 457	
4,CC	Tan-colored piece of pumice, very soft.
Hole 458	
27-1, 130–132	Olive-green, fine-grained sandstone, cut by carbonate-lined fracture.
28-1, 58–64	Heavily altered, light-green-gray, spherulitic basalt, one large vesicle (5 × 3 mm).
28-1, 125–130	Heavily altered, light-green-gray, spherulitic basalt.
28-1, 140–146	Dark gray, aphyric, fine-grained basalt, 3 percent vesicles (< 2 mm), a few larger vesicles lined by blue-gray clay.
29-1, 54–57	Olive-green, fine-grained, aphyric basalt, 1 percent vesicles (< 1 mm).
29-2, 37–42	Dark-green-gray, fine-grained aphyric, altered basalt, < 1 percent vesicles (< 1 mm).
30-1, 56–59	Heavily altered, olive-green, spherulitic basalt, 5 percent vesicles (2–5 mm), lined by gray-blue clay and white mineral (zeolite?).
31-1, 39–41	Heavily altered, light olive-green, fine-grained, aphyric basalt, one vesicle (2 + 2 mm).
31-1, 131–136	Light-gray (green tinges), fine-grained, aphyric basalt, 3 percent vesicles (< 1 mm).
32-1, 116–119	Light-gray-green, medium-grained, aphyric basalt, 1 percent vesicles (< 1 mm).
32-3, 34–36	Light-gray-green, aphyric, aphanitic basalt, 5 percent vesicles (< 1 mm).
33-2, 19–22	Gray-green, medium-coarse grained (ca. 1 mm) basalt, few vesicles (< 1 mm).
34-1, 39–42	Light-green-gray, medium-grained, basalt, 2 percent vesicles (< 1 mm), one surface of sample is a fracture covered by a light-olive-green clay and carbonate.
35-1, 42–45	Light-green-gray, medium-grained, aphyric basalt, 5 percent vesicles (< 1 mm); one surface of sample is a fracture; basalt heavily altered, but no coating of secondary minerals.
35-2, 69–73	Light gray, aphyric, aphanitic basalt, several trains of small vesicles (< 0.5 mm).
36-1, 27–31	Light gray-green, aphyric, aphanitic basalt, few vesicles, cut by carbonate and clay/chlorite(?)-lined vein.
37-1, 52–55	Gray-green, fine-grained, aphyric basalt.
37-2, 62–64	Gray-green, medium-grained, aphyric basalt, few vesicles.
38-1, 51–53	Battleship-gray, fine-grained basalt, 2 percent vesicles (< 2 mm), odd plagioclase(?) phenocrysts(?).
39-1, 37–40	Gray, very fine-grained basalt, 5 percent vesicles, often lined or infilled by gray clay and calcite.
40-2, 90–93	Battleship-gray, aphyric, aphanitic basalt, 1 percent vesicles (< 0.5 mm), sample cut by carbonate-lined fracture.

Table 1. (Continued).

Sample (interval in cm)	
41-1, 22–26	Heavily altered, olive-gray, aphyric, aphanitic basalt, 3 percent vesicles (< 0.5 mm).
42-1, 61–64	Green-gray, fine-grained aphyric basalt, few vesicles, slickenside surface on sample covered by chlorite.
42-1, 86–88	Dark-gray, aphyric, aphanitic basalt, 2 percent vesicles often surrounded by light-gray alteration zone and lined by light-blue clay and zeolites or chalcedony. Sample cut by zeolite or chalcedony-lined vein.
43-1, 118–121	Gray, fine-grained basalt, 2 percent vesicles, heavily altered to green clays, a few zeolites(?) in vesicles.
44-1, 53–60	Gray, aphyric, aphanitic basalt, 2 percent vesicles lined by zeolites and blue-gray clay.
45-1, 8–12	Gray, aphyric, aphanitic basalt, 2 percent vesicles lined by zeolites and blue-gray clay, similar to previous sample.
45-1, 24–27	Olive-green-gray, aphyric, fine-grained basalt, 10 percent vesicles (< 3 mm).
46-1, 75–81	Gray-green, fine-grained, aphyric basalt, few vesicles.
46-1, 83–86	Gray-green, aphyric, aphanitic basalt, few vesicles, one vesicle filled by a zeolite(?), trains of fine vesicles (< 0.5 mm).
47-1, 67–71	Light-green-gray, aphyric, aphanitic basalt; three parallel trains of fine vesicles (< 0.5 mm) cut sample, plus a few larger vesicles (1–2 mm).
48-1, 79–82	Gray-green, aphyric, aphanitic basalt, lustrous, black glassy margin on one side of sample, very fresh, but coating of clays/chlorite on outer surfaces.
49-1, 136–138	Olive-green-gray, fine-grained, aphyric basalt, 5 percent vesicles, gray-blue clay lining to vesicles.
Hole 459	
60-2, 80–83	Gray-green, medium-grained inequigranular basalt, 3 percent vesicles (< 1 mm).
61-1, 115–118	Light-gray-green, medium-grained inequigranular basalt, 15 percent vesicles (< 2 mm), specks of Fe^{III} oxides present.
61-2, 47–50	Green-gray, medium-grained inequigranular basalt, 2 percent vesicles (< 2 mm), mesostasis altered to light-olive-green and tan clays.
63-1, 53–54	Olive green-gray, fine-grained aphyric basalt, 2 percent vesicles, generally < 0.5 mm, a few 1–2 mm.
64-1, 41–44	Dark green-gray, fine-grained, aphyric basalt, 3 percent vesicles (< 1 mm).
65-1, 59–63	Heavily altered, dark green-gray, aphyric, aphanitic basalt, 1 percent vesicles (< 1 mm); sample also includes part of glassy margin (black, lustrous, relatively fresh), and is cut by carbonate and clay and/or chlorite(?)-lined vein.
66-1, 73–77	Heavily altered, olive-green-brown, medium-grained, inequigranular basalt, 3 percent vesicles (< 2 mm), brown clay lining to some vesicles.
66-2, 147–150	Heavily altered, olive-green-brown, medium-grained, inequigranular basalat, 1 percent vesicles (< 2 mm), one large vesicle (5 mm).
67-1, 118–120	Olive-green, medium-grained, inequigranular basalt, 3 percent vesicles, bright olive-green secondary mineral—malachite? Infilling and replacing mesostasis near some vesicles.

Table 1. (Continued).

Sample (interval in cm)	
68-1, 51–54	Olive-green, fine- to medium-grained, inequigranular basalt, bright-olive-green mineral (malachite?), replacing mesostasis and lining fracture with carbonate.
69-1, 144–146	Gray, fine-grained, aphyric basalt, 2 percent vesicles, sample surface covered by green and brown clays.
69-3, 83–86	Olive-green, very fine grained aphyric basalt, 2 percent vesicles (<2 mm).
70-1, 49–53	Dark-olive-green-gray, fine-grained, aphyric basalt, 4 percent vesicles (<0.5 mm), 1 percent vesicles (1–2 mm); sample cut by slickensided, chlorite-lined fracture.
71-2, 38–40	Heavily altered, olive-green-gray, fine-grained basalt, 3 percent vesicles (<1 mm).
71-2, 105–108	Heavily altered, olive-green-gray, fine-grained basalt, 3 percent vesicles (<1 mm); similar to previous sample, cut by slickensided chlorite-lined fracture.
73-1, 38–40	Heavily altered, olive-green-gray, fine-grained, aphyric basalt, 3 percent vesicles, similar to previous two samples.
73-3, 118–120	Heavily altered, olive-green-gray, fine-grained, aphyric basalt, 2 percent vesicles (<2 mm).
Site 460	
460-9,CC, 7–8 (#2)	Heavily altered, olive-green-brown, fine-grained, plagioclase-phyric (5%) basalt, 1 percent vesicles (0.5–2 mm).
460A-9,CC, 11–13	Olive-green-gray, aphanitic, aphyric basalt, 2 percent vesicles (<5 mm).
460A-11-1, 29–33	Green-gray, medium-grained basalat, odd vesicle (<2 mm), lined by dark-green clay.
Hole 461A	
3-1, 60–62	Green-brown, fine-grained, aphyric basalt, light-tan and dark-green clays ± chlorite coating surface of sample, cut by fracture lined by Fe^{III} oxides.